Numéro d'ordre : 19/19

Université polytechnique des Hauts-de-France

Detection of fouling factor by ultrasonic coda wave during contamination and cleaning of solid substrate

Thèse de Doctorat

par

CHEN Bowei

Soutenance le 10 juillet 2019, à Valenciennes

Président :	Guy Feuillard,*Professeur, INSA Centre Val de Loire*
Rapporteurs :	Emmanuel Le Clézio, *Professeur, Université de Montpellier* Romain Jeantet, *Professeur, Agrocampus Ouest*
Examinateurs :	Marieke Van Audenhaege, *Chargée de Recherche, Responsable du pôle Technologie Laitière, SODIAAL* Guillaume Delaplace, *Directeur de Recherche, INRA* Dorothée Callens-Debavelaere, *Maître de Conférences, Université Polytechnique Hauts-de-France* Pierre Campistron, *Maître de Conférences, Université Polytechnique Hauts-de-France*
Directeur de thèse :	Emmanuel Moulin, *Professeur, Université Polytechnique Hauts-de-France*
Discipline :	Electronique
Ecole Doctorale :	Sciences Pour Ingénieur (ED SPI 072)

IEMN DOAE- UMR CNRS 8520

Numéro d'ordre : 19/19

Université polytechnique des Hauts-de-France

Détection du facteur d'encrassement par onde de coda ultrasonore lors de la contamination et le nettoyage d'un substrat solide

Thèse de Doctorat

par

CHEN Bowei

Soutenance le 10 juillet 2019, à Valenciennes

Président :	Guy Feuillard,*Professeur, INSA Centre Val de Loire*
Rapporteurs :	Emmanuel Le Clézio, *Professeur, Université de Montpellier* Romain Jeantet, *Professeur, Agrocampus Ouest*
Examinateurs :	Marieke Van Audenhaege, *Chargée de Recherche, Responsable du pôle Technologie Laitière, SODIAAL* Guillaume Delaplace, *Directeur de Recherche, INRA* Dorothée Callens-Debavelaere, *Maître de Conférences, Université Polytechnique Hauts-de-France* Pierre Campistron, *Maître de Conférences, Université Polytechnique Hauts-de-France*
Directeur de thèse :	Emmanuel Moulin, *Professeur, Université Polytechnique Hauts-de-France*
Discipline :	Electronique
Ecole Doctorale :	Sciences Pour Ingénieur (ED SPI 072)

IEMN DOAE- UMR CNRS 8520

Remerciements

Je souhaite tout d'abord remercier les Professeurs Emmanuel Le Clézio et Romain Jeantet d'avoir accepté la charge de rapporteur de ma thèse. Je tiens également à remercier messieurs Professeur Guy Feuillard et Docteur Marieke Van Audenhaege pour avoir examiné mes travaux.

Je remercie directeur de thèse, Professeur Emmanuel Moulin, et co-directeur Docteur Pierre Campistron, Docteur Dorothée Callens-Debavelaere. Vous m'avez guidé dans la recherche et m'avez inspiré pour surmonter les difficultés dans les travaux. Grâce à vous, je peux comprendre l'essentiel de la recherche scientifique.

Cette thèse a été réalisée en collaboration entre l'Institut National de la Recherche Agronomique de Lille (INRA PIHM) et l'Institut d'Electronique, Microélectronique et de Nanotechnologie - Département Opto-Acousto-Electronique (IEMN-DOAE), respectivement au sein des équipes Processus aux Interfaces et Hygiène des Matériaux (PIHM), Transduction, Propagation et Imagerie Acoustique (TPIA), Matériaux et Acoustiques pour MIcro et NAno systèmes intégrés (MAMINA). Je remercie Guillaume Delaplace, le responsable de thèse de la partie INRA. Vous avez fourni des support significatif pour la thèse sur les matériaux expérimentaux et m'avez aidé sur l'expression scientifique.

Je remercie Pascal Debreyne, Marwan Abdallah, Simon Oussama Khelissa. Votre contribution sur les manipulations est indispensable. Je remercie également Laurent Bouvier, Thierry Six, Nour-Eddine Chihib, et les autres membres de INRA pour les aides dans les manipulations.

Je remercie Lynda Chehami, Salah-Eddine Hebaz, Martin Robin et les autres membres de IEMN-DOAE pour l'aide sur l'enseignement et la vie dans laboratoire. Je remercie également les secrétaires, Virginie Schafer, Françoise Desruelles, Maureen Courbez et Marie-Hélène Frappart pour l'aide administratif.

Abstract/Résumé

Abstract

Fouling of equipment occurs in many industrial sectors. For example, contamination of surfaces in contact with foodstuff, caused by fouling, causes considerable economic losses and increases public health risks. The cleaning of the fouled surface is generally carried out using highly polluting chemicals. Therefore, it is important to develop devices to monitor the formation / removal of fouling on these surfaces (without disrupting production) in order to reduce the microbiological risks and environmental/economic impacts associated with the cleaning processes. In this work, the detection of fouling factor using a non-invasive ultrasonic method, called "coda wave interferometry", abbreviated in English (CWI), was investigated. This technique has been tested for various types of applications (wax cleaning, biofilm formation detection and protein deposit cleaning). The results obtained are very promising and show that the CWI is able to detect even a slight change in the fouling factor. In particular, the evolution of the decorrelation coefficient for each application shows good agreement with the actual fouling factor. Overall, this work has provided evidence that the CWI method is applicable to the monitoring of fouling factor of solid surfaces.

Keywords : Fouling detection, Coda wave, Ultrasound

Résumé

L'encrassement des équipements a lieu dans de nombreux secteurs industriels. Par exemple, la contamination des surfaces de contact avec les aliments, provoquée par un encrassement, entrainent des pertes économiques considérables et augmentent les risques

de santé publique. Le nettoyage de l'encrassement est généralement réalisé à l'aide de produits chimiques très polluants. Par conséquent, il est important de développer des dispositifs permettant de surveiller la formation/l'élimination des encrassements sur ces surfaces (sans perturber la production) afin de réduire les risques microbiologiques, les impacts environnementaux et économiques liés aux processus de nettoyage. Dans ce travail, on s'intéresse à la détection du facteur d'encrassement à l'aide d'une méthode ultrasonore non invasive, dite "interférométrie d'ondes de coda", abrégée en anglais (CWI). Cette technique a été testée pour différents types d'applications (Nettoyage de cire, détection de la formation de biofilm et nettoyage de dépôts protéiques). Les résultats obtenus sont très prometteurs et montrent que la CWI est capable de déceler même un léger changement du facteur d'encrassement. En particulier, l'évolution du coefficient de décorrélation pour chaque application montre une bonne concordance avec l'état d'encrassement réel de la surface. Dans l'ensemble, ces travaux fournissent un ensemble de preuves montrant que la méthode CWI, est applicable au suivi du facteur d'encrassement de dépôts sur des surfaces solides.

Mots-clés : Détection du dépôt, Onde coda, Ultrason

Table des matières

Introduction

In many industry, an undesirable deposition layer often occurs where there is a contact of device surface and product. The existence of deposit will damage the manufacture procedure and cause negative influences on the efficiency and the quality of production.

Among all the industry, the food production is a typical field which is extremely strict to the quality of products. Contamination in the food industry due to the presence of fouled deposition on the inner surface of the equipment is a serious problem. A large number of food products are lost due to the contamination of foulant. The cost of production rises with the loss of products. And the source of food supply for human society then diminish. The fouling inside the equipment leads to a hygiene risk for industrial products. In heat treatment, deposition fouling is inevitable by current production technology. For the contaminated product, it is difficult to separate the polluted part or eliminate the contamination without damaging the product. Therefore, cleaning the equipment frequently is the best solution to minimize the influence of contamination and guarantee the quality of production.

Fouling occurs frequently in many kinds of industrial equipment, especially the heat treatment devices. The cleaning of food stains is carried out everyday. Consequently, the cleaning treatment is very expensive due to a large number of repetition. In addition, the detergent used in cleaning has a significant environmental impact. Today, people have realized that the sustainable development is important. Environmental protection has already become a major social concern. Thus, the development of industry should also satisfy it. It means that the cleaning protocol need to be more efficient.

The essential of cleaning improvement is the detection and monitoring in order to know the current state of deposit inside the equipment. Then it will be possible to optimize the cleaning procedure and minimize the use of detergent. The objective of an

NDT/E (Non-Destructive Testing/Evaluation) method is to detect and characterize the state of structure or materials, without modifying the studied specimen, which means the methods are certainly non-invasive. Thanks to a good penetration of acoustic waves, ultrasonic methods are widely used in detections of liquid or solid materials since the last century. Considering the economy and safety, NDT/E ultrasonic methods have an excellent potential in many field, but they are rarely applied on the deposition monitoring of food industry.

Among all the NDT/E methods, the ultrasonic coda wave is a suitable method for deposit detection. Briefly, coda wave is the late part in signals after the direct wave, which propagate directly from acoustic source to the receiver. It is a summation of waves along all possible paths with multiple reflections and diffusions. Thus, the classic acoustic parameters are difficult to be used for analyzing coda wave. The Coda Wave Interferometry (CWI) is a quite recent technique. The detection methods by using coda wave are more sensitive than the classic acoustic methods. It is verified in this thesis that the detectable thickness with of a deposit layer coda wave could be less than $50\mu m$. So far, this type of method has not yet applied to the fouling detection in food industry.

Nowadays, there is still few research in the field of coda. An NDT/E method using the coda wave is proposed in this thesis to detect and monitor the fouling state on a solid substrate. The objectives of this work are :

— Verify the feasibility of fouling detection on solid substrate by the coda wave ;

— Propose a parameter to quantify the variation of coda ;

— Construct an acquisition system for measuring signals experimentally ;

— Complete the detection method and test it with real fouling deposit ;

This thesis project is enrolled at the Doctoral School Engineering Sciences (ED SPI 072) of Lille University Nord-de-France. Funding is provided by the Hauts-de-France region (50%) and the University of Valenciennes and Hainaut-Cambresis (UVHC) (50%). The work is carried out at the laboratory IEMN-DOAE (Institute of Electronics, Microelectronics and Nanotechnology - Department Opto-Acousto-Electronics) and in collaboration with the INRA-UMET-PIHM (Institut National de la Recherche Agronomique - Unité Matériaux Et Transformations - Equipe Inra Processus aux Interfaces et Hygiène des Matériaux).

In this manuscript, the current state of industrial production and detection techniques will be introduced in the first chapter. Industrial food production process and fouling cleaning techniques are discussed. The biofilm generated by bacteria is introduced as a special deposit. In addition, in order to study the biofilm deposit, the experimental preparation of biofilm is also explained. Then, recent methods of deposit detection in different field are briefly mentioned. The CWI method, as essential of this thesis, is detailed at the end of this chapter.

In chapter 2, the theoretical signal processing method will be introduced. In order to study the phenomenon of the fouling change on substrate, a simple multi-layer model is constructed. Several simulations have been realized with this model. A modeling of the propagation of the wave in this geometry is established in this chapter.

In chapters 3,4, three experimentations are presented. A measurement of a cleaning procedure with a piece of wax is detailed in chapter 3 to verify experimentally the feasibility of this method. The thickness of wax is controlled and the cleaning is carried out by a circulation of hot water. The second part of chapter 3 is a manipulation of a measurement on the protein deposition cleaning. The properties of protein fouling is prepared very close to the real dairy fouling in the food industry. The protein fouling is eliminated by sodium hydroxide solution. In chapter 4, biofilm formation is measured statically with a particular container. The biofilm is generated by a common bacteria (*Staphylococcus aureus*). The detail of this measurement will be presented.

At the end of the manuscript, the results obtained by this thesis are generally concluded. A perspective is given on the further works or the feasibility in other particular cases.

Chapitre 1

Context

1.1 Fouling : a major issue for different industrial sectors

Fouling is a problem for industry in many sectors [1], such as petrochemistry ; nuclear, naval and food industries. The appearance of such kind of undesired organic or mineral deposits leads to a decrease of performances of many equipments, especially the heat exchangers (reduction of heat transfer efficiency, increase in frequency of maintenance and cleaning operations, etc.). As example, Figure 1.1 shows a heat exchanger in a ship which is fouled by mineral deposit.

The economical cost due to the presence of fouling is far from being negligible.

In dairy industry, the fouling in heat exchangers and the associated cost of cleaning procedure account for 80% of the total production cost [2]. The cost of dealing with the fouling problem is also high in other industry sectors [3, 4].

Thus, a lot of studies are interested in understanding the underlying mechanisms behind the adhesion of deposit on a surface of equipment, especially for the heat exchangers. The formation of fouling is a complex phenomenon which is related to several factors, including the process parameters, the physico-chemical composition of the product which is in contact with the equipment surface, but also materials of the surface and its properties (roughness, surface energy...), etc.

So, it is clear that the fouling type is not the same in different industry sectors and

FIGURE 1.1 – Photo of fouled inner surfaces of tubular heat exchanger used in a ship (Navy Currents Winter 2015)

fouling growth is closely linked to the operating conditions.

Hygiene issue is also a major concern for certain industries, especially pharmaceutical and food sectors. Microbial contamination is the most common reason of hygiene issue in the production [5]. This problem can cause a serious consequence on the health of consumers. Food safety accident is not tolerable in food industry, which is our concern. The elimination of contamination is an essential step in the food production process and the best way to avoid contamination is to mitigate fouling.

1.1.1 Fouling in heat exchanger of dairy industries

Since the beginning of human civilization, fire, as a method of heat treatment, is used to improve the quality of food. With correct processing parameters, heat treatment is able to eliminate contamination without destroying the nutrients. The principle of this basic idea is still applied presently [6]. Heat treatment techniques are widely applied in the dairy industry, for example Pasteurization (Figure 1.2). The advantages of heat treatments are the guarantee of elimination of the majority of pathogenic microbial, without secondary

contamination and low cost of production.

FIGURE 1.2 – Pasteurization heat exchanger

Heat treatment techniques mainly used in the food industry is pasteurization and sterilization [7]. Most of the enzymes found in nature will be deactivated at a temperature higher than 60 °C. Microorganism can be destroyed by deactivating the enzymes. In the pasteurization, the temperature is around 70 - 80 °C and the process last for 15 - 20 s. The number of microbials could be effectively decreased with pasteurization. Sterilization is a strict heat treatment technique. The sterilization temperature is usually higher than 110 °C and it last for 2 - 5 s. Food products can be stored for long periods with the sterilization treatment.

Deposits is formed very frequently during heat treatment. Fouling in the equipment are always formed in an undesirable way [8, 9].

Other authors have proposed that in agriculture and food industry, the fouling could be classified into 3 types by their composition [10] :

— Organic fouling : Organic molecule is one of the essential component in dairy products, for example the protein. And it is common to have organic fouling in dairy production.

— Mineral fouling : Mineral component existed in water and products may adhere on surfaces, especially during heat treatment.

— Microbiology fouling : This kind of fouling is caused by the contamination of microorganisms.

In fact, in the real production, the industry have to face the combination of several fouling types [11, 12]. For example in dairy industry, both the protein (organic) and the calcium (mineral) in milk will take part in the fouling formation.

1.1.2 Importance of the French dairy sector and requirement to control fouling

As a motor of French economy, the dairy industry's exports in 2018 are 7 billion euros, while the total volume of business is about 30 billion euros. This sector provide more than 250,000 jobs in France, which contribute a lot to the social stability and prosperity. In fact, the agriculture and food sector (more than 11.5 billion euros) is the second largest contributor after the aeronautic industry (more than 22 billion euros) (Source : douanes 2011). In the agriculture sector, 13% product come from dairy industry. The value of dairy products in 2018 is about 8.7 billion euros (Source : La filiére laitière française). As the second producer in Europe and the 8th producer in the world (Eurostat, 2011 ; Agreste, 2011), 23.8 billion litres of milk is used to produce dairy product in France every year.

1.1.3 Importance of heat treatment for texturing and stabilization of dairy product

Heat exchanger is widely used in dairy industry. This kind of equipment is used in many production step, especially for the heat treatments, in order to guarantee the quality of product.

Different kinds of heat exchangers, in form of plate or tube, are used to achieve heat treatments (Figure 1.3). Nevertheless, heat treatments are not the perfect solution. In

many food production, for example the dairy industry, heat treatments will cause the formation of deposit on the inner surfaces of equipment [2, 13, 14].

FIGURE 1.3 – Deposit on inner surfaces of heat treatment equipment ; heat exchanger in form of plate (left) ; heat exchanger in form of tube (right)

In dairy industry, the product will always be heated at least once during the heat treatment. The mechanism of the heat exchanger is a transfer of heat. Certain liquid (which is usually water) with high temperature pass through the heat exchanger and transfer the heat to the product. In most of the case, the transfer procedure is achieve by a substrate between the two liquid. The fouling will then formed on the substrate surface because of the heat transfer.

1.1.4 Economic and environmental impact of dairy fouling

As introduced before, the pasteurization and sterilization treatment of milk will lead to the formation of fouling absolutely (Figure 1.2). The fouling problem in dairy industry is much more severe than other sectors (petrochemistry, nuclear industry, etc.).

The cleaning procedure is often automatic in the production line. In the petrochemical industry, equipment cleaning is at the frequency of once a year or less. On the other hand, the frequency of cleaning in the food industry is at least once per day [15], in order to satisfy the hygienic requirement strictly. In the food production line, a cleaning procedure lasts for a few hours. It means that the production time is notably decreased by the cleanings. For example, in the dairy industry 4 to 6 hours is used for cleaning the fouling every day.

Deposit has a significant influence on the production. It is able to damage the heat

transmission, weaken the pumpability, increase the production loss [16]. The thermal conductivity of fouling is rather low. The thermal conductivity of steel, which is a common material of substrate in heat exchangers, is about 16 $Wm^{-1}K^{-1}$, while the thermal conductivities of mineral fouling ($CaCO_3$,$CaPO_4$) and protein fouling are about 3 $Wm^{-1}K^{-1}$ and 0.1-0.5 $Wm^{-1}K^{-1}$ [17]. So, the presence of deposit on the inner wall of heat exchanger will reduce the heat transfer efficiency of the heat treatment.

The fouling could also cause a reduction of flow. The section inside the heat exchanger will absolutely decrease when deposit is formed. Consequently, there will be an increase of pressure drop in the heat exchanger [18]. In this case, the design of heat exchangers needs to be oversized by $70\% - 80\%$ in order to meet the requirement of the heat transfer efficiency. Nevertheless, $30\% - 50\%$ of the additional size is consumed by fouling [2]. Besides, the fouling will also lead to hygienic risks of the product. The microorganism in deposit could contaminate the product [19].

Since it is difficult to avoid the formation of fouling deposit, cleaning is a widely used solution in the industry to keep the products in good quality. The cleaning of deposit needs to be applied scrupulously. If the cleaning is incomplete somewhere, the contamination of microorganism will still exist [20]. However, the industrial production has to be stopped during cleaning procedure. The cost of operations for dealing with fouling and the time loss of production should also be regarded as additional cost of production.

The precise number of economy loss caused by fouling is difficult to be determined, but the magnitude could be deduced. About several billion euros every year is lost because of fouling [21]. Some authors have concluded that the fouling cost caused by fouling is between 0.15 and 0.3 % of GNP (France, US, UK, Japan, Germany, Australian, New Zealand) [13, 21, 22].

In general, considering these information, the fouling leads to a tremendous economic loss every year.

1.1.5 Dairy composition and its fouling

As presented in Table 1.1, milk is a complex biological fluid, containing numerous of thermally unstable components (protein, mineral, fat, etc.). Among these components, the whey protein is the major material for fouling, especially the β-lg.

Component	**Quantity in Milk (%)**
Water	87.6
Protein Total	3.3
Caseins	2.5
Whey Protein (β-lactoglobulin)	0.3
Whey Protein (α-lactalbumin)	0.07
Fat	3.8
Carbohydrate	4.7
Na	0.050
K	0.150
Ca	0.120
Mg	0.012
P	0.095
Fe	0.00005
Cu	0.00002
Zn	0.00035
S	0.030
Cl	0.095

TABLE 1.1 – Chemical composition and the concentration of milk [23]

The dairy fouling can be classified into two type. The first type, known as Type A, is formed at lower temperatures ($75 - 110°C$). In this case, the fouling deposit consists of denatured and unfolded whey protein. The deposits of this type are usually white, soft and spongy. The deposits consist of 50 to 70% protein, 30 to 40% minerals and 4 to 8% fats.

The other type of dairy fouling, known as Type B, is formed at high temperature ($> 110°C$) containing noticeably mineral compositions, especially calcium phosphates [15]. The deposits of Type B are usually hard, brittle, granular and grey. The deposits consist of 70 to 80% minerals (mostly calcium phosphate), 15 to 20% protein and 4 to 8% fats.

There are lots of differences in fouling growth whether dairy protein solution contains casein or not. Whey protein solution are free of casein.

1.1.6 Fouling mechanisms

The mechanisms of fouling are complicated involving chemical reactions and physical parameters (momentum, heat and mass) [15]. Some processes which are involved in the fouling formation are listed [21] :

1. Reactions inside the product which make some of its constituents capable to be deposit
2. Transportation of those foulant constituents to the surface
3. Attachment of some foulant material on the surface to form an initial fouling layer
4. Removal of the fouling deposit (spalling or sloughing of the deposit layer)
5. Transport from the deposit-fluid interface to the bulk of the fluid

The first stage is before the appearance of fouling. The two major underlying destabilizing mechanisms inducing fouling during heat treatment of milk-based product (whey, milk, solutions of inorganic ions with milk proteins) are the formation of activated β-lg protein molecules due to heat denaturation and the precipitation of salts (calcium, calcium phosphate or calcium phosphate-lipoprotein complexes) contained in the fouling solution. Salts precipitation and denaturation can directly occur on the hot layer in the vicinity of stainless steel wall surface or in the bulk of the solution due to the increase of temperature and the 'reverse solubility' of salts. The period of this stage depends on temperature, flow velocity, fouling composition and surface conditions.

The mechanisms involved in the second stage (transportation of foulant material) are variety. Some possible mechanisms are : Diffusion, Electrophoresis, Thermophoresis, Diffusiophoresis, Sedimentation, Inertial impaction, Turbulent downsweeps.

The mechanisms involved in the third stage consist of physical and chemical processes. An overview of the heat-induced fouling mechanisms of whey or milk can be schematically addressed [2, 15, 24].

Upon heating, active molecules β-lg proteins are generated on the hot surface of the stainless steel wall of the PHE or in the bulk of the fouling fluids. The former stick on the hot surface to constitute a first fouling layer while the latter form aggregate in the bulk or contribute to the build-up of deposit [25, 26] after being transported to the surface. Simultaneously, under the increase of temperature, the calcium complexing substances

precipitate calcium salts (calcium, calcium phosphate or calcium phosphate-lipoprotein complexes). These solid calcium-based elements are susceptible to provide a link with heat denaturated β-lg protein molecules (β-lg alone or aggregated to β-casein of milk micelles) forming stable co-precipitates with the protein and accelerating the growth of the fouling layer.

In milk, it is likely that calcium phosphates are the solid calcium-based elements agent, linking the heat denaturated β-lg protein molecules. Indeed, for temperatures around 80 °C, Sadeghinezhad et al. [27] observed an open interconnected calcium phosphate-protein network (see also Andritsos et al., 2002 [28]). The interaction calcium phosphate-protein might involve phosphoserine groups in milk caseins [24].

For whey protein solutions, ionic calcium is supposed to be the linking agent since calcium phosphate concentration are not expected to be as much important as with casein-based products.

The interaction calcium-protein might be done through carboxylate groups of soluble proteins (aspartate, glutamate) [24].

The 3 most important factors for the attachment stage are surface conditions, surface forces and sticking probability.

The removal of fouling deposit is possible to happen at the same time of fouling deposition. The mechanisms of this stage are shear forces, turbulent bursts, re-solution and erosion.

Once there is a sloughing of deposit, the sloughed part of deposit may be transported from the deposit-fluid interface to the bulk of the fluid. But if the sloughed piece is large enough, it may moved and adhere on other surface in the system. The sloughing of deposit depends on the age of fouling.

These stages could be classified as deposition process (the first 3 stages) and removal process (the last 2 stages). The rate of deposition growth could be regarded as the difference between the deposition rate (Φ_d) and the removal rate (Φ_r) (equation (1.1))

$$R_f = \Phi_d - \Phi_r \tag{1.1}$$

1.1.7 Factors affecting fouling formation

The fouling formation is a very complicated process. It could be influenced significantly by the operating conditions (process parameters-flow and heat transfer, geometry, surface, ..) and the physico-chemical properties of product (dairy derivative).

a) Geometry, wall surface properties and process parameters in the heating zone

The geometry of heat exchanger is a significant factor that influence the fouling formation. In stagnation parts, like the connections of equipment or branch of pipeline, there are usually more fouling than other parts [29].

The condition of the surface which contact with product is another factor to the fouling formation. The fouling formation happens more easily on rough surfaces than smooth surfaces [30, 31]. But, the roughness will not influence the fouling formation any more if the formation of first fouling layer is complete [31, 32].

Flow of product will also influence the fouling formation. Even through fouling could not be avoid by changing the flow, but rising the flow velocity could decrease the formation of deposit [30, 33].

b) Dairy derivative properties

The properties of dairy derivative itself is essential for the fouling formation. Accordingly, even though a general dairy fouling mechanism can be proposed involving interaction between heat denatured protein and calcium compounds, it appears clearly that the fouling mechanisms are strongly different, depending whether the derivative milk-based product (whey, milk, ...) contains casein micelles or not. Indeed, the presence of casein micelles reduces the opportunities of foulant intermediate (activated β-lg protein molecules and calcium phosphate) to feed the fouling layer by allowing on one hand calcium phosphate to insolubilize in casein micelles (as Micellar Calcium Phosphate) and on the other hand enable activated β-lg protein to aggregate on casein micelles surface on heating. In other words, presence of casein micelles increases the stability of milk-based product in regard the growth of the fouling mass deposit on the surface of PHE.

Milk, which is the common product in dairy industry, is proposed here as an example. The nature pH value of milk is about 6.7 ± 0.1 at 20°. If the pH of milk is smaller than the interval, the fouling rate will increase [31, 34].

The milk age has a special influence on the fouling. If the milk is conserved for 12-24 hours before heat treatment, the fouling formation could be reduced [35]. This phenomenon is considered as the consequence of lipoclasis of fat in milk [36]. However, if the period of conservation before heat treatment is longer than 24 hours, the fouling rate will increase [37]. The increase may be caused by the appearance of enzymes produced by psychrotrophic bacterium [38].

Milk is a complex liquid and the composition is not stable.There are always natural variations caused buy climate, age of cow, location etc. This composition variation could also change the fouling formation process [39].

There is always gases (air) dissolved in milk before heat treatment. When heating the milk, the dissolved air will be separated from milk. Air bubbles will appeared on the surface of heat exchanger if the pressure is low [40]. The dissolved air itself do not influence the fouling formation, but the air bubbles on the heat exchanger surface will behave as the core of deposit and increase the fouling rate [35, 40, 41].

c) Preheating

It has been demonstrated that a preheating treatment could reduce the fouling formation effectively [42]. With a higher temperature of preheating, the reduction of fouling formation is more significant. The principal of preheating treatment is the denaturation of whey protein [43].

1.2 Biofilm formation in dairy industries

The biofilm structure is lively and dynamic. Pathogenic bacteria exist widely in nature (in animals, plants, etc.). Nevertheless, the presence of biofilm is not indubitable with the existence of bacterium. In food and dairy industry, the contamination of pathogenic bacteria will always lead to the hygienic problems in product. Naturally, the bacteria have tendency to adhere on surfaces and to form a complex structure, which is known as

a layer of biofilm. The contamination could happen in any step of industrial production. The Center for Disease Control (CDC) mentioned that there are 48 million medical case of illness in the USA every year. The biofilm could also lead to the contamination of medical instruments. There are 3.2 million cases of healthcare-associated infections (HAIs) in Europe per year [44].

1.2.1 Economic, environmental and health impact of biofilm formation on processing surfaces

Biofilm is able to help the bacteria surviving in unsuitable environment. This characteristic leads to intractable problems in many sectors. Recently, studies in the medical field have shown that bacterial biofilms are the reason for some chronic and refractory diseases [45]. Antibiotics are widely used in the medical field. Unfortunately, biofilms have the inherent resistance for the antibiotic and host immunity [46, 47]. Biofilm infections are difficult to be cured by antibiotic or immunity [48]. Problems caused by biofilm exist in many industries (water system industry, medical industry, etc.). In addition, biofilms can reduce the quality of drinking water [49].

In food industry, some studies have mentioned that the meat product, seafood product and dairy food product were found to be contaminated by bacteria [50, 51, 52]. Even the retail raw chicken sample was found to be contaminated by *S. aureus* (a kind of common pathogenic bacteria) in China [53].

The contamination source in food industry is variety. It could be water, dust, equipment, crude materials, food handlers, etc. Sharma and Anand have stated the persistence of biofilms on pasteurization lines of commercial plants [54]. Since the adhesion of biofilm is rather persistent, a completely formed biofilm on food contact surfaces could play a role of continuous contamination source. The biofilm is now known as the major contamination source of food product contaminations. It has been enumerated that most of the food contact surfaces (including dairy, meat and seafood sectors) were contaminated by biofilms [55, 56].

All these studies lead to a fact that the food sector provide a suitable environment for the development of biofilm. The food safety will then be challenged, and the public hygienic risks will be increased.

Presently, bacterial contamination and biofilm formation is difficult to be avoided [57, 58, 59]. Monitoring the appearance of the biofilm is always an essential insurance for industrial production and public hygiene. Once a layer of biofilm is formed on a surface, a biofilm elimination treatment is needed to avoid the influence. In this case, research on biofilm cleaning technology is important [60], and online biofilm monitoring is needed for research and characterization of microorganisms [61].

1.2.2 Mechanisms of biofilm formation

Biofilms are communities of microorganisms adhering to an inert or living surface (Figure 1.4). They are structured by cells and enclosed by extracellular macromolecules [62].

FIGURE 1.4 – Bacterial biofilm on a stainless steel substrate

Bacterial contamination on the surface is the prerequisite of a presence of the biofilm. A favorable microenvironment for bacteria on the surface can encourage biofilm formation [63]. The 3 essential conditions of the biofilm formation are : the existence of bacterial cell, the adhesion of bacteria on the surface and the medium around the surface [64]. The growing of biofilms is not even on the surface. The formation of biofilm includes 4 phases [65][66] :

— Adhesion of bacteria on surface

— Formation and growth of microcolonies

— Biofilm maturation

— Dispersion

If the environment on the surface is changed and the bacteria can not adapt to the new environment (such as a change in temperature or pH of the surface), the bacteria can no longer be alive and the biofilm will be detached from the surface. If the environment is still favorable for bacteria, microbial dispersion occurs after the maturation phase [67]. This dispersion will causes new contaminations at other surfaces.

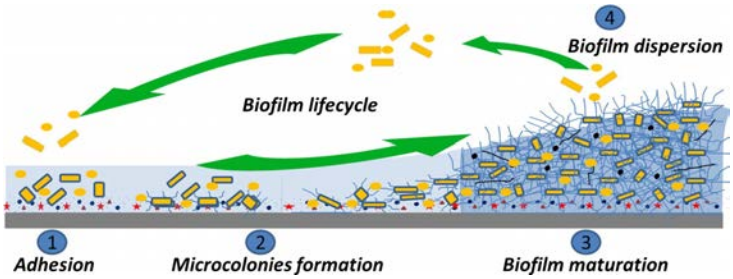

FIGURE 1.5 – 4 biofilm formation steps [65]

a) Microbial adhesion

The adhesion of bacteria is the origin of biofilm (Figure 1.5). The biofilm formation is always started by this step. The adhesion of bacteria is a reversible process and can be influenced by physical, chemical or biological interactions [68]. Once the bacterial cell is closed to a surface of interest, the cell will be given physiochemical forces which help the bacterial cell to achieve the adhesion on the surface [69]. Many studies have shown that the bacteria is able to sense the abiotic surface by the appendages to confirm that if the surface is suitable for the biofilm formation [70]. If there is a surface of interest, the appendages could contribute on the bacterial adhesion [71]. Environmental parameters, such as temperature and pH, are also the factors which influence the bacterial adhesion.

b) Bacterial growth and matrices production

While the adhesion step is complete, the bacterial cells will start to grow into microcolonies. At this step, exopolymeric substances will be secreted to form biofilm matrix. This

is a extracellular matrix that consists of polymeric compounds [72]. The extracellular matrix gives cells the ability to aggregate together and stick tightly to the surface [73]. Then the biofilm formation become irreversible. The biofilm development tends to mature as the bacterial cells are encased and protected in an extracellular matrix, which also offer a stable structure for the biofilm [74]. These exopolymers in biofilm play an important role in the resistance of biofilm to antimicrobial agents by stopping the biocides penetration.

It has been verified that the formation of biofilm is also related to some environmental parameters, such as temperature and nutrient. Bacteria are able to sense those parameters and modulate the formation of biofilm [70]. Besides, the communication between the cells and the quorum sensing could also regulate the biofilm formation [75].

c) Biofilm maturation and Dispersion

After the extracellular matrix is formed completely, the biofilm is considered to be mature. Sessile cells start to leave the biofilm structure and contaminate other surfaces. For the whole lifecycle of biofilm, the important factors that influence these biofilm formation steps could be classified into 2 categories : the species of pathogenic bacteria (*S. aureus*, *P. aeruginosa*, etc.) and environmental conditions (temperature, nutrient, pH, oxygen, surface, etc.).

1.3 Cleaning of deposit

The influence of fouling and biofilm has been detailed in the sections before. The growth of fouling will lead to hygienic problems and consumers complain. Thus, the production is interrupted regularly to clean the fouling deposit.

Fryer and Asteriadou (2009) have defined 3 wide ranges of fouling deposit and the cleaning methods [76] :

— Viscoelastic fluids : These kind of deposit could be easily removed by water

— Microbial films and gel-like layers : Chemical agent is needed to be used with water

— Solid-like deposit formed during thermal treatment : Chemical agent is indispensable and the chose of chemical agent should consider the nature of deposit.

A large number of techniques are brought out for the cleaning of fouling in heat treatment devices [77]. Cleaning technology is classified into two categories, offline cleaning and online cleaning. In offline cleaning, it is unavoidable to disassemble the heat exchangers. The cleaning is carried out either by the chemical agent or by mechanical sollicitations [17]. After cleaning all the components of the exchangers, the reinstallation of the devices is executed in order to continue producing procedure. The result of offline cleanings is obvious and easy to monitor. However, disassembly and reinstallation of heat exchangers is always with a large time consuming and complicated operations. The off-line cleanings result in a significant increase in the cost of production. Consequently, the use of offline cleaning is limited and is not the current practice in industry.

Disassembly and reinstallation is not necessary to the cleaning-in-place (CIP) methods [78]. Production costs could be extremely reduced. So, online cleaning is widely used in the industry. CIP has been widely applied for the last 50 years in dairy industry. The principle of CIP is to apply a circulation of water or chemical agent to the equipment for a certain time, which depends on the fouling properties and equipment [79]. For example, alkaline solution could be used to remove milk fouling.

The alkaline solution is able to break up protein and make it dissolved into water. However, dairy fouling is usually a complex mixture of protein and mineral components. After the circulation of alkaline solution, the mineral deposit will still stay on the surfaces. So, more than one chemical solution is needed for the cleaning procedure. In this case, acid is used to remove the mineral part of fouling in the dairy deposit so that the cleaning of fouling could be complete [80]. In addition, sequestering and wetting agents have the function of amplifying the cleaning efficiency of alkaline solution [81].

In the most simple cleaning, single-stage cleaning, there are usually 3 steps : (1) rinsing ; (2) cleaning ; (3)rinsing, while for the two-stage cleaning there are 5 steps : (1) rinsing ; (2) alkali cleaning ; (3) rinsing ; (4) acid cleaning ; (5) rinsing [82].

1.3.1 Cleaning mechanisms of dairy deposits and biofilms

The dairy product has a great number of consumers all over the world. It is necessary to increase cleaning efficiency as much as possible. The dairy fouling that appeared in heat exchangers is usually with strong adhesive to the equipment surfaces. Then the study of

cleaning mechanism can make important contribution to the development of cleaning.

There are usually 3 stages in the cleaning of dairy fouling [83]. The first stage is swelling . As the initial stage of cleaning, only the top layer of fouling deposit is contacted with alkaline solution. The deposit starts swelling and the top layer will be removed. The cleaning rate increases at this stage. The next stage is erosion. In this stage, most of the remaining deposit will break up and be removed. The cleaning rate will meet its maximum during this stage. The final stage is removing of mineral deposit. After the protein is all removed by alkaline solution, the mineral layer will be cleaned by acid.

1.3.2 Factors affecting cleaning

Mechanistic studies state that the cleaning of dairy fouling is influenced by the factors such as temperature, chemical agent concentration [83]. Temperature could modify the solubility of circulation fluid and the chemical reactions rate. These will extremely change the efficiency of cleaning process. It has been found that the increasing of temperature could increase the penetration velocity of the NaOH [84].

It has been indicated that the cleaning is strongly influenced by choice of cleaning agent [85]. For example, sodium hydroxide has an impressive efficiency on cleaning of dairy fouling. The concentration of chemical agent is also an important parameter for the cleaning efficiency. Using concentrated sodium hydroxide solutions in the cleaning of whey protein fouling will reduce the cleaning rate [86]. The optimum concentration of sodium hydroxide is found to be 0.5 $wt\%$ at 50 $^{\circ}C$ [87].

Another important factor for cleaning is mechanical action. This factor is essential for removing loosened parts of deposit and break large deposit bulk into small pieces [83]. The mechanical action is related to the flow velocity, surface shear stress, etc. To remove a piece of the deposit by mechanical action, fluid shear forces need to be more than the adhesion and cohesive forces of the deposit. Timperley and Smeulders showed that the cleaning time of a deposit in a plate heat exchanger decreased with increasing flow velocity [82]. The shortest cleaning time is observed when the flow velocity increase from 0.2 to 0.5 m/s.

1.3.3 Environmental footprint of cleaning

Industrial heat exchangers are always made of opaque materials. As a result, cleaning progress is difficult to monitor and no optical method is possible to apply to online detection in heat exchangers.

Recently, society and governments are paying more and more attention to the protection of environment. Sustainable development is significantly considered in industrial production. Consumers concern a lot about the influence of industry on the environment. Unfortunately, the chemical agents used in the cleaning of the fouling cause significant environmental impact (such as the alkaline solution or the acid solution). In addition, large amount of water is used in the cleaning operation, and a certain amount of water is sent directly to the purification device. By neglecting the type and size of equipment, about 0.5 to 5 L of water is wasted for every liter of milk production [88, 89]. Majority of production cost (80%) is related to fouling of deposit and cleaning in the dairy industry [90].

Thus, research to improve cleaning efficiency is needed by the industry to reduce the cost of production. It is difficult to improve the technology of cleaning, and chemical agents are always indispensable. In industry, the cleaning procedure is rarely optimized [20]. In daily cleanings, some amount of water and chemical agent is wasted because of the uncertainty of fouling state on the inner surface of equipment. So real-time information of deposit is needed to reduce the waste in the cleaning process.

As introduced before, the formation of deposit on the inner surfaces of devices depends on numerous factors in online production. So, in order to deal with this problem, a real-time monitoring and cleaning of fouling is a proper solution. With a detection system, the presence of fouling on the inner surfaces could be known immediately. The cleaning time can be determined more favorably. The deposit information is also obtained by the detections. In the cleaning procedure, the cleaning method (using either chemical agent or water pressure) can be optimized. The accurate time for achieving the elimination of all the deposit could be also precisely quantified. Thus, the moment to stop the cleaning can be more precise and the waste can be reduced. The technology of monitoring fouling deposition and cleaning is the key to the reduction of cleaning cost.

1.4 Monitoring of surface fouling factor and cleaning endpoint

In the previous sections, the need of detection and monitoring on fouling deposit in closed equipment and cleaning procedure is introduced. For all cleaning methods, on-line or off-line, a proper fouling monitoring of a specific situation will result in the reduction of operating time, chemical agent consuming and industrial effluents [78]. Current detection methods are based on the principle of different fields (mechanics, electronics, acoustics, etc). These detection techniques can be classified by direct method and indirect method.

1.4.1 Direct methods - off-line detection techniques

The direct methods of deposit detection are mainly in the mechanical and optical domains. The thickness and the mass of deposit are the classic parameters used by the direct methods. Dos Santos et al. have used the section projection of the deposit to detect the thickness of biofilm [91]. There are also other direct methods and tools proposed for the detection of fouling thickness [92, 93].

The thickness is not a parameter which contains all the information in the sample. The detection on the mass of fouling is also useful. As the deposit mass is largely affected by the moisture of sample [94], most of the measurement of fouling is performed by weighing the dried deposit [95, 96, 97, 98, 99, 100, 101, 102].

There are also some methods for evaluating fouling other than the detection on mass or thickness [25, 103, 104, 105]. But all the direct methods are more or less invasive. A probe contacted with the sample is often necessary for the detection system. Even if the optical probe does not need to touch the sample, a transparent medium between the probe and the sample is always required. Therefore, disassembly and reassembly of the equipment is necessary for every measurement. For this reason, the use of direct methods is limited to off-line detections. In on-line detections, for example real tubular or plate heat exchangers, these methods can not be applied.

1.4.2 Indirect methods

Indirect detection methods are usually used for CIP. It is widely recognized that CIP could be rationalized by the use of sensors and rational indicators, to reduce operating time and the volume and load of effluents [106]. But an effective monitoring method to validate the cleaning end-point is still a challenge. Then, many studies of fouling detection in CIP systems have been in progress for the past 40 years. A large number of detection techniques have been developed on the basis of knowledge in thermology, optics, acoustic, electrics and hydromechanics. However, there is rarely a significant breakthrough in CIP systems.

Among the indirect detection methods in all the fields, the techniques based on thermal performance are widely applied in the food industry. As presented in the section above, heat treatment is widely used in the food industry, and deposit is very common due to heat treatment. Thus, measuring the thermal parameters is also the main monitoring method in this field. Recently, acoustic methods for detection and monitoring have been developed. More and more acoustic techniques are being used in different fields of detection non-destructive. Acoustic detection techniques have the advantages of non-contact, non-invasive and these techniques could adapt majority of installation requirements. Including the detection methods in other fields, these different techniques are detailed below.

a) Non-acoustic methods

At first, some detection techniques without using acoustic theory will be introduce in this part. As indirect methods, classic physical parameters of fouling, such as mass and thickness, will not be measured directly. In this case, some other physical parameters are used as indicators of fouling.

In hydrodynamics, a modification of cross-section surface at a part of tunnel will result in a pressure change at the outlet. Actually,the input and output pressure of heat exchangers (P_{in} and P_{out}) is measured regularly during the production. When fouling is appeared and increased on the inner surface of equipment, the decrease of mean square area in a flow channel will lead to a pressure drop ($\Delta P = P_{in} - P_{out}$) at constant flow rate. This method can often be used with other systems such as artificial neural network (ANN) [107] or mass and heat transfer measurement [108]. Even though there are still

other needs for the measurement of inlet and outlet pressure, the capacity of pressure drop on fouling detection is not impressive. With this method, the sensitivity is not good for thin layer and the location of fouling cannot be detected.

Since the heat exchanger, in which the fouling is formed frequently, is used for a thermal treatment, the monitoring of temperature is definitely executed all the time, especially the inlet and outlet temperature. The measurement of temperature is applied on the product (inlet or outlet) in order to control the status of production. Just like the pressure drop phenomenon, the outlet temperature is also influenced by the fouling. Assuming that the inlet temperature and thermal treatment power is constant, with the presence of fouling, the outlet temperature will decrease. This detection method is similar to the pressure drop. Obviously, it has the same drawback as pressure drop : low sensitivity and no information of fouling location. And this method is usually used with other systems [109, 110, 107, 111, 112].

Another thermal parameter called heat transfer coefficient (U) is widely used for the industrial fouling detection. This parameter is defined as : $U = \frac{Q}{A\Delta T_{LM}}$, where Q is the heat transfer rate between hot and Cole fluid, A is the contact area between heat exchanger and fluid, the ΔT_{LM} is the log-mean temperature difference calculated from the inlet and outlet temperatures. This coefficient (U) represents the capacity of thermal treatment with a certain heating medium. The heat transfer coefficient depends on the heat quantity received in product and the heat contributed by heating medium. Practically, heat transfer coefficient can be monitoring indirectly by measuring the mass flow rate of product and temperature difference between heating medium and product.

The presence of fouling, as an additional layer on the substrate surface of heat exchanger, will inevitably modify the heat transfer coefficient. This modification is considered as an extra heat flux resistance. The additional heat flux resistance is related to the fouling thickness and its thermal conductivity. Thus, comparing the heat transfer coefficient of arbitrary heat exchanger states with the heat transfer coefficient of a clean heat exchanger could determine the presence of fouling [113]. These measurements can also used with numerical simulations for further treatment [114].

The disadvantage of heat flux measurement is that bulk temperature, which is measured by intrusive sensors, is always needed. Besides, it is hard to achieve a high precision because of the difficulties in calibration.

Electrical parameters are also possible to be used in some particular cases. Electrical resistance and conductivity are the parameters most used in the detection. Chen et al. have achieved a relation between electrical resistance and thermal resistance [115]. Ayadi et al. have found out that the fouling will increase the electrical resistance and lead to energy dissipation [116]. The electrical conductivity is also dependent on the current fouling state. By monitoring these parameters, the fouling thickness can be determined [117]. This is a sensitive detection technique. However, in order to use this detection method, it is indispensable to install electrodes with invasive means. Some parameters like consumed electrical power can only measured when using an electrical heating device for thermal treatment. With these limitation, electrical parameter is difficult to apply on industrial production.

Fluid Dynamic Gauging (FDG) is an accurate and cheap detection method [118, 119]. The principle of this method is to use the flow rate of certain liquid to determine the fouling thickness. Suppose that there is a sample of a plan surface with or without deposit on it. A nozzle is placed vertically toward the surface (Figure 1.6). The size of nozzle is fixed. A kind of steady fluid (usually a kind of proper liquid) is filled on the surface. Then, because of the hydrostatic principles, a suction flow of fluid will go through the nozzle by a siphon tube connected to the tail of nozzle.

The flow rate of the suction flow in the nozzle is related to the diameter of nozzle (d_t) and the distance between the nozzle and the surface (h). Since the diameter of nozzle is controlled, the distance between the nozzle and the surface can be monitored by measuring the flow rate. With knowing the distance of clean surface, the thickness of deposit could be determined. Nevertheless, the nozzle should be placed at the same side of fouling surface and close enough to the surface in order to keep the sensitivity.

b) Classic acoustic methods

Acoustic methods are widely used for many detection sectors (imaging, damage evaluating, etc.). For a particular case as the fouling detection of sealed equipment, the ultrasonic sensor [121] is installed on the outside surface of substrate to detect the fouling on the other side (process side). Acoustic parameters change when fouling occurs and can be measured in transmission (one transducer as sender, one as receiver) and in pulse-echo mode (one transducer as sender and receiver). Since the acoustic properties of fouling

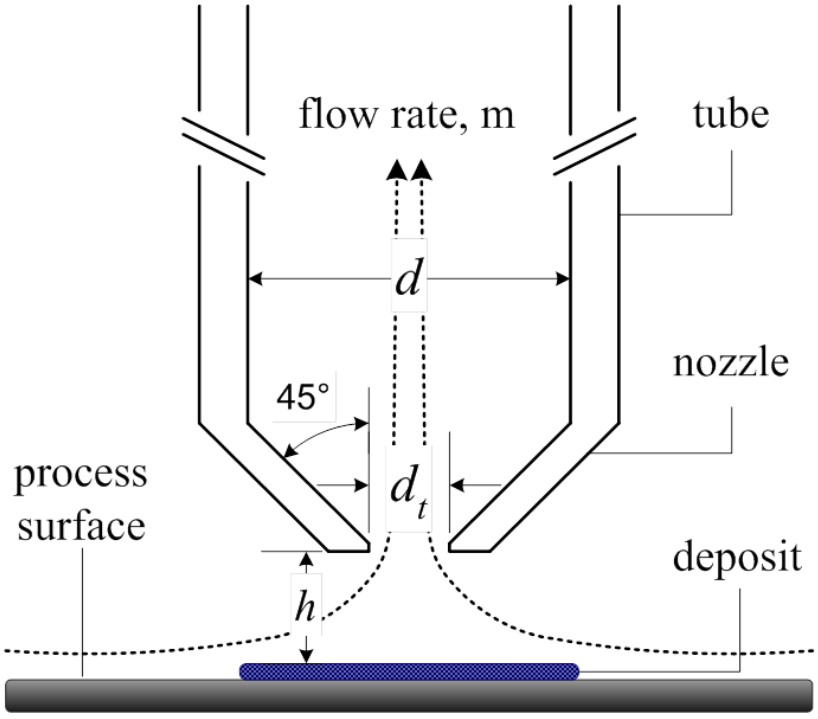

FIGURE 1.6 – Schematic of Fluid Dynamic Gauging [120]

deposit are different from processed liquid, the appearance of fouling deposit will change the characteristic acoustic impedance of the medium, such as the time of flight, the reflection coefficient at an interface. Echo energy is also another physical variable which changes when fouling develops due to changing reflection/transmission and attenuation coefficients. Thus, damping and signal attenuation can be also used. The indicator of fouling deposition could be obtained from these parameter changes [7]. Collier et al. have successfully used reflection coefficient for determining the fouling adhesion on a substrate. It is considered as a case of multi-layer (Figure 1.7). At each interface, the acoustic wave will be divided into transmission wave and reflection wave. Every reflection at an interface gives an echo in received signal. With different adhesion at the interface fouling-substrate, the reflection coefficient will also be different. This difference will be embodied by echoes in the signals [122]. However, few information of fouling layer itself could be obtained by reflection coefficient.

Ultrasound tests can be classified into two groups, those based on vibration resonance [123] and those based on ultrasound propagation. Ultrasonic guided waves have a good

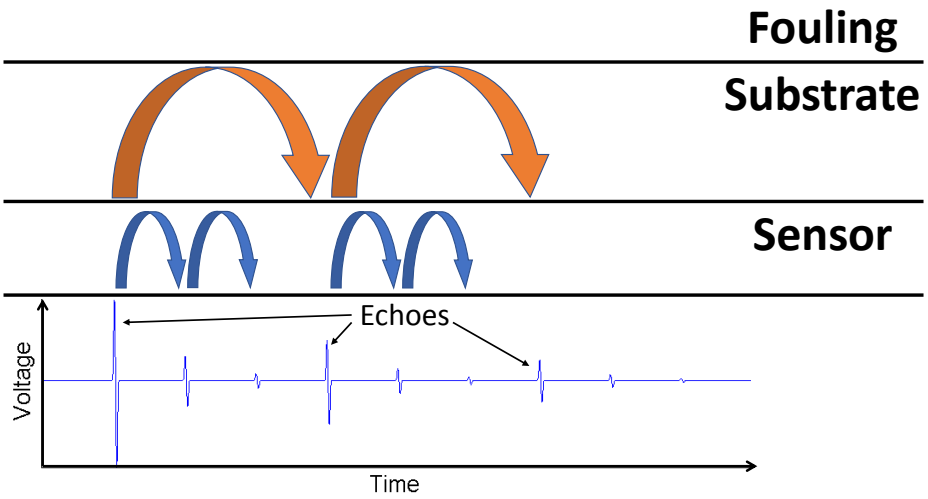

FIGURE 1.7 – Using reflection coefficient to detect the adhesion of fouling on substrate

effect of fouling detection in a pipe [124, 125, 126]. However, very low frequency is needed to adapt to the equipment and test specimen. In that case, small magnitude of deposit is hard to detect. Concerning ultrasound propagation-based tests, ultrasonic guided wave methods [125, 126] and acoustic impact techniques [127, 128, 129] have been mainly used to detect fouling formation. Acoustic impact techniques usually use a pulse signal as an excitation source to the sample and observe the performance of the reception signal. Among acoustic impact techniques, Mechatronic Surface Sensor (MSS) is developed to monitor deposit inside a pipe, using the vibration properties of surface waves, such as amplitude and damping factor [128, 129]. These methods are still not very sensitive, especially for thin layer. The decay of the echo energy is also used to detect the fouling. This method is able to detect the present of layers of $800\mu m$, but the irregular in fouling, like uneven fouling surface, could raise the error of results.

1.4.3 Monitoring fouling : still a challenge

As presented in Table 1.2, there is no difficulty to achieve an accurate, cheap off-line detection. But in order to adapt the CIP systems, on-line detection techniques are indispensable. According to the survey of available on-line methods for monitoring fouling

factor, most of the common drawbacks of the existing tools are : the reliability, the significance and easiness of interpretation of the information contained in the indicator (if it is a local or global fouling factor, representing several certain properties of local fouling layer or concluding the whole state of fouling deposit in the heat exchanger), sensitivity to thin layer detection, invasiveness, duration for establishing the fouling diagnosis, computational load for being easily included in any supervision software, easiness of device for measuring fouling factor including set-up, tuning and maintenance stages, robustness, economic cost...

So many points have to be considered when developing a detection method. It is hard to find a perfect way satisfying all the concerns. Definitely, some requests could be compromised within specific ranges (device set-up, economic cost,...). But there are still limitations which should be fully obeyed (reliability,invasiveness,...). The detection of local thin deposit and tiny change of the deposit in real time is still a challenge to be achieved [108][130]. Some methods are not sensitive enough to describe a small change occurred at the interface and others need special conditions or equipment which is not always compatible with actual applications.

In industry, it is essential to have a non-invasive, on line, fast, reliable, robust and not expensive method for fouling factor monitoring. It is also vital that the analyzing and signal processing systems are simple and that the sensitivity of fouling detection methods is high. Unfortunately, at the state of the art this is not the case and consequently, most of the time cleaning cycles are conducted in an unsupervised manner. Currently, industrial CIP procedures rely on practical experience with excessive safety margins in terms of duration and environmental footprint, but this situation is no longer acceptable. Some tools have to be proposed to enable on-line diagnosis of the fouling factor for helping in the decision process and revisiting cleaning sequences on the basis of rational knowledge.

One major constrain is to avoid placing fouling sensors on process side (at the bulk or at the inner surfaces of heat exchanger in contact with the processed fluid). Indeed, industrials are often reluctant to use sensors directly in contact with the processed products since sensors could induce additional hygienic problems and false fouling detection, which should be definitively avoided in the food industry. Moreover, embedded sensors would not have a long service life with such on-line severe operating conditions (temperature, shear stress due to flow rate, chemical agent..), which add extremely the difficulty to the

maintenance operation.

Equipment in industrial production is often sealed and isolated. These industrial devices are also made by opaque materials. There is no light path that could reach the fouling deposit inside the equipment. Consequently, any optical methods is impossible to be applied directly in this case. Then, acoustic methods, as another type technology frequently used in detection, have a good potential in overcoming the difficulties in food industry. The current acoustic detection methods have already satisfied most of the requests above. The major challenge is to increase the sensitivity so that thin layers could be also detected.

1.5 Generality on coda wave and CWI (Coda Wave Interferometry)

Acoustic waves in solid can be classified into 2 types, longitudinal waves (the propagation direction of wave is the same as the oscillation) and transverse waves (the propagation direction of wave is perpendicular to the oscillation). In non-viscous fluid medium, transverse waves cannot propagate and only longitudinal waves exist. Like optical waves and electromagnetic waves, the propagation of acoustic waves depends on the medium. In common solid medium (which is not always transparent), the propagation of acoustic waves is much more applicable than optical waves and electromagnetic waves. This makes the acoustic technology the best detection method in solid structure.

1.5.1 Acoustic wave propagation

The acoustic field of the fouling monitoring in industrial applications could be simplified into a model of two layers as in Figure 1.8. Substrate represents the wall of equipment in contact with fouling. Acoustic sources and sensors are installed at the other surface of substrate.

During the acoustic monitoring, the source will send acoustic waves into the substrate. Then the acoustic waves start to propagate in the acoustic field (substrate, deposit, etc.). Each time the acoustic waves meet an interface, there will be a part of energy pass through the interface and the other part of energy reflect by the interface. In this model, since

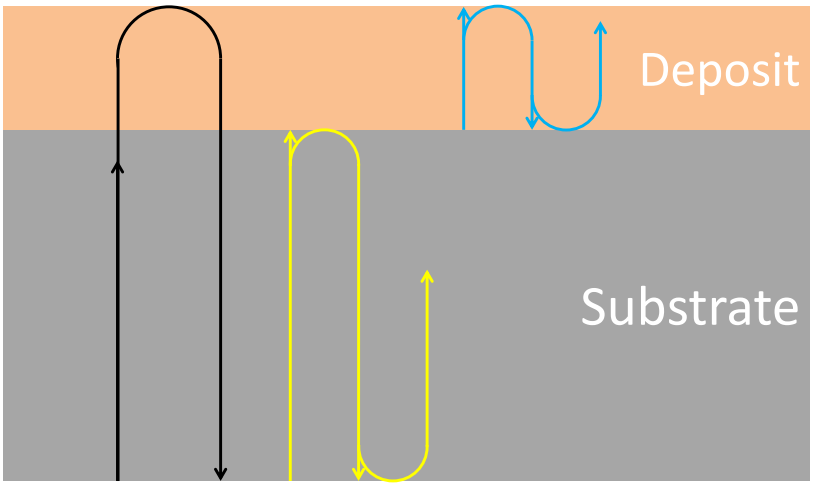

FIGURE 1.8 – Schema of wave propagation in an acoustic field substrate-deposit

the acoustic waves are always reflected partly by the interfaces, they will pass through the substrate layer and deposit layer many times. The acoustic energy pass through the inner surface of deposit is considered as energy loss. The waves pass through the outside surface of substrate will be received by acoustic sensors as measured signals.

1.5.2 Principle of coda wave interferometry

Acoustic wave signals can be classified into 3 parts according to their nature, ballistic waves, coda waves and noise (Figure 1.9). The ballistic waves, also known as direct waves, are the first arrived waves which propagate directly from acoustic source to sensor along the shortest path (Figure 1.10). Most of the acoustic energy is carried by the direct waves. Direct wave is widely used in acoustic detection as it carries lots of evident information (reflection coefficient, attenuation, time of flight,...), which could be related directly to the nature of test sample.

Coda waves are the tails after the ballistic waves in the later part of signal with weak amplitude (Figure 1.9). The propagation of coda waves go through every possible path in the medium (Figure 1.10). Obviously, the paths of all the coda waves are longer than direct waves, which makes coda waves received by the sensor after direct waves. Then the received coda signal is a summation of coda waves along all the paths in the medium. Since coda waves are strongly scattered in the medium, it is difficult to analyze the wave

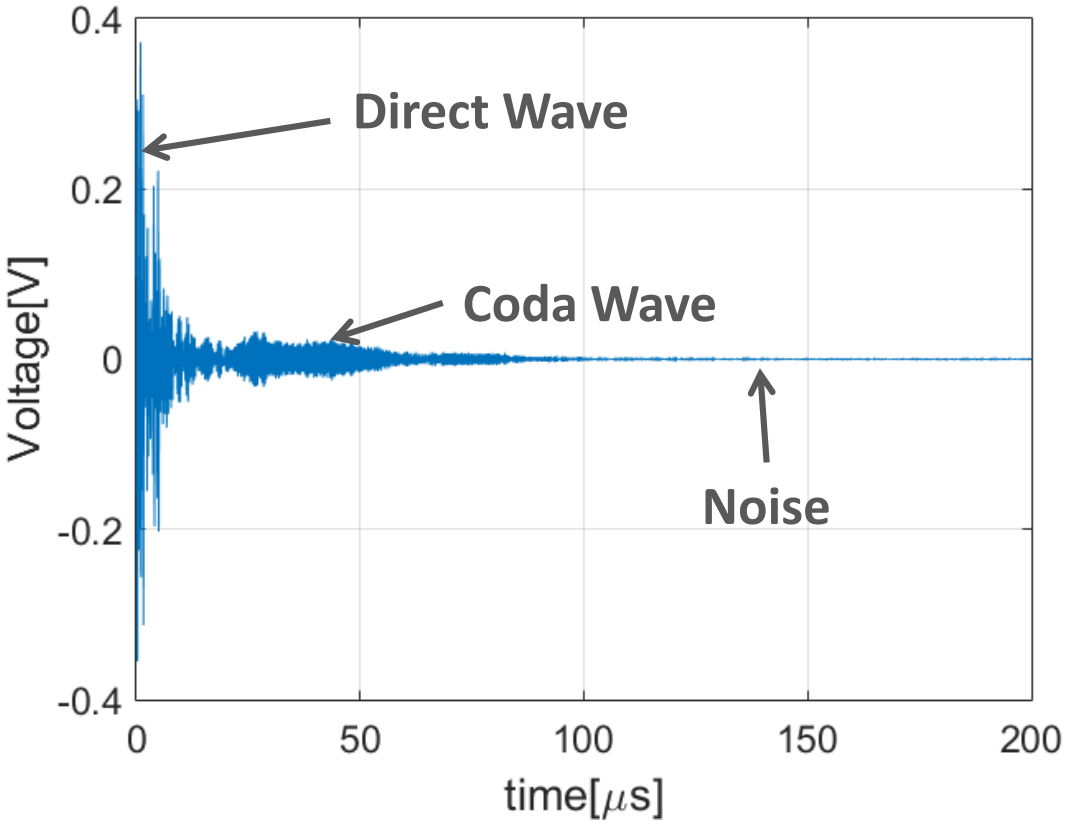

FIGURE 1.9 – Picture of an acoustic signal measured in complex medium

of each path like direct waves [131]. That is why the coda waves have been treated as an useless part of signal like noise for a long period since it is discovered.

However, the coda waves do carry the information of medium. In detail, supposing that acoustic waves propagate through an arbitrary complex medium, if the state of medium is kept constant, the propagation of coda waves along each path will not change, then, as a result, the received coda signals will also be identical. On the other hand, if there is even a slight perturbation in the medium, there must be some propagation paths which are modified. These modification will lead to variations in coda signals. The coda waves propagate many times through the medium, which means it is much more sensitive than the direct waves for detection [132][133][134].

Coda Wave Interferometry (CWI) is a tool for analyzing coda signals, which is recently proposed by Snieder et al. [135][136]. The principle of CWI is to analyze the global differences of coda signals measured with different states of sample. Using the changes in

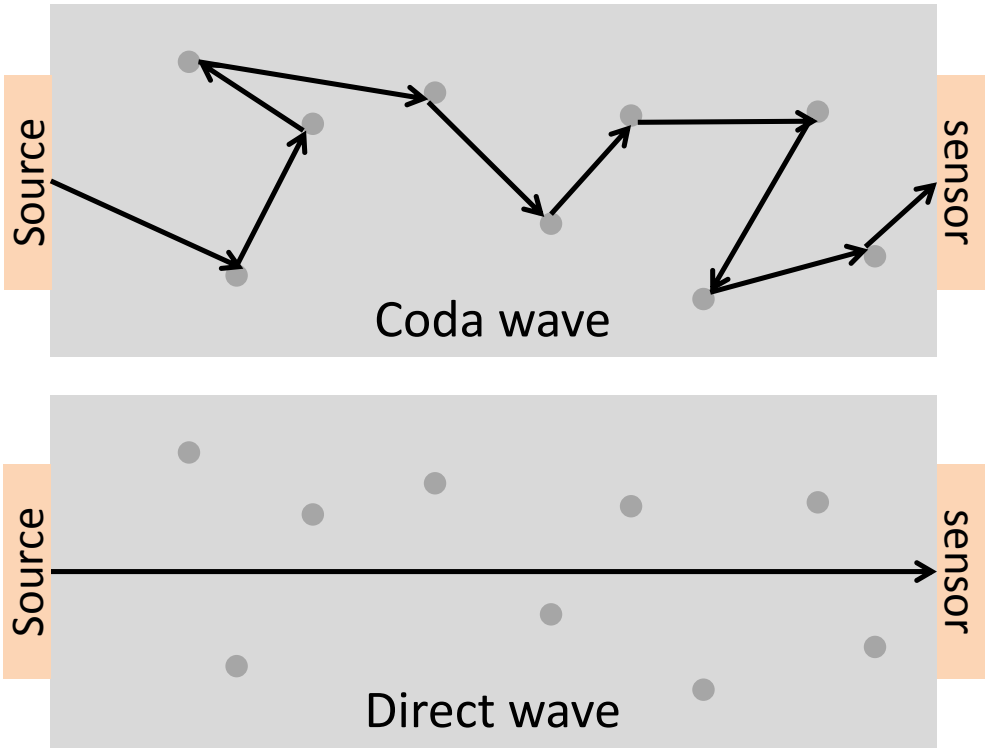

FIGURE 1.10 – Propagation of direct wave and coda wave in complex medium

coda (Figure 1.11), the variation of sample states could be somehow quantified.

For a received signal $u_0(t)$, it consists of numerous waves along all the possible paths. The expression of $u_0(t)$ could be defined as :

$$u_0(t) = \sum_n s_n(t) \tag{1.2}$$

Where n indicates the propagation paths, and s_n is the wave propagating along the path n. If there is a perturbation in the wavefield, some waves will be modified. Then the definition of a perturbed wavefield could be defined as :

$$u_p(t) = \sum_n s_n^{(p)}(t) \tag{1.3}$$

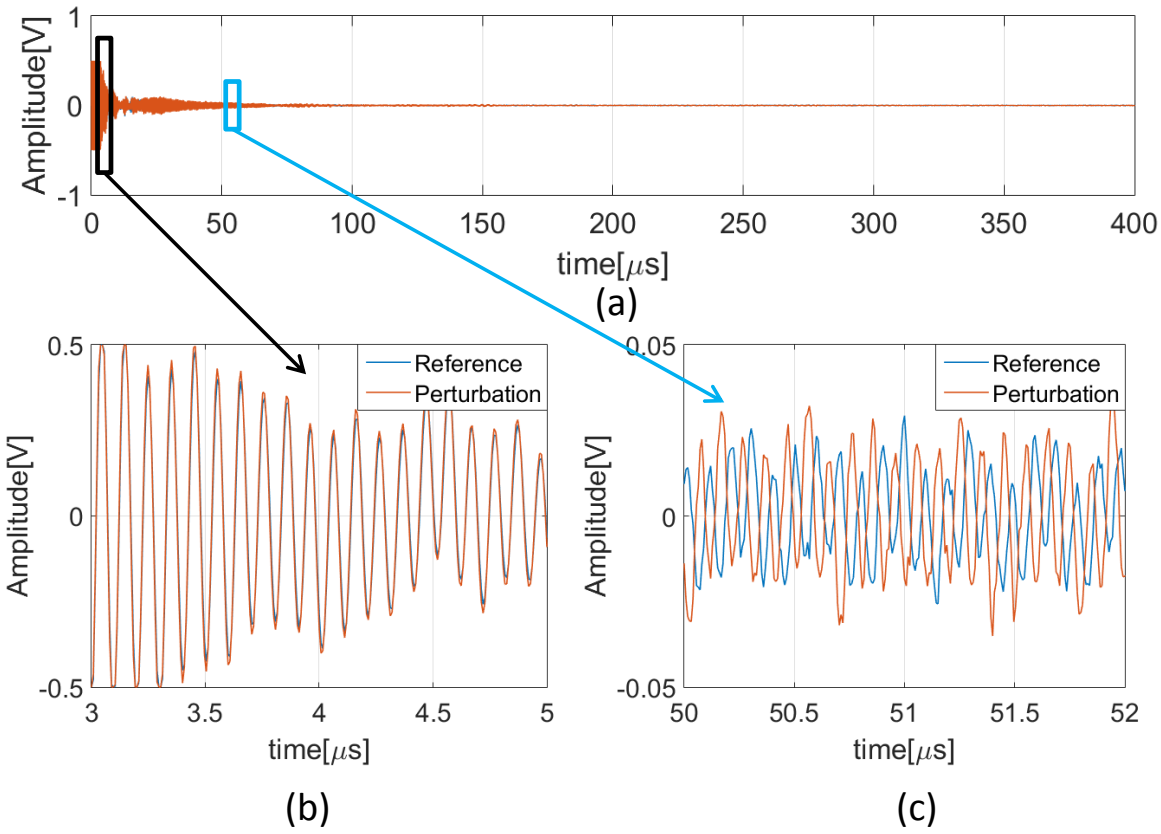

FIGURE 1.11 – Coda signals measured at a reference sample state and at a perturbed sample state

Where $s_n^{(p)}$ is the perturbed wave propagating along path n. With some particular kinds of perturbation, s_n and $s_n^{(p)}$ could be related. For example if the perturbation does not change the wave shape, $s_n^{(p)}$ could be written as :

$$s_n^{(p)}(t) = s_n(t - \tau_n) \tag{1.4}$$

Where τ_n is the change in the travel time of the wave propagates along path n. Knowing these coda properties is not enough for an effective detection. In order to have readable results, a parameter is needed to indicate the level of difference between signals. For example correlation coefficient $C_D(t_s)$ is used for comparing the reference and perturbed signals. It is defined as :

$$C_D(t_s) = \frac{\int_T u_0(t')u_p(t'+t_s)dt'}{\sqrt{\int_T u_0^2(t')dt' \int_T u_p^2(t')dt'}} \tag{1.5}$$

Here, the correlation coefficient is calculated within a finite time window T, representing the similarity between the reference signal u_0 and the perturbed signal u_p. By using the correlation coefficient, some parameters of wavefield could be determined in particular cases.

For a perturbation which is a change of wave velocity, the velocity variation could be determined under conditions. Supposing that the relative velocity perturbation $\delta v/v$ is constant everywhere in the wavefield ($\frac{\partial \delta v/v}{\partial x} = \frac{\partial \delta v/v}{\partial y} = \frac{\partial \delta v/v}{\partial z} = 0$), the velocity perturbation will be quantified by the correlation coefficient. By the Doublet method [136], the expression of velocity perturbation could be written as :

$$\frac{\delta v}{v} = \frac{t_{max}}{t} \tag{1.6}$$

The t represent the center of time window. t_{max} is the value of t_s that make the correlation coefficient $C_D(t_s)$ reach the maximum value. Stretching is another method which has a different explanation for the variation in signals [137]. The influence of perturbation to the signals is considered to be a time dilation instead of a phase change. The expression of correlation coefficient is then evolved :

$$C_S(\alpha) = \frac{\int_T u_0(t'(1+\alpha))u_p(t')dt'}{\sqrt{\int_T u_0^2(t'(1+\alpha))dt' \int_T u_p^2(t')dt'}} \tag{1.7}$$

As presented in Equation 1.7, α is the time dilation of signal. By this Stretching method, the velocity change could be quantified evidently :

$$\frac{\delta v}{v} = \alpha_{max} \tag{1.8}$$

The correlation coefficient could also be used to quantify another wavefield parameter. Supposing that the perturbation is movements of scatterers with a mean displacement δ, and the average of length and travel time of paths does not change, then the mean displacement δ can be somehow quantified [138][139]. By using CWI, the mean displacement is related to the maximum value of correlation coefficient C_D [136] :

$$MAX(C_D) = 1 - \frac{\overline{\omega^2}\delta^2 t}{v l_*} \tag{1.9}$$

Where $\overline{\omega^2}$ is the mean-squared angular frequency, l_* is the transport mean free path. Even though the coda signals are much more difficult to be analyzed than direct waves, we can still extract some information under conditions.

Some other parameters could also used for quantifying the difference level of signals, such as the distance between signals ($\sqrt{\int (u_0(t) - u_p(t))^2 dt}$), time shift and time dilatation rate. The detail of these indicators will be addressed in chapter 2.

1.5.3 Current applications of CWI

Since the use of coda wave is a relatively recent technique and the analyze of coda signals are complicated, coda wave is not widely used in various fields. Seismology is the first domain in which the CWI is applied [140][141][134][142]. Recently, the coda wave has been used in rock properties monitoring [132], mining monitoring [143], Volcano change monitoring [144][145][146], Concrete test [147][148][149]. In each domain, the coda wave shows a good result in sensitivity. CWI also has a potential on the application in other fields such as fouling/cleaning detection but so far has not been investigated.

1.6 Conclusion

With the development of industry, fouling deposition has been a problem that cannot be neglected. Considering the consequence of fouling, cleaning processing ought to be applied on industrial production. The efficiency of cleaning protocol has always been a major challenge for the industrial production, as it causes additional cost and environmental impact.

The coda wave has been widely used in seismology detection and monitoring, but it also has a potential on the application in other fields. The use of coda wave remain undiscovered in many domains. Industrial fouling detection and monitoring is a application which can be carried out by the coda wave. This technology can satisfy the industrial requirements, such as high sensitivity, non-invasive and low cost. The substrate between sensor and test sample could extend the duration of coda in received signals which helps the selection of

time window. Since the substrate usually exists in industrial detections, the coda wave technique is very adaptable for these applications. In last section, the two particular perturbations presented are common in many applications. However, the industrial fouling detection may not fit these conditions very well.

Nowadays, it is still impossible to find out a general solution for analyzing all the detail of coda waves propagation. Fortunately, other authors have shown a feasible way of coda wave analyzation. As presented in last section, each particular case may have a special analyzation method for coda. Then in the following chapters,one aim will be to set for suitable methods of coda wave analyzation for fouling detection and monitoring.

Monitoring methods	Advantages	Disadvantages
Direct methods	Very sensitive ; Local monitor	Cannot be used for CIP
Pressure drop	Measurement available and traditionally carried out on process line ; Overall monitor	Bad sensitivity ; Fouling place unknown
Temperature	Measurement available and traditionally carried out on process line ; Overall monitor	Bad sensitivity ; Fouling place unknown ; Do not work for thin layers
Heat transfer coefficient	Flow/temperature usually measured ; Overall monitor	Bad sensitivity ; Fouling place unknown ; Invasive
Electrical parameters	Very sensitive even for thin layers ; Able to determine fouling thickness	Invasive ; Fouling place unknown
FDG (Fluid Dynamic Gauging)	Very sensitive ; Local monitor	Invasive especially for soft deposits
Classic acoustic methods	Very sensitive ; Local monitor ; Non-invasive	Temperature change and presence of air bubble have a serious impact on the monitoring results ; Sensitivity limited by acoustic wavelength

TABLE 1.2 – The advantages and disadvantages of different fouling detection methods

Chapitre 2

Theoretical analyze and modeling of coda wave propagation in multilayer

This chapter will discuss the signal processing used for the experimental detection and the modeling of the acoustic field. In industrial applications there is always the presence of a substrate. The substrate is not the goal of detection, but it has a significant influence on the monitoring results. For this reason, it is necessary to study the influence of substrate in the whole acoustic detection field.

Modeling of the acoustic field corresponding the case of applications is useful for the study of substrate. Thus, an one dimension model of a multi-layer structure is constructed to study the wave propagation and substrate behavior. Then, the influence of substrate on the monitoring results could be achieved.

With the model, an expression of reception signals in function of emission signal and acoustic parameters is deduced. A simulation by impedance matrix is used to verify the correctness of the theoretical analyze result.

Nomenclature

$s(t)$	signal (time domain)
$S(\omega)$	signal (frequency domain)
$h(t)$	transfer function (time domain)
$H(\omega)$	transfer function (frequency domain)
$\delta(t)$	dirac delta function
Z	impedance
k	wave number
e_s	substrate thickness
v_s	sound velocity in substrate (stainless steel)
r_{so}	Reflection coefficient from substrate (stainless steel) to water
r_{sm}	Reflection coefficient from substrate (stainless steel) to detection zone
r_{ms}	Reflection coefficient from detection zone to substrate
t_{so}	Transmission coefficient from substrate (stainless steel) to water
t_{os}	Transmission coefficient from water to substrate (stainless steel)
t_{sm}	Transmission coefficient from substrate (stainless steel) to detection zone
t_{ms}	Transmission coefficient from detection zone to substrate (stainless steel)

2.1 Introduction of the studied structure and modeling

The studied model consists of a stainless steel substrate layer (with 2 parallel surfaces) and a detection zone containing the test sample. As presented in Figure 2.1, the detection zone is at the right side of substrate. This part could be considered as a black box. This black box could be identified by the transfer function h(t). The left side of substrate is supposed to be a semi-infinite zone of transducer that is different in acoustic parameters from the substrate.

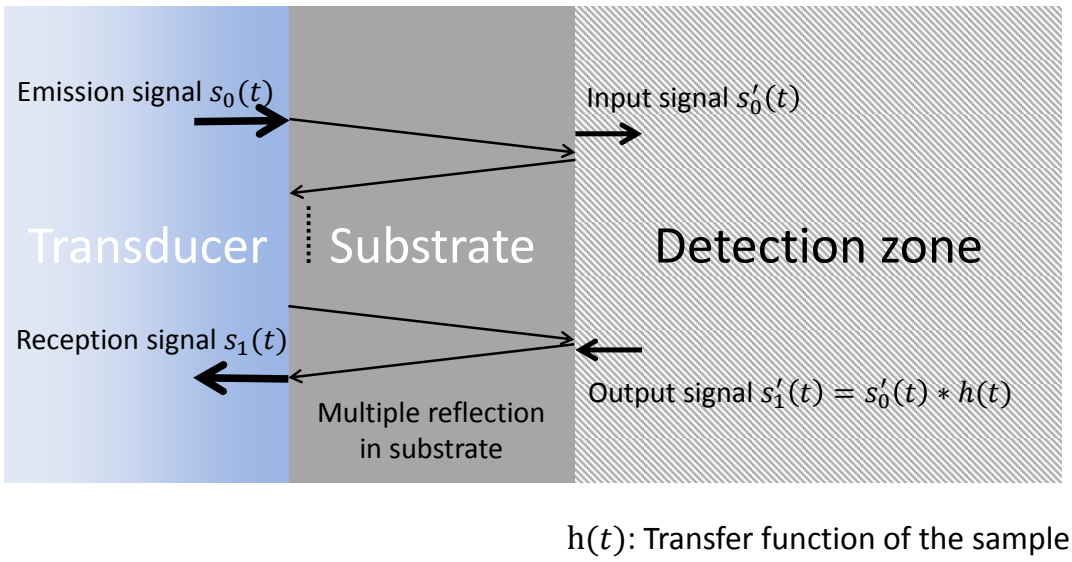

FIGURE 2.1 – Schema of the model which is studied in this chapter. Substrate is made of known material (stainless steel). Test sample is in the detection zone. h(t) is the transfer function which define the state of sample

The transfer function h(t) is defined as the ratio between the output signal and the input signal of the detection zone.

$$s_1'(t) = s_0'(t) * h(t) \tag{2.1}$$

This calculation could be simplified in frequency domain as in (2.2).

$$H(\omega) = \frac{S_1'(\omega)}{S_0'(\omega)} \tag{2.2}$$

Then, this transfer function $H(\omega)$ could be obtained by a modeling of only the detection zone which gives the input signal $S_0'(\omega)$ and the output signal $S_1'(\omega)$.

To have a better correspondence with the fouling monitoring applications, the detection zone in this model is a fouling layer followed by a semi-infinite zone of water. The material of substrate in the modeling is stainless steel which corresponds to the experimental implementation. The physical parameters of each material used in the simulation is detailed in Table 2.1.

Material	Density (kg/m^3)	sound velocity (m/s)	Impedance ($Pa \cdot s/m$)
Water	998	1482	1.5 10^6
Stainless steel	7891	6000	47.3 10^6
Fouling	1497	2223	3.3 10^6

TABLE 2.1 – Parameters of each material used in the model

2.2 Hypotheses and limited conditions

The problematic is studied in the frequency around 10 MHz, which corresponds to the experimental measurement detailed in the following chapters. In the applications, the structures that need to be detected, such as heat exchangers and ducts, are usually very large. Thus, in the modeling (Figure 2.1), there is no boundary at the top side and bottom side for each layer and the model could be constructed in one dimension.

In industrial applications, the fouling is usually under an unknown state between solid and liquid. The attenuation of transverse wave may be extremely large in liquid or fouling with unknown viscosity. Then, only longitudinal wave is considered in the modeling and theoretical analyze.

Most of the energy loss in acoustic propagation is due to the reflection and transmission at each interface. Thus, the influence of attenuation in substrate is rather weak, especially when the thickness of substrate is small. So, in the modeling the attenuation is neglected.

Once the emission signal is sent into the model, acoustic waves will reflect repeatedly at

the two surfaces of substrate. Each reflection at the interface substrate/detection zone will be followed by a series of output signals from the detection zone which will be explained in the next section. These two kinds of waves will then arrive to the interface water/substrate and be measured as an echo in signal. The substrate is supposed to be thick enough to separate echoes, so that there will not be any overlap between two different echoes of a signal.

2.3 Propagation of acoustic waves

In the model of Figure 2.1, the propagation of waves is started at the substrate surface. The acoustic source is at the left boundary of substrate. The emission signal is sent into the substrate and then arrive to the interface substrate/detection zone. The propagation of signal will separate at this interface. A part of energy will reflect at the interface, the other part of energy will enter the detection zone as the input signal, and then an output signal, which depend on the transfer function, will return to the substrate/detection interface. A part of this output signal will cross the interface and join the direct reflected signal. The other part of output signal will return to the detection zone as a new input signal. This loop happens many times in the detection zone and a series of output signals traverse the interface (Figure 2.2).

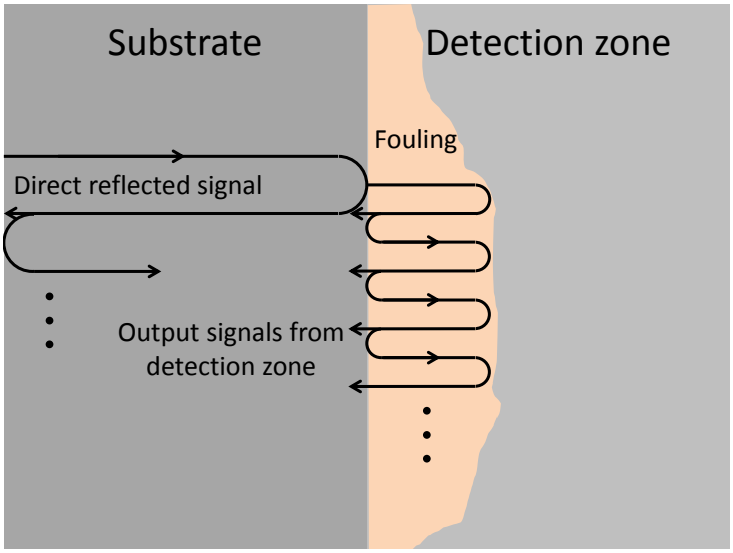

FIGURE 2.2 – One reflection happened at the interface substrate/detection zone

For all of the propagation paths (direct reflection signal and the output signals from detection zone), the signals will then arrive at the interface water/substrate. The signal will also separate into 2 parts at this interface. One part of the signal cross the interface and received by acoustic sensor. The other part of the signal reflect at the interface and propagate in the substrate from left to right like a new emission signal. Then, theoretically the same process happens in the model for infinite times. Gathering all the signals that cross the water/substrate interface, the entire reception signal could be obtained.

2.4 Mathematical modeling

The goal of this modeling is to investigate the substrate behavior for the results, which are related to the signals received at the interface water/substrate. The material of substrate in industrial applications is usually a common material. Moreover, changing the substrate material may cause other biological problems in the production. So, in this modeling, the substrate material is considered to be stainless steel and the goal is to study how the substrate thickness influence the result of measurements.

Thus, the first thing to do is to find the mathematical relation between reception signal and substrate thickness. In this section, the wave propagation in the model will be studied in detail. The reception signal will be expressed in function of known parameters and the transfer function of detection zone.

The acoustic parameters (reflection coefficient and transmission coefficient) could be obtain by the physical parameters of each layer. Since the material of each layer is defined in Table 2.1, the acoustic parameters in this model could also be regarded as known parameters. The parameters, which are useful for the mathematical modeling, are listed in the nomenclature.

As mentioned in the last section, the existence of interface will lead to a reflection of the output signal in the detection zone. The global output signal which arrives in the substrate and joins the direct reflected wave should be defined by the summation of all the output signals that cross the interface from the detection zone as in equation (2.3).

$$S_{\text{out}}(\omega) = S_{\text{input}}(\omega) \sum_{j} H^{j} t_{ms} t_{sm} r_{ms}^{j-1} \tag{2.3}$$

Since the substrate is supposed to be thick enough to separate the echoes in the reception signal, it is reasonable to analyze every single wave packet individually. Mathematically, a wave packet consists of the direct reflected wave at the interface substrate/detection zone and the output waves in the detection zone. Then, in frequency domain , considering the equation (2.3), the first echo in the reception signal $S_{r,1}(\omega)$ could be defined as in equation (2.4)

$$S_{r,1}(\omega) = S_0(\omega) r_{sm} t_{os} t_{so} + S_0(\omega) \sum_j H(\omega)^j t_{ms} t_{sm} r_{ms}^{j-1} t_{os} t_{so} \tag{2.4}$$

Where S_0 represents the original emission signal and H is the transfer function of detection zone.

At the interface water/substrate, there will be a reflection wave with the same waveform as the first echo. This reflection wave could be treated as the emission wave of the second echo. Overall, all the echo could be explained by this loop. Then an arbitrary echo could be defined as in equation (2.5).

$$S_{r,i}(\omega) = S_{r,i-1}(\omega) r_{sm} r_{so} + S_{r,i-1}(\omega) \sum_j H(\omega)^j t_{ms} t_{sm} r_{ms}^{j-1} r_{so} \tag{2.5}$$

Where i is the number of echo, and $i \geq 2$. The summation corresponds to the form of a geometric sequence. It could be simplified as in equation (2.6).

$$\sum_j H(\omega)^j r_{ms}^j = \frac{H(\omega) r_{ms}}{1 - H(\omega) r_{ms}} \tag{2.6}$$

This geometric sequence needs to satisfy 2 conditions to make the simplification correct, which are :

— This is an infinite geometric sequence ($j \to \infty$)

— The module of the common ratio is less than one ($|H((\omega) r_{ms}| < 1$)

Theoretically, there are infinite times of reflection at the interface in the detection zone. So the sequence should be an infinite sequence. Physically, the energy of output waves will always decrease compared to the input signal (reflection, transmission, attenuation, diffusion,...). So, the absolute value of transfer function $H((\omega)$ is always less than 1. On the other hand, it is widely known that the absolute value of reflection coefficient r_{ms}

is always less than 1. So the sequence meet those conditions and the simplification in equation (2.6) is correct.

With the simplification in equation (2.6), the equation (2.5) could then be written as equation (2.7).

$$S_{r,i}(\omega) = S_{r,i-1}(\omega)(\frac{H(\omega)r_{ms}}{1 - H(\omega)r_{ms}}a + b) \tag{2.7}$$

Where $a = \frac{t_{sm}t_{ms}r_{so}}{r_{ms}}$ and $b = r_{sm}r_{so}$ are constants which depend on the acoustic parameters. The second term in equation (2.7) could be defined as a new function (equation (2.8)).

$$T(\omega) = \frac{H(\omega)r_{ms}}{1 - H(\omega)r_{ms}}a + b \tag{2.8}$$

And the equation (2.7) could be written as :

$$S_{r,i}(\omega) = S_{r,i-1}(\omega)T(\omega) \tag{2.9}$$

Using the recurrence relation, the arbitrary echo ($S_{r,i}(\omega)$) could finally expressed by the emission signal ($S_0(\omega)$) (equation (2.10)).

$$S_{r,i}(\omega) = a_0 S_0(\omega)T^i(\omega) \tag{2.10}$$

Where $a_0 = \frac{t_{so}t_{os}}{r_{so}}$ is a constant related to the acoustic parameters. Gathering all the echoes, the whole reception signal could be defined (equation (2.11)).

$$s_{\text{reception}}(t) = \sum s_{r,i}(t) * \delta(t - \frac{2ie_s}{v_s}) \tag{2.11}$$

Where e_s is the thickness of substrate and v_s is the sound velocity in the substrate. $s_{r,i}(t) = IFT[S_{r,i}(\omega)]$ is the time domain signals of echoes.

2.5 The simulation results by impedance matrix method

The theory explained in the last section will be confirmed in this section. The impedance matrix is a well known method in studying multi-layer structure. The impedance matrix method calculate the total impedance of whole model. And this impedance gives the ratio between reception signal and emission signal (reflection coefficient) in frequency domain. So the reception signals could be obtained by the impedance and emission signal.

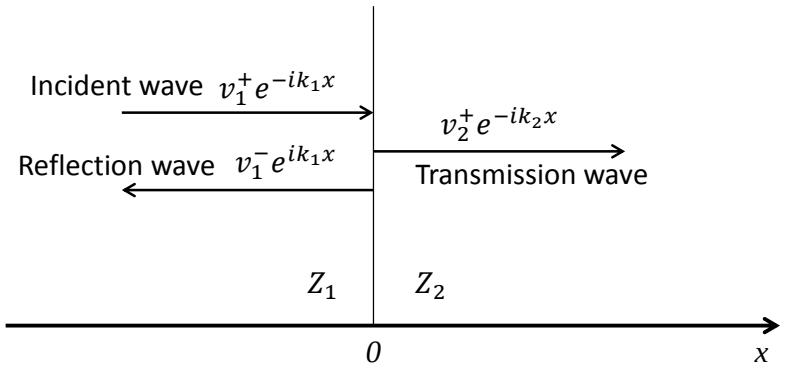

FIGURE 2.3 – Propagation of acoustic wave at an interface between 2 semi-infinite mediums

For an interface between two different semi-infinite mediums where the wave propagation is perpendicular to the interface (Figure 2.3), the displacement (2.12) and constraints (2.13) of waves (incident wave, reflection wave and transmission wave) at the interface (x=0) are continue.

$$\begin{aligned} v_1(x) &= v_1^+ e^{-ik_1 x} + v_1^- e^{ik_1 x} \\ v_2(x) &= v_2^+ e^{-ik_2 x} \end{aligned} \tag{2.12}$$

$$\begin{aligned} \tau_1(x) &= -Z_1(v_1^+ e^{-ik_1 x} - v_1^- e^{ik_1 x}) \\ \tau_2(x) &= -Z_2 v_2^+ e^{-ik_2 x} \end{aligned} \tag{2.13}$$

The wave number $k_{1/2}$ is known as $2\pi f/v_{1/2}$ with neglecting the attenuation. $v_{1/2}$ represents the sound velocity in medium Z_1/Z_2.

Thus, at x=0, the reflection coefficient $r_{12}^{(v)}$ and the transmission coefficient $t_{12}^{(v)}$ of movement velocity could be obtained as Eq. (2.14)

$$\begin{aligned} r_{12}^{(v)} &= \frac{v_1^-}{v_1^+} = \frac{Z_1 - Z_2}{Z_1 + Z_2} \\ t_{12}^{(v)} &= \frac{v_2^+}{v_1^+} = \frac{2Z_1}{Z_1 + Z_2} \end{aligned} \tag{2.14}$$

The combination of a finite layer (Z_1) and a semi-infinite medium (Z_2), as presented in Figure 2.4, is known as a transmission line. The thickness of layer is defined as l. The medium Z_1 and Z_2 together could be regarded as an entire structure with an impedance of $Z = -\frac{\tau_1(-l)}{v_1(-l)}$.

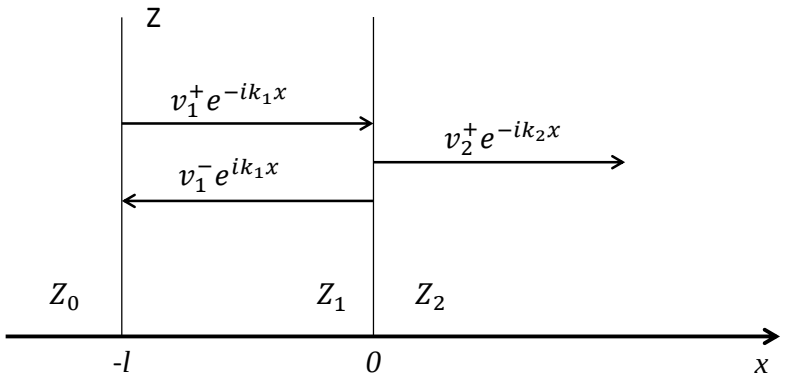

FIGURE 2.4 – Acoustic transmission line

With Eq. (2.14), the expression of $v_1(-l)$ and $\tau_1(-l)$ could be defined as Eq. (2.15) and Eq. (2.16).

$$v_1(-l) = \frac{Z_1 + Z_2}{2Z_1} v_2^+ e^{ik_1 l} + \frac{Z_1 - Z_2}{2Z_1} v_2^+ e^{-ik_1 l} \tag{2.15}$$

$$\tau_1(-l) = -\frac{Z_1 + Z_2}{2} v_2^+ e^{ik_1 l} + \frac{Z_1 - Z_2}{2} v_2^+ e^{-ik_1 l} \tag{2.16}$$

Then, this two expression could be simplified into Eq. (2.17) and Eq. (2.18).

$$v_1(-l) = v_2^+ cos(k_1 l) + i\frac{Z_2}{Z_1} v_2^+ sin(k_1 l) \tag{2.17}$$

$$\tau_1(-l) = -Z_2 v_2^+ cos(k_1 l) - iZ_1 v_2^+ sin(k_1 l) \tag{2.18}$$

Thus the the displacement (v) and constraints (τ) at two surfaces could be related as Eq. (2.19), and the impedance Z of the entire structure could be obtained as Eq. (2.20)

$$\begin{vmatrix} \tau_1(-l) \\ v_1(-l) \end{vmatrix} = \begin{vmatrix} cos(k_1 l) & -iZ_1 sin(k_1 l) \\ -i\frac{sin(k_1 l)}{Z_1} & cos(k_1 l) \end{vmatrix} \begin{vmatrix} \tau_2(0) \\ v_2(0) \end{vmatrix} \tag{2.19}$$

$$Z = Z_1 \left(\frac{Z_2 cos(k_1 l) + iZ_1 sin(k_1 l)}{Z_1 cos(k_1 l) + iZ_2 sin(k_1 l)} \right) \tag{2.20}$$

With knowing the impedance Z at the interface $x = -l$, the reflection coefficient in frequency domain r_{01} here could be obtained as Eq. (2.21).

$$r_{01} = \frac{Z - Z_0}{Z + Z_0} \tag{2.21}$$

Where Z_0 is the impedance of the medium at $x < -l$. If the emission signal at the medium Z_0 is known, the reception signal could be easily achieved by the reflection coefficient r_{01}.

A concrete model is proposed in Figure 2.5-(a) with the structure of detection zone defined. The detection zone here consists of a certain thickness of fouling layer and a semi-infinite zone of water. By using both methods, a reception signal could be achieved. The correspondence between the reception signals obtained by the two methods could verify the correctness of equation (2.11).

The emission signal is defined as one single period of sinus at 10 MHz. By using the impedance matrix, the reception signal of the model (Figure 2.5-(a)) could be achieved.

Another model is used for obtain the transfer function h(t) (Figure 2.5-(b)). This model is the detection zone of the first model. By using the impedance matrix, the reception signal of model 2 could be easily obtained and the transfer function h(t) of the detection zone could also be deduced by Equation (2.22).

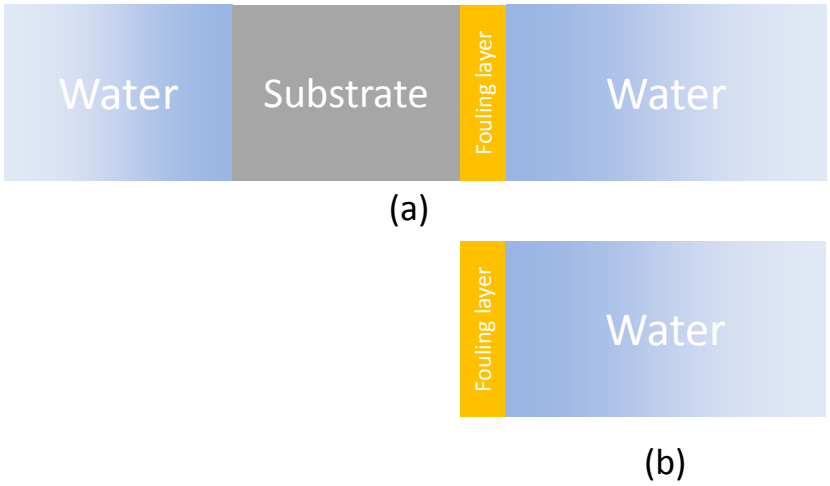

FIGURE 2.5 – Schema of 2 models simulated by impedance matrix

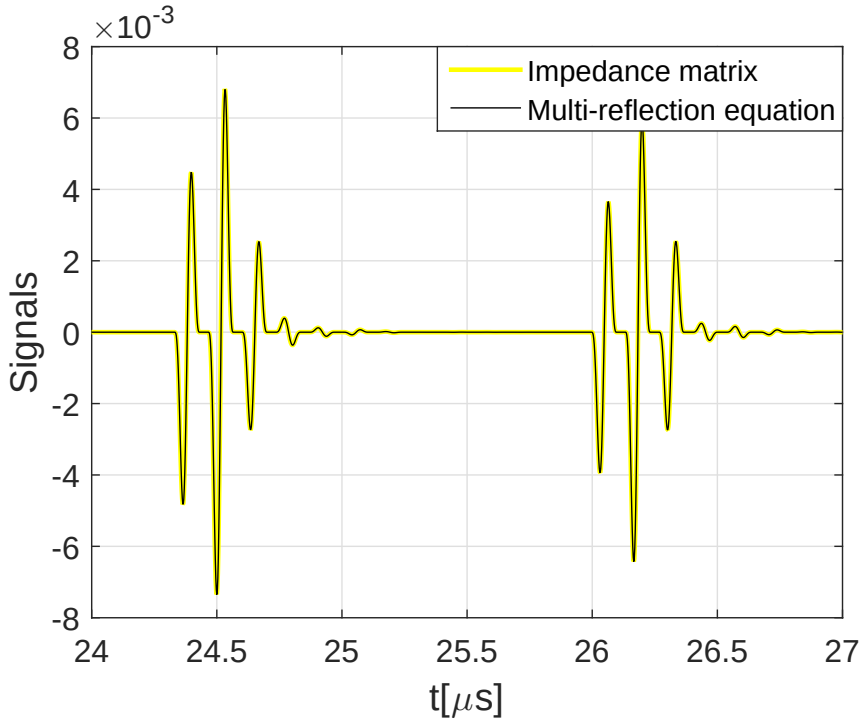

FIGURE 2.6 – Two reception signals obtained by impedance matrix and multi-reflection theory (equation (2.11)

$$H(\omega) = \frac{S_{\text{reception}}(\omega)}{S_{\text{emission}}(\omega)} \tag{2.22}$$

Then, with the transfer function and the theory mention before, the reception signal could also be obtained by the equation (2.11). Figure 2.6 shows the reception signal simulated by impedance matrix (yellow), and the reception signal obtained by equation (2.11) (black). These two lines are almost identical, which means both of the methods finally produce the same result. In this figure, only 2 echoes are presented in order to have good clarity for the signals. But in the other parts of the signals, these two lines are always identical like in this figure.

This phenomenon could confirm that the theory explained in the last section is correct. However, this theory is not suitable for thin substrate. The limit of substrate thickness will be discussed in sections below.

2.6 Useful indicators of coda signals

The crude reception signals cannot be used directly to quantity the state change of sample during the monitoring process. A parameter that extracted from the signals is usually used as an indicator to represent the sample state in real time. The classic acoustic parameters, such as time of flight, are difficult to be extracted from the coda waves, because the coda waves is a summation of multiple waves propagating different paths which makes the coda waves difficult to be decomposed to study the wave propagation of each path.

In order to complete the monitoring process, it is necessary to find an indicator which can be applied on coda wave signals. For example, other authors have proposed Doublet [150] and Stretching [151] methods to study the velocity variation [147]. Time shift or time dilatation rate is used as an indicator to quantify the velocity change in the acoustic propagation field. In our case, the state change of fouling is not always the same type. Thus the indicator suppose to be capable to represent the global change in coda.

The distance is an indicator which could represent the difference between signals. The definition of the distance between 2 coda signals $s_1(n)$ and $s_2(n)$ could be presented as Equation (2.23) (non-normalized) and Equation (2.24) (normalized).

$$d^2_{1,2,\text{non-normalized}} = \int (s_1(t) - s_2(t))^2 dt \tag{2.23}$$

$$d_{1,2}^2 = \int (\frac{s_1(t)}{\sigma_1} - \frac{s_2(t)}{\sigma_2})^2 dt \tag{2.24}$$

Where σ_1 and σ_2 are the root of variance of signals s_1 ands_2. The variance σ^2 could be obtain as in Equation (2.25).

$$\sigma^2 = \int (s(t) - m)^2 dt \tag{2.25}$$

The m is the mean value of signal $s(t)$ which could be defined by Equation (2.26).

$$m = \frac{1}{T} \int_0^T s(t) dt \tag{2.26}$$

Obviously, it is feasible to use this parameter in quantifying the difference between signals. The advantage of the distance of non-normalized signals is that the calculation is simple, which make the signal processing speed rather fast. However, the absolute value of distance is also depend on the energy of each signal, and there is no limitation for the max value. The absolute value of this parameter might be meaningless for the monitoring of sample change.

In order to have a reasonable result which is independent of signal energy, the distance of normalized signals (Equation (2.24) is a better choice. For the two signals $s_1(t)$ and $s_2(t)$ with the offset regulated to 0 ($m = 0$), the expression of $d_{1,2}^2$ could be decomposed into equation (2.27).

$$d_{1,2}^2 = \frac{1}{\sigma_1^2} \int s_1(t)^2 dt + \frac{1}{\sigma_2^2} \int s_2(n)^2 dt - \frac{2}{\sigma_1 \sigma_2} \int s_1(n) s_2(n) dt \tag{2.27}$$

In Equation (2.27), the two first terms $\frac{1}{\sigma_1^2} \int s_1(t)^2 dt$ and $\frac{1}{\sigma_2^2} \int s_2(n)^2 dt$ are equal to 1. The third term ($\frac{2}{\sigma_1 \sigma_2} \int s_1(n) s_2(n) dt$) is the only part which gives the information of the difference between signals. However, the form of this term is close to the decorrelation of signals (Equation (2.29)).

2.6.1 Decorrelation coefficient

Time-shifted correlation coefficient is another parameter which can be extracted from coda waves [136].The definition of normalized correlation coefficient $C_{1,2}$ between 2 signals

($s_1(t)$ and $s_2(t)$) could be simply expressed as equation (2.28).

$$C_{1,2}(\tau) = \frac{\int_{t_0}^{t_1} s_1(t)s_2(t+\tau)dt}{\sqrt{\int_{t_0}^{t_1} s_1^2(t)dt \int_{t_0}^{t_1} s_2^2(t)dt}} \tag{2.28}$$

This normalized parameter gives the similarity between the two signals. The correlation coefficient could always be extractable from signals no matter which kind of change happenes in the acoustic propagation field.

In the signal processing of CWI, the signals $s_1(t)$ and $s_2(t)$ in the equation (2.28) are the reception signals. The integrations are calculated with the same time window($[t_0, t_1]$).

Other authors have used the max value of $C_{1,2}(\tau)$ and the corresponding value of τ to extract information from signals (velocity variation, mean scatterer displacement,...) [136]. However, the perturbation type of our model in the acoustic propagation field is not similar to any of those special cases, and these two parameters are not suitable.

In industrial applications, the perturbation which needs to be monitored is the growing or cleaning of fouling. In other words, the change of fouling quantity is the main target to be detected. The fouling formation and elimination never goes with a predictable way. The time shift between signals may caused by the fouling thickness change. If the max value of $C_{1,2}(\tau)$ is used as an indicator, this change will not be detectable. The corresponding value of τ may able to give the information of surface change with knowing the initial fouling thickness under an ideal condition. But the fouling in application is usually not uniform and the fouling surface may not be a flat, which makes τ difficult to be related with fouling thickness. In this case, τ is not useful to be an indicator for this monitoring either.

Therefore, zero lapse-time decorrelation coefficient is used as the indicator of coda. The Equation (2.29) is the definition of the decorrelation coefficient. This parameter gives the dissimilarity between two windowed signals without time shift. In fact, the definition of decorrelation coefficient is equal to the definition of half normalized distance (Equation (2.27)). Thus, the optimal result obtained from the signal distance could also be achieved by decorrelation coefficient.

$$D_{1,2} = 1 - \frac{\int_{t_0}^{t_1} s_1(t)s_2(t)dt}{\sqrt{\int_{t_0}^{t_1} s_1^2(t)dt \int_{t_0}^{t_1} s_2^2(t)dt}} \tag{2.29}$$

All kinds of changes happened in the acoustic propagation field will lead to the variation of decorrelation coefficient. Since there is no state change in the substrate, the decorrelation coefficient will be influenced only by the changes happened in detection zone, which is of cause the fouling evolution. Then, the decorrelation coefficient is used as the indicator for the acoustic monitoring in the experiments.

As the substrate always plays an important role in the wave propagation, it is worthy to know the behavior of decorrelation coefficient as a function of the substrate. The acoustic parameters of substrate are usually stable as they depend on the physical properties of the material (sound velocity, density,...). The thickness is another important factor for the acoustic model. In this section, the influence of substrate thickness on the decorrelation coefficient will be detailed by theoretical analyze and verified by the impedance matrix method.

2.6.2 Decorrelation coefficient result with impedance matrix method

By using the impedance matrix, the reception signals with different thicknesses of substrate could be simulated. In order to study the decorrelation coefficient behavior, the fouling layer of two different thickness, 40 μm and 50 μm, is used as two different sample states.

Thus, simulated signals could be classified by two series :

— The reception signals simulated with different substrate thicknesses and the first sample state (40 μm fouling)

— The reception signals simulated with different substrate thicknesses and the second sample state (50 μm fouling)

Decorrelation coefficient between the two sample states with an arbitrary substrate thickness could then be calculated by the simulated signals (equation (2.29)). However, the decorrelation coefficient is also a time window dependent parameter. In order to involve all parts of reception signal, the end of time window (t_1) is always fixed at the 29th echo (correspond to a threshold (5×10^{-4}) in amplitude) and the beginning of the time window (t_0) move from the beginning of reception signal to the 29th echo. Then, a series of decorrelation coefficients which related to the beginning of time window is obtained

(equation 2.30). The average value of the result ($D_{1,2}(t_0)$) is used as the indicator of the decorrelation coefficient behavior at a substrate thickness.

$$D_{1,2}(t_0) = 1 - \frac{\int_{t_0}^{t_1} s_1(t)s_2(t)dt}{\sqrt{\int_{t_0}^{t_1} s_1^2(t)dt \int_{t_0}^{t_1} s_2^2(t)dt}} \tag{2.30}$$

Gathering this indicator at each substrate thickness, a figure of the mean value of decorrelation coefficient in function of substrate thickness could be obtained (Figure 2.7).

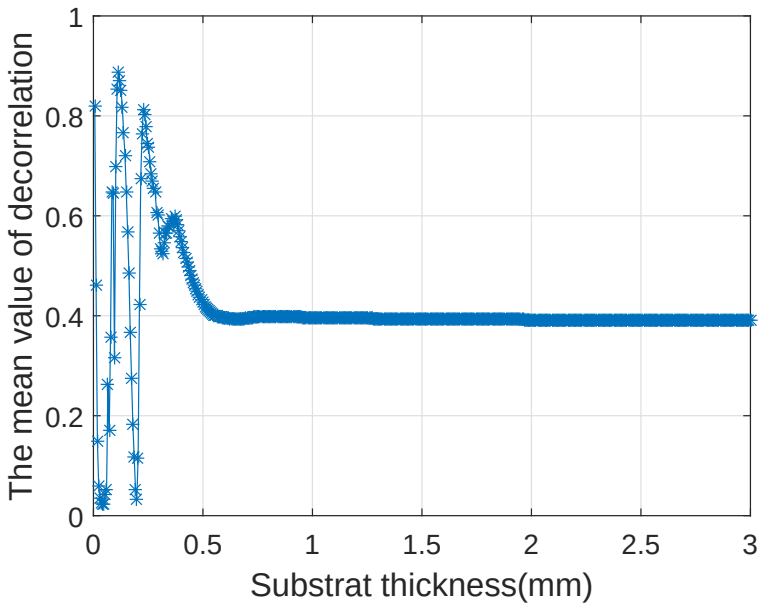

FIGURE 2.7 – Mean value of decorrelation coefficient with different time windows in function of the substrate thickness.

In Figure 2.7, it is evident that the decorrelation change a lot if the substrate is thinner than 0.6 mm. At the other part (substrate thickness more than 0.6 mm) the decorrelation coefficient is stable. This means that if the thickness of substrate is thick enough, the decorrelation result may not depend on the substrate thickness.

The advantage of impedance matrix method is that it can deal with the thin substrate condition. However, the simulation by this method could give us no more information. The impedance matrix simulation method gives directly the reception signals by the emission signal. Thus, it is difficult to extract relations between the decorrelation coefficient and an arbitrary parameter. Even though the Figure 2.7 shows that the decorrelation coefficient become stable after 0.6 mm, but it does not mean that other parameters, such

as reflection/transmission coefficient and state change level in detection zone, could not modify this value of thickness.

It is impossible to do the same simulation for all the useful values of parameters. Therefore, another simulation method by using mathematical analyze of wave propagation will be detailed below to study that the decorrelation coefficient depends on which parameter(s) and how this or these parameter(s) influences the decorrelation coefficient.

2.6.3 Decorrelation coefficient result with theoretical analyze result

The most essential part in the decorrelation coefficient definition (equation (2.29)) is the integration between $s_1(t)$ and $s_2(t)$. Thus the analyze starts with this part.

The integrations in equation (2.29) is calculated within a chosen time window. Obviously, the time window is an important parameter for the decorrelation coefficient. Experimentally, the decorrelation coefficient is calculated directly with the windowed signals. In the simulation with impedance matrix, the decorrelation coefficient is obtained by the same way. Theoretically, knowing the expression of reception signals, the decorrelation coefficient may have another definition.

For the integration (equation (2.31)), echoes of the signals could be regarded as individual terms.

$$I_{1,2} = \int s_1(t)s_2(t)dt \tag{2.31}$$

Each reception signal, $s_1(t)$ or $s_2(t)$, could be considered as a summation of all the echoes as in the equation (2.11). Then, those signals could be defined with the same form (equation (2.32)).

$$s_1(t) = \sum_i s_{1,i}(t) \tag{2.32a}$$

$$s_2(t) = \sum_j s_{2,j}(t) \tag{2.32b}$$

Where i and j are the number of echo and the signals $s_{1,i}(t)$ or $s_{2,j}(t)$ are the signals of each echo. The product of the signals $s_1(t)$ and $s_2(t)$ is then the summation of products

of each term (equation (2.33)).

$$s_1(t)s_2(t) = \sum_{i=j} s_{1,i}(t)s_{2,j}(t) + \sum_{i\neq j} s_{1,i}(t)s_{2,j}(t) \tag{2.33}$$

In the equation (2.33) the products of terms are classified into two categories, diagonal terms ($i = j$) and cross terms ($i \neq j$) (Figure 2.8). As the thickness of substrate is supposed to be thick enough to separate echoes, the products between cross terms ($i \neq j$) could be considered as zero. So the product of $s_1(t)$ and $s_2(t)$ could be simplified into equation (2.34).

$$s_1(t)s_2(t) = \sum_{i} s_{1,i}(t)s_{2,i}(t) \tag{2.34}$$

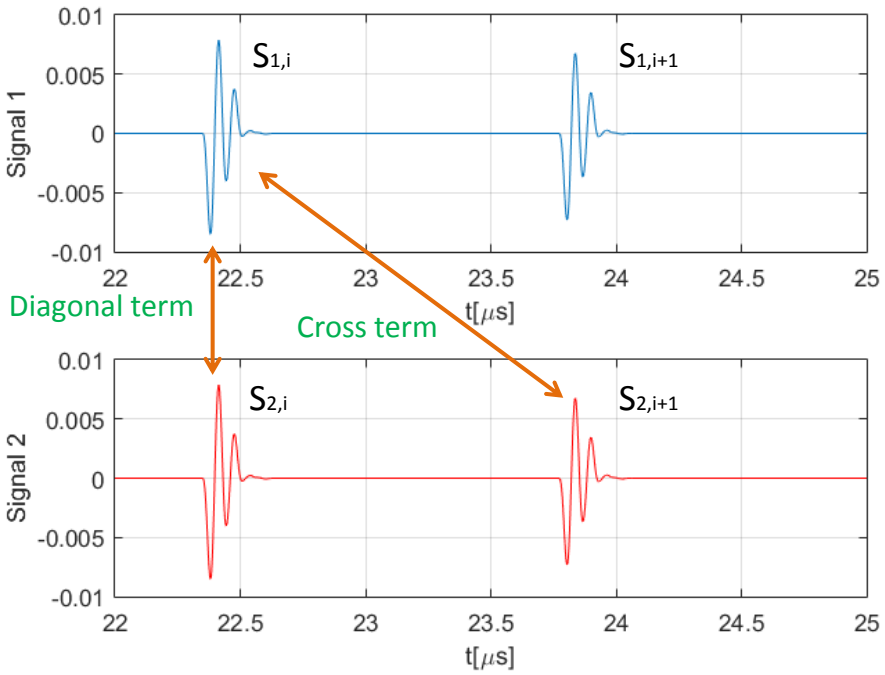

FIGURE 2.8 – Diagonal terms and Cross terms of signals

Inserting expressions (2.34) in equation (2.31), the expression of the integration is then :

$$I_{1,2} = \sum_{i} \int s_{1,i}(t)s_{2,i}(t)dt \tag{2.35}$$

The integration of $s_{1,i}(t)s_{2,i}(t)$ could be transformed in frequency domain (equation (2.36)).

$$\int s_{1,i}(t)s_{2,i}(t)dt = IFT[S_{1,i}(\omega)S^*_{2,i}(\omega)](0) \tag{2.36}$$

The definition of each echo in frequency domain has already been given in equation (2.10). Then, the integration could be transform into equation (2.37).

$$\int s_{1,i}(t)s_{2,i}(t)dt = IFT[a_0^2||S_0(\omega)||^2(T_1(\omega)T_2^*(\omega))^i](0) \tag{2.37}$$

The integrations at the denominator in equation (2.30) could also be expressed by the same way. The expression of decorrelation coefficient could finally be transform into equation (2.38).

$$D_{1,2} = 1 - \frac{\sum_i IFT[||S_0(\omega)||^2(T_1(\omega)T_2^*(\omega))^i](0)}{\sqrt{\sum_i IFT[||S_0(\omega)||^2||T_1(\omega)||^{2i}](0)\sum_i IFT[||S_0(\omega)||^2||T_1(\omega)||^{2i}](0)}} \tag{2.38}$$

In time domain, the expression (2.38) could be written as expression (2.39).

$$D_{1,2} = 1 - \frac{\sum_i (s' * h'_{d,i})(0)}{\sqrt{\sum_i (s' * h'_{1,i})(0)\sum_i (s' * h'_{2,i})(0)}} \tag{2.39}$$

Where $s' = IFT[||S_0(\omega)||^2]$, $h'_{d,i} = IFT[(T_1(\omega)T_2^*(\omega))^i]$, $h'_{1,i} = IFT[||T_1(\omega)||^{2i}]$, $h'_{2,i} = IFT[||T_2(\omega)||^{2i}]$.

In the expression (2.38) or (2.39), the decorrelation coefficient with an arbitrary window could be considered as the decorrelation coefficient of consecutive echoes.

The expression (2.38) could be verified by calculating the decorrelation coefficient directly by simulated signals. The substrate is now supposed to be thick enough and the thickness is supposed to be fixed. Then, a relation between the decorrelation coefficient value and the time window could be constructed by the two methods.

In the Figure 2.9, the red curve is the decorrelation coefficient calculated directly by the definition (equation (2.29)) with the simulated signals s_1 and s_2. These two signals are simulated with different sample states. The two sample states are still defined by setting the fouling layer thickness at 40 μm and 50 μm. In this figure, the ending of time windows

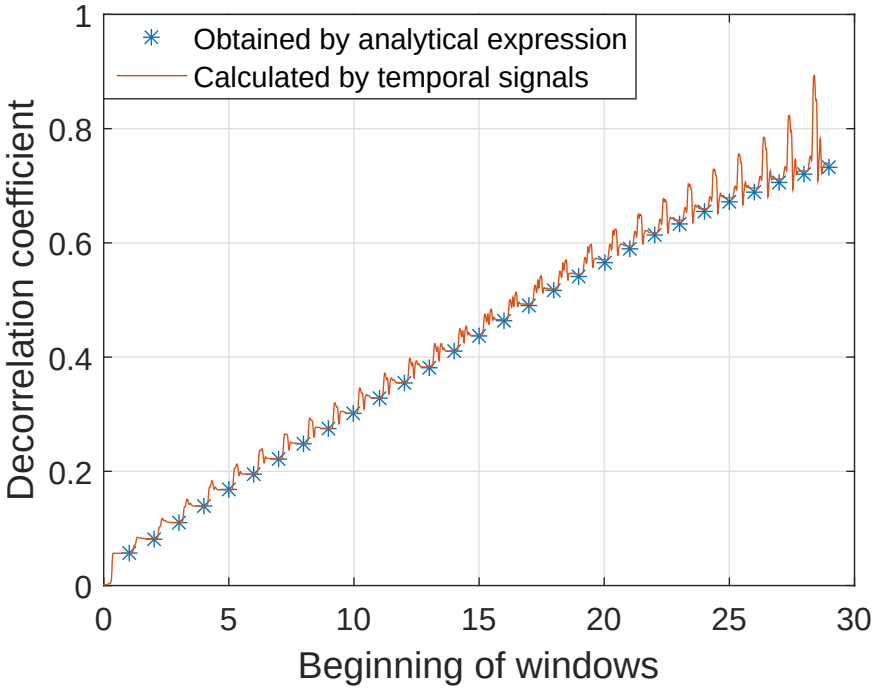

FIGURE 2.9 – Decorrelation coefficient in function of the beginning of time windows. Theoretical solution of decorrelation coefficient (Blue stars) ; Decorrelation coefficient calculated directly by simulated signals (Red curve)

is always fixed at the 29th echo and the decorrelation coefficient is as a function of the beginning of windows, which changes from the first echo to the last echo (29th echo).

The decorrelation coefficient could also be calculated by using equation (2.38). The change of time window is achieved by modifying the echo numbers i. The maximum value of i is fixed at 29, since the ending of time window is always at 29th echo. The minimum value of i varies from 1 to 29. Then, the decorrelation coefficient in function of the minimum value of i could be obtained.

The blue stars in Figure 2.9 is the result of decorrelation coefficient calculated with the expression (2.38). In the figure, it is evident that the result of expression (2.38) match the result of decorrelation definition (equation (2.29)). This could verify that the expression (2.38) is correct.

In the theoretical expression (2.38), the decorrelation coefficient is only related to the emission signal and the term T. For the two simulated signals s_1 and s_2, there are corresponding transfer functions of detection zone. As in equation (2.8), the expression

of T_1 and T_2 consist of the transfer functions and acoustic parameters. However, the substrate thickness is not involved in the expression of T. This result could justify that the decorrelation coefficient does not depend on substrate thickness if the substrate is thick enough.

This consequence leads to other questions for the theoretical explanation of the instability of decorrelation coefficient with thin substrate and the value of substrate thickness after which the decorrelation coefficient could be independent of the substrate thickness.

For the theoretical expression of decorrelation coefficient (equation (2.38)), the cross terms in equation (2.33) is neglected. However, for the condition of thin layer of substrate, there is no reason to neglect the influence of cross term. This may explain why the decorrelation coefficient in Figure 2.7 is unstable with thin substrate layer.

The next thing to do is to study the influence of cross terms on the integration result (equation (2.35)). The influence of cross terms could be presented by the ratio between the cross terms and diagonal terms. As in Figure 2.8, the attenuation of each echo signal makes the diagonal terms much more important than the cross terms. For the same reason, the cross terms of two contiguous echoes also have much more influence to the result than the other cross terms. In this case, the cross/diagonal ratio could be simplified into the ratio between contiguous cross terms and the corresponding diagonal term (expression 2.40).

$$P_i(e_s) = \frac{\int s_{1,i}(t)s_{2,i+1}(t)dt + \int s_{1,i+1}(t)s_{2,i}(t)dt}{\int s_{1,i}(t)s_{2,i}(t)dt} \tag{2.40}$$

Where e_s is the substrate thickness. By this way, all the cross terms between contiguous echoes are considered. The critical substrate thickness could be defined as the thickness which makes the absolute value of $P_i(e_s)$ small.

With the equation (2.37), the expression of cross/diagonal ratio could be defined as expression (2.41).

$$P_i(e_s) = \frac{\sum_i IFT[a_0^2||S_0(\omega)||^2(T_1(\omega)T_2^*(\omega))^i(T_1+T_2^*)](\frac{2e_s}{v_s})}{\sum_i IFT[a_0^2||S_0(\omega)||^2(T_1(\omega)T_2^*(\omega))^i](0)} \tag{2.41}$$

Where v_s is the sound velocity in substrate. In equation (2.41), we have the cross/diagonal ratio in function of the substrate thickness. This result could be compared to the mean

decorrelation value in Figure 2.7. Figure 2.10 shows the trend of these two parameters in function of substrate thickness. When the cross/diagonal ratio is approach to 0, the decorrelation value is also stable.

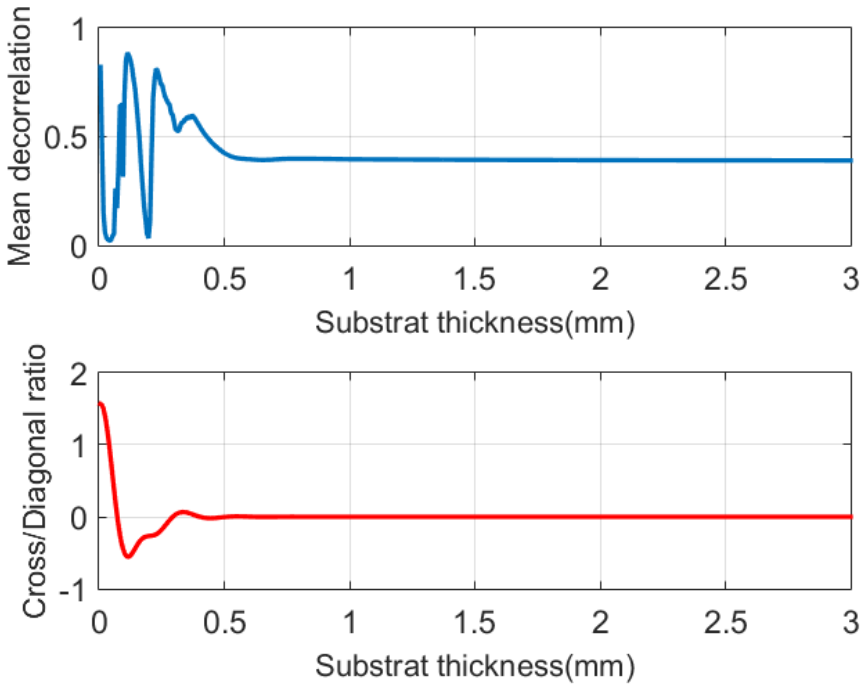

FIGURE 2.10 – Mean value of decorrelation coefficient and the cross/diagonal ratio in function of the substrate thickness.

2.7 Conclusion

The attenuation is not considered in this chapter. With the condition that the substrate is thick enough and the echoes of reflection in the substrate are totally separated, the expression of a reception signal in a multi-layer system (Figure 2.1) could be defined by the acoustic parameters, transfer function in detection zone and the emission signal (expression (2.10)). Due to the simulation by Impedance matrix, this analytical result could be validated (Figure (2.6)).

By using the analytical definition of reception signals, the decorrelation coefficient could also be defined by the acoustic parameters, transfer functions and the emission signal (expression (2.38) and (2.39)). This expression could be verified by calculating the decorrelation coefficient directly by the signals (Figure (2.9)).

Consequently, none of the useful result (the theoretical expression of received signal and the decorrelation coefficient) is related to the thickness of substrate. The presence of substrate will make the coda part last longer in signals and the acoustic waves will pass through the detection zone more times. If the substrate is thick enough, the thickness itself has few influence to the acoustic detection.

The decorrelation coefficient becomes unstable if the substrate thickness is small (Figure 2.7). This phenomenon is considered to be caused by the cross terms in the integration (equation (2.33)). A way to find the critical substrate thickness, which makes the decorrelation coefficient stable, is presented at last. The thicknesses of substrates used in the experiments in Chapter 3 and Chapter 4 are always at the interval that the decorrelation coefficient is stable.

Chapitre 3

Monitoring of cleaning procedure

In this chapter, two fouling cleaning procedures are studied. The first experiment is cleaning of wax deposit. This measurement is aimed at verifying the feasibility of coda wave detection of fouling. In this experiment, a piece of wax is used to simulate the fouling and a circulation of hot water is used to eliminate the wax fouling as a cleaning procedure. Acoustic measurements are applied during the cleaning of wax. And then, measured coda signals are used to verify the cleaning process. (This part is principally taken from the published article [152])

After studying the feasibility of coda wave detection by the wax cleaning experiment, we focus on the detection of real industrial fouling in the second part of this chapter. After all, testing real fouling is more convictive for practical applications. This time, whey protein deposit is chosen to be the fouling sample. This kind of protein deposit occurs frequently in the food industry, and the cleaning of protein fouling is an important procedure for the quality of product. Experimentally, as this research is aimed at the detection of fouling but not the cleaning technology, the protein deposit is cleaned by alkaline solution, which is a simple and effective way. Like in the first experiment, acquisitions of acoustic signals are executed during the cleaning procedure. And coda waves are used in the signal processing to monitoring the fouling states.

3.1 Wax cleaning procedure

A piece of wax is used to simulate a fouling layer. Flux of hot water is used to flush out the wax as the cleaning procedure. This cleaning process of wax is monitored by acoustic sensors to show the feasibility of the coda wave detection method. The difference between the monitoring results with and without wax is then discussed.

3.1.1 Materials and method

As evoked earlier in Chapter 1 and Chapter 2, acoustic signals can be measured experimentally to study the information in the specimen (medium in which fouling layer is to be characterized). Coda waves are a combination of waves that propagate along numerous paths and are difficult to separate. However, they are not random. If there is no change in the medium, there will be no change in the path of each scattered wave either. Conversely, if the state of medium is different, the paths of the scattered waves will change. Experimentally, a reference signal, which generally corresponds to an initial state, is measured. The signal is then measured after a change of the medium state and compared with the reference signal. Therefore, the evolution of a specimen can be monitored with good sensitivity by analyzing the evolution of coda waves at different times.

Most of the acoustic parameters frequently used such as time-of-flight and reflection coefficients, are difficult to extract from coda waves. Decorrelation coefficient representing the degree of dissimilarity in coda waves is therefore proposed to analyze the information carried by the coda. By using this indicator, the change of the medium can be fully characterized and quantified.

a) Presentation of the cleaning loop and positioning of the fouling deposit

In the experiment, a wax layer of controlled thickness was used to represent the industrial deposit in a cleaning loop (Figures 3.1 and 3.2) comprising two parts : a water bath and a rectangular duct made of stainless steel and measuring $51.5cm \times 11cm \times 0.8cm$. The top plate of the duct, which could be opened, was used as the substrate on which the wax layer was placed. Wax was chosen here as the fouling material essentially for practical reasons : it is soft, cheap, and easy to obtain. It melts easily when heated and solidifies

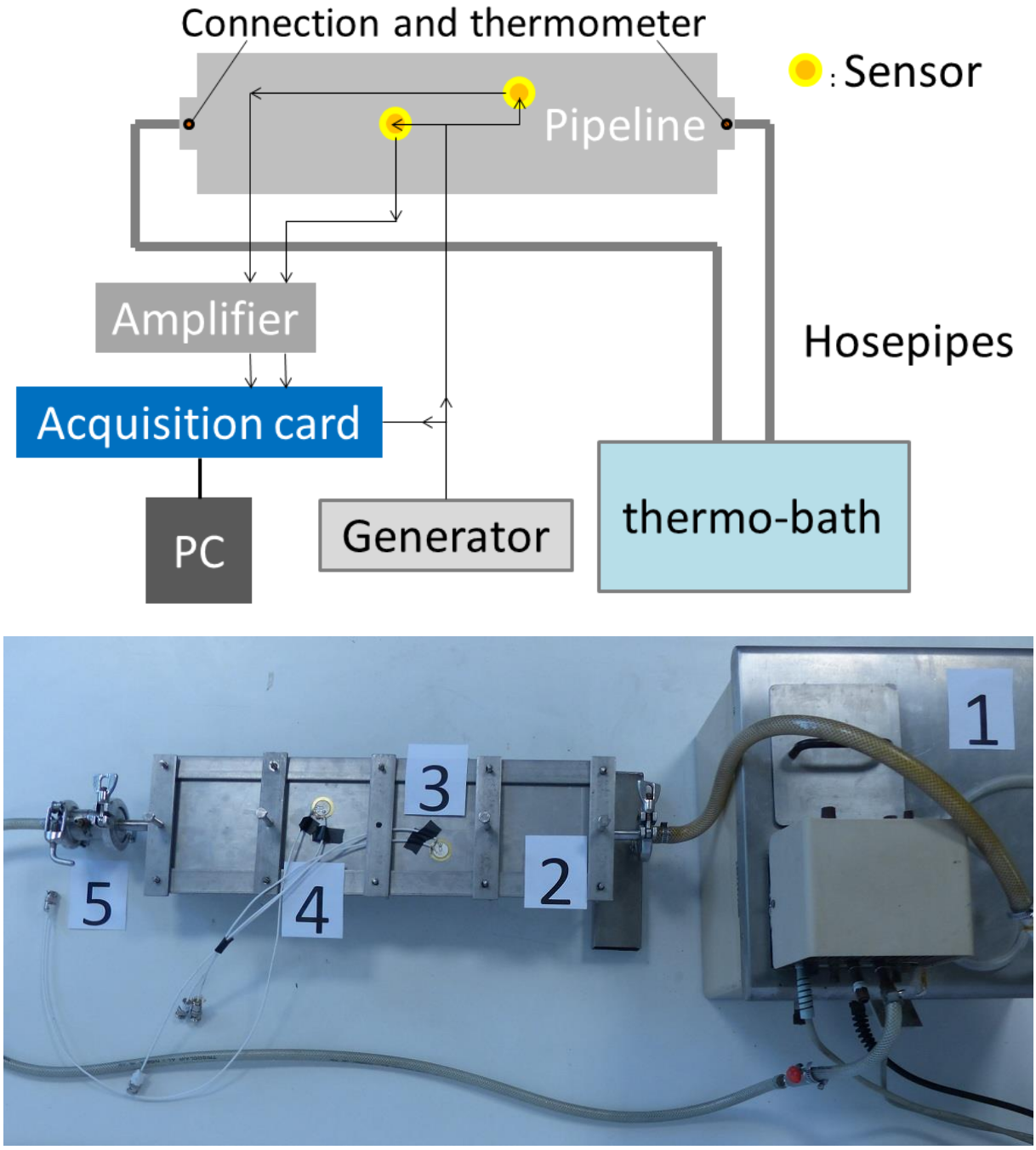

FIGURE 3.1 – Diagram of the monitoring system (top) ; Photo of the cleaning system (bottom), 1 : water bath ; 2 : duct ; 3 : measurement sensor with wax ; 4 : control sensor without wax ; 5 : connection of duct and hosepipe with thermometer

when cooled. A piece of wax can be placed on a clean substrate by solidifying liquid wax ;

the shape is easy to control mechanically during or after the solidification step.

The piece of wax was placed on the inner surface of the substrate as follows : after cleaning the substrate surface with alcohol and acetone, a rectangular mask consisting of a hole measuring 6 cm by 3.2 cm in a metallic plate 6 mm thick was put on the substrate and filled with liquid wax. After several minutes, the wax solidified and the mask was removed leaving a 6-mm thick rectangular piece of wax on the substrate. This represented the initial fouling state.

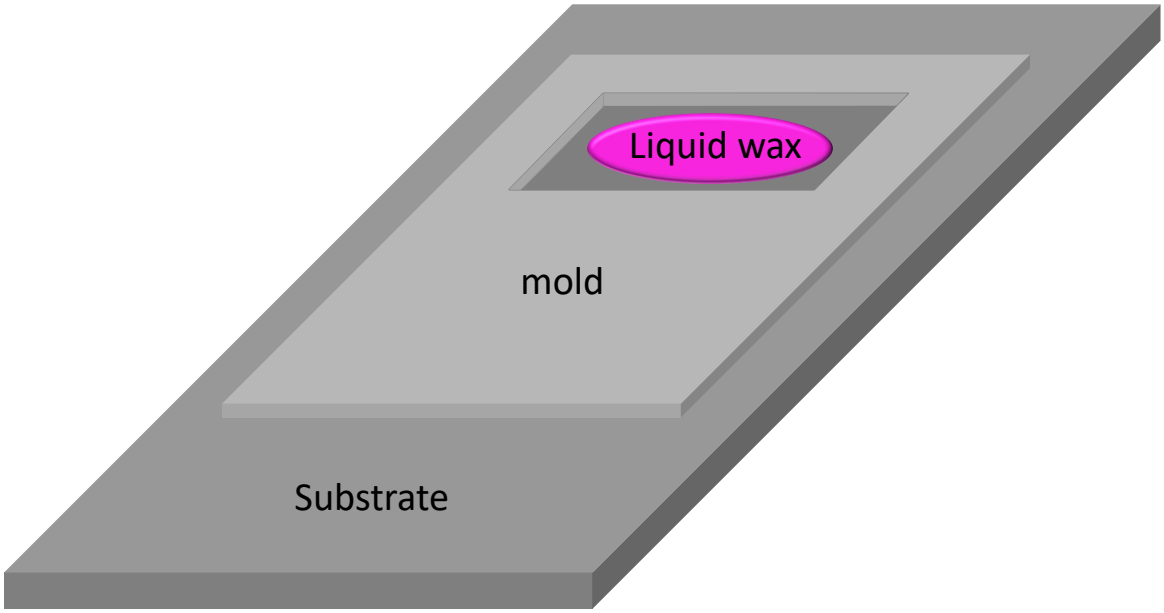

FIGURE 3.2 – Installation of wax

A water bath was used to heat the water and keep the cleaning water circulating inside the duct at a fixed temperature (70 °C here). The water flow was about 16 ml/s. The average circulation velocity was 18 mm/s. The bath and the duct were connected by hosepipes. The input and output temperatures were monitored using thermometers installed at both extremities of the duct. The cleaning process was monitored using acoustic sensors to show the feasibility of the CWI method as detailed below.

The signal acquisition system consisted of a laptop computer, an amplifier, an acoustic generator (Function / Arbitrary Waveform Generators, Keysight 33600A Series), a USB acquisition board (PicoScope 5000 Series), and two sensors (one for measuring the clea-

ning and the other used as a control) glued to the outer surface of the duct using a strong adhesive. The sensors used in the experiment were piezoelectric transducers consisting of two concentric active parts (Figure 3.3). The active inner part was for emission (ultrasound source). The other part was for acquisition (receiver). The generator created a pulsed signal of one sinusoid period that was sent to the emission transducers. The source transducer converted the electrical signal to an acoustic signal, which was emitted into the substrate. The acoustic waves propagated, reflected, and scattered inside the substrate, the deposit, and the duct. Part of these waves was intercepted by the receiving transducer and recorded using the acquisition board. There are 3 channels of acquisition board used in the experiment : one was used to monitor the source signal from the generator, and two were used to receive the signals from the sensors. The sampling frequency was 125 MHz. The amplifier was connected between the acquisition board and the sensors to amplify the signals received and filter out any low-frequency noise caused by the vibration of the support. The signal data in the acquisition board was transmitted to the PC for further processing (Figure 3.1).

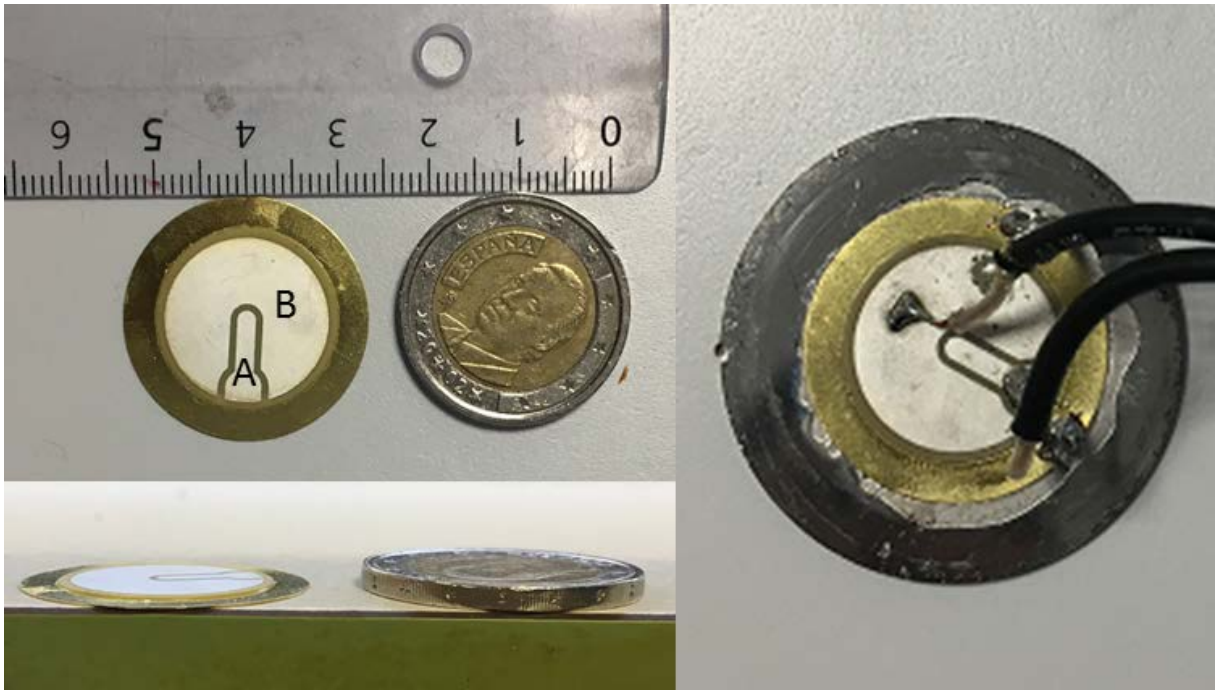

FIGURE 3.3 – Piezoelectric transducer consisting of two parts : Receiver (A) ; Source (B) ;

b) The cleaning protocol

The duct was cleaned with alcohol before each measurement. The wax was placed on the inner surface of the duct beneath sensor 2 (Figure 3.4). The physical parameters of the paraffin wax used were as follows : density 900 kg/m^3 ; Young's modulus 61.4 MPa ; sound velocity 1300 m/s [153]. After installing the wax, the duct was sealed and inserted in the water circulation loop at a slight angle and the cleaning process was started. This angle was designed to help the water flow and rapidly expel any air bubbles remaining in the duct. The temperature of the water bath was set to 70 °C. Simultaneously, the acquisition system started recording the data measured by the sensors. Sensor 2 was used to monitor the wax cleaning process. Sensor 1 recorded the data at another position without wax located upstream in the duct, which served as the control. The delay between two acquisitions was 15 seconds.

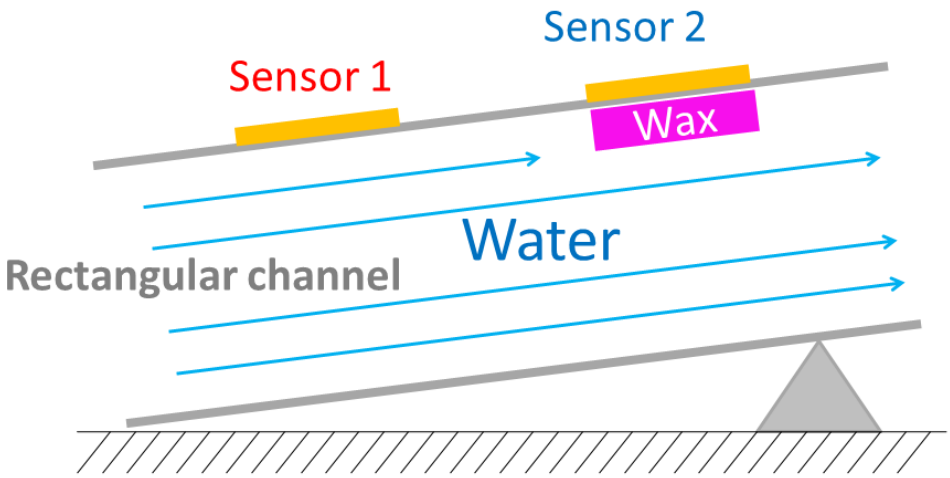

FIGURE 3.4 – Diagram detailing the inside and the outside of the duct. The hot water flows through the duct from left to right. A small support is placed under the right side of the duct to create a slight angle. Sensor 2 measures the evolution of the wax in the cleaning system. Sensor 1 records the data without wax as a control.

c) The wax cleaning process

The entire measurement sequence lasted for about 3 hours. During the measurement, two thermometers monitored the water temperature at the inlet and outlet of the duct.

There was a slight drop in temperature at the beginning, but it stabilized at 70 °C after 15 minutes. During that time, a lot of air was exhausted from the duct, which could have a negative effect on the measurement. Therefore, to ensure neither the temperature nor the air had an influence, the acquisitions at the beginning of the measurement were ignored. After acquisition, the circulation of the hot water was stopped and the duct was opened to visually confirm the result of the wax cleaning process. After each cleaning sequence, it was observed that the piece of wax on the inner surface had indeed disappeared.

In order to obtain further information on the dynamics of the wax cleaning, additional cleaning cycles were performed after replacing the stainless steel top plate of the duct with a transparent glass plate of similar dimensions. A video of the cleaning sequence was captured and the images were processed. In the video, it appeared that the wax had totally disappeared after about 2.2 hours.

After cooling down the circulating water, the wax dispersed in the water could be observed. This observation was expected as the cleaning process with hot water had progressively melted the wax in the duct, which then solidified as the water temperature decreased.

3.1.2 Experimental results

a) Ultrasonic signals of the measurement

Figures 3.5-(a) and 3.5-(c) show typical echograms received by sensors 1 and 2, respectively. Sensor 2 was located on the upper side of the surface fouled with wax while sensor 1 (control) was placed on the upper side of a clean surface.

For both sensors (Figure 3.5-(a) and Figure 3.5-(c)), it could be observed that the signal amplitudes of the direct waves were rapidly attenuated whereas the attenuation of the signal was more progressive for the coda waves.

The signals in the time window $[20\ \mu s - 22\ \mu s]$ are presented for both sensors (Figure 3.5-(b) for sensor 1 and Figure 3.5-(d) for sensor 2), which shows the coda wave signals in more detail. Each colored curve in Figure 3.5-(b) and Figure 3.5-(d) corresponds to an echogram obtained after a different period in the cleaning cycle : 0 hours (immediately after starting signal acquisition), 0.75 hours, 1.5 hours, and 2.25 hours. The signal to

noise ratio at [20 $\mu s - 22\ \mu s$] was about 30 dB (the ratio between the energy of this part of signal and the last part of signal), which was good enough for the analysis. Here, an average of 10 signals measured continuously was used to reduce the noise level for all the other signals recorded.

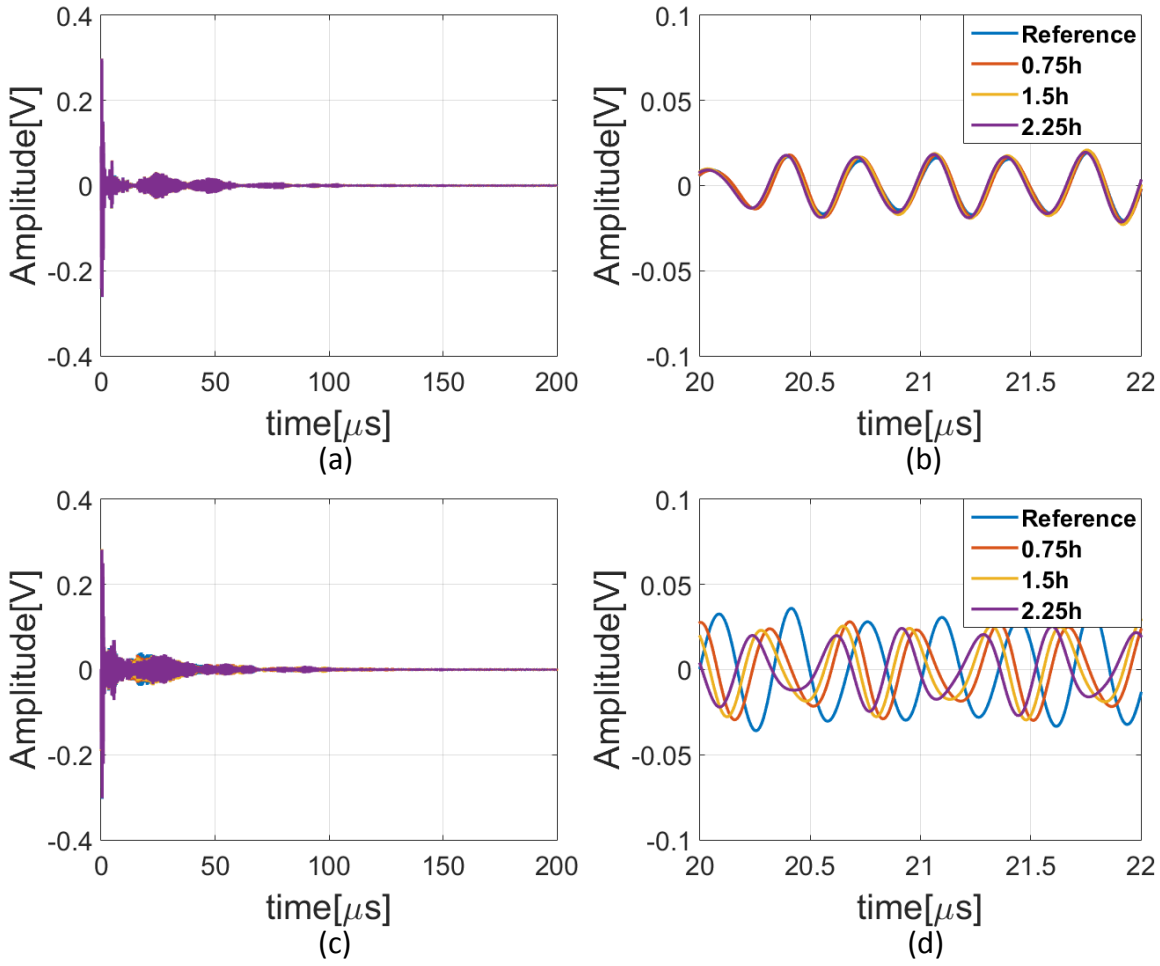

FIGURE 3.5 – Measurement signals with a 2 MHz - 5 MHz filter : entire signals of control sample (a) ; signals of control sample over the interval (20 $\mu s - 20.5\ \mu s$) (b) ; entire signals of wax cleaning process (c) ; signals of wax cleaning process over the interval (20 $\mu s - 20.5\ \mu s$) (d). The lines with different colors are the results acquired at different moments during the measurement. Blue : reference state ; Red : measured at 0.75 hours ; Yellow : measured at 1.5 hours ; Purple : measured at 2.25 hours

For sensor 2 (Figure 3.5-(d)), the signal varied in both amplitude and time shift ac-

cording to the stage of the cleaning protocol.

For sensor 1 (control), regardless of the period in the cleaning cycle, the signals looked very similar and could be superimposed. This trend was expected, as sensor 1 was placed on the upper side of a clean surface, the state of which was not supposed to change during the cleaning protocol. This result illustrates the fact that coda wave can show any change in the state of the sample, provided there are no other perturbations in the acoustic propagation field (temperature variation, flux variation, loud noise...).

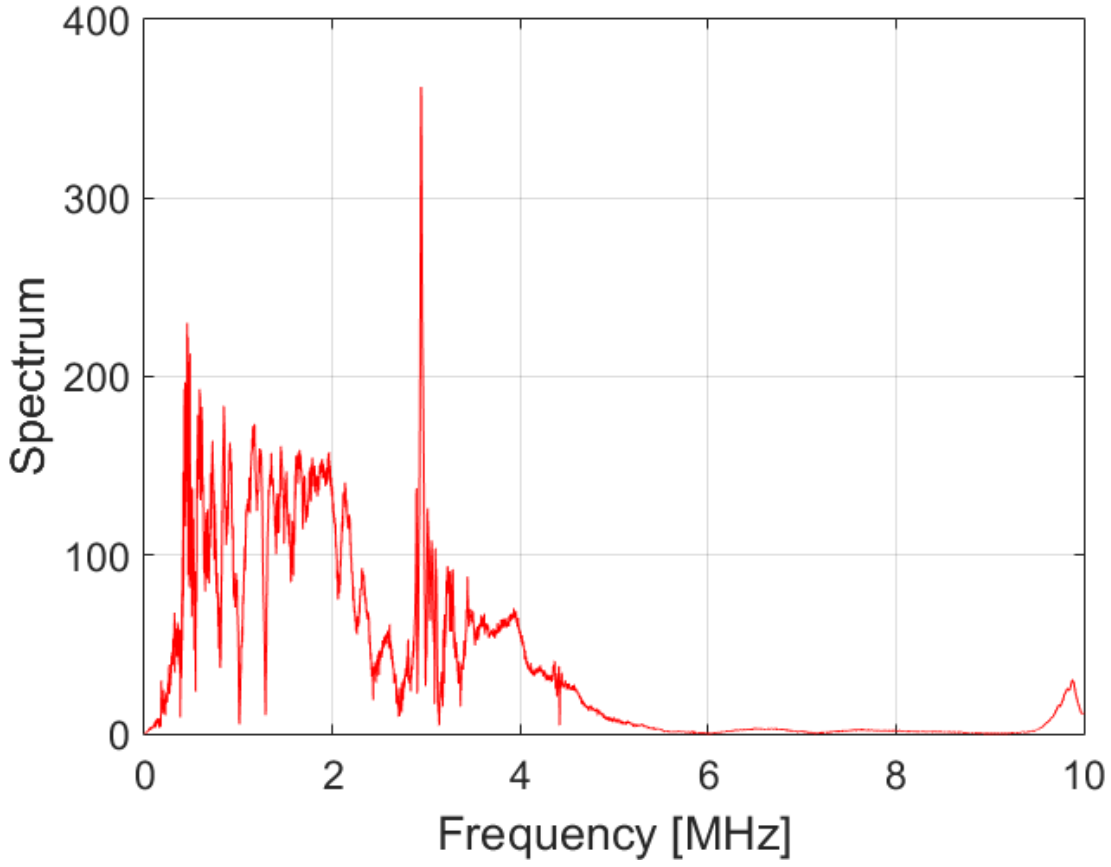

FIGURE 3.6 – Spectrum of signals received between 0 MHz and 10 MHz

For all the graphs in Figure 3.5, the sinusoid period of the source signal was 3 MHz. The aim of the band-pass filter was to adjust the sensitivity to the specific conditions and reduce the influence of noise. As the emission signal was a single sinus period, its spectrum was wide band. However, in the spectrum of signals received (Figure 3.6), there was only a narrow peak at 3 MHz, which is resulted by the interaction between the excitation

frequency band and the effect of substrate. The high-frequency bound of 5 MHz simply corresponds to the highest frequency in the received signal spectrum. The lower bound of the band-pass filter (2 MHz) was selected so that the central excitation frequency was 3 MHz. In addition, after testing several frequencies, the optimum decorrelation sensitivity was obtained for the band [2 MHz - 5 MHz]. The energy at low frequencies is usually come from the other undesired vibration on the transducer (surface waves, transverse waves, etc.).

b) The decorrelation coefficient with and without wax

The decorrelation coefficient was used as an indicator to quantify the evolution in fouling compared to a reference state. As highlighted before, the decorrelation coefficient provides a global overview of the dissimilarity between two signals. Here, the dissimilarity between the coda signals measured at time t and the initial state (fouled state) was computed and served as an indicator of fouling. In this work, 720 signals were recorded over about 2.75 hours, which corresponds to the duration of the cleaning protocol.

Only part of the coda signals was used to compute the decorrelation coefficients. Hence, five different time-domain windows of 10 μs wide were tested ($[0\ \mu s - 10\ \mu s], [4\ \mu s - 14\ \mu s], [8\ \mu s - 18\ \mu s], [12\ \mu s - 22\ \mu s], [16\ \mu s - 26\ \mu s]$) to find out which parts of the echogram were more sensitive to the degree of fouling. In our case, the width of the time window was 30 times the excitation signal period and the chosen band-pass filter was such that $\Delta f \cdot \Delta t \gg 1$, which fully satisfies the conditions mentioned in chapter 2. Figure 3.7 shows the evolution of the decorrelation coefficient for sensors 1 and 2 for the five different time-domain windows.

For sensor 2, the evolution of the decorrelation coefficient depends on the time-domain window used for the analysis. For the last three time-domain windows ($[8\ \mu s - 18\ \mu s], [12\ \mu s - 22\ \mu s], [16\ \mu s - 26\ \mu s]$), a drastic increase in the decorrelation coefficient with cleaning time was observed, then a plateau was reached. This increase in the decorrelation coefficient was correlated to the decrease in wax fouling. Furthermore, the fact that at that time the substrate surface was almost clean and all the wax in the duct had been washed away could explain the plateau.

Conversely, for the first two time-domain windows chosen ($[0\ \mu s - 10\ \mu s]$, $[4\ \mu s - 14\ \mu s]$), no increase in the decorrelation coefficient was observed during the cleaning

process.

Theoretically, the sensitivity of different parts of the coda waves varies because of differences in overall propagation distance in the specimen. In our case, it is clear that the time-domain window [16 $\mu s - 26$ μs] was more sensitive and likely to inform us of any change in fouling state. Conversely, the first two time-domain windows ([0 $\mu s - 10$ μs], [4 $\mu s - 14$ μs]) were not suitable for detecting any change in fouling state.

For the first two time-domain windows chosen ([0 $\mu s - 10$ μs], [4 $\mu s - 14$ μs]), the signals analyzed were very similar to the direct waves, so it is logical that the sensitivity was not remarkable and that the decorrelation coefficient did not evolve.

For sensor 1 (control), the decorrelation coefficient was relatively stable whatever the time-domain window, as expected.

The window selection corresponds to a compromise between sensitivity and signal-to-noise ratio. Indeed, the latter parts of the coda should theoretically correspond to a better decorrelation sensitivity. However, since the amplitudes are lower, the SNR is lower too, resulting in a mitigation of the sensitivity gain when using later coda windows. Figure 3.8 shows the sensitivities of the different parts of the signals. The width of the windows was 10 μs. The center of the windows shifts from 5 μs to 45 μs. The maximum decorrelation coefficient after 2.25 h was chosen as an indicator of sensitivity. From Figure 3.8, it appears that the time window [16 $\mu s - 26$ μs] corresponds to the best compromise. The oscillation of the maximum value after 20 μs comes from the narrow peak at 3 MHz in the spectrum (Figure 3.6). As mono-frequency signals, if 2 signals are in-phase the decorrelation coefficient will equal to 0, and if 2 signals are opposed-phase the decorrelation coefficient will equal to 2, which implies some periodicity in the received signals. On the other hand, the decrease of SNR will also rise the result, as explained above.

Hence, the decorrelation coefficients for sensors 1 and 2 have been plotted simultaneously on the same graph (Figure 3.9) using the time-domain window [16 $\mu s - 26$ μs].

In addition, several pictures extracted from the video at different times during the cleaning process are also presented to show the evolution in fouling over time. These pictures confirm that the evolution of the decorrelation coefficient is directly related to the substrate surface state.

Of course, it was not possible to ascertain that the two cleaning processes for the two

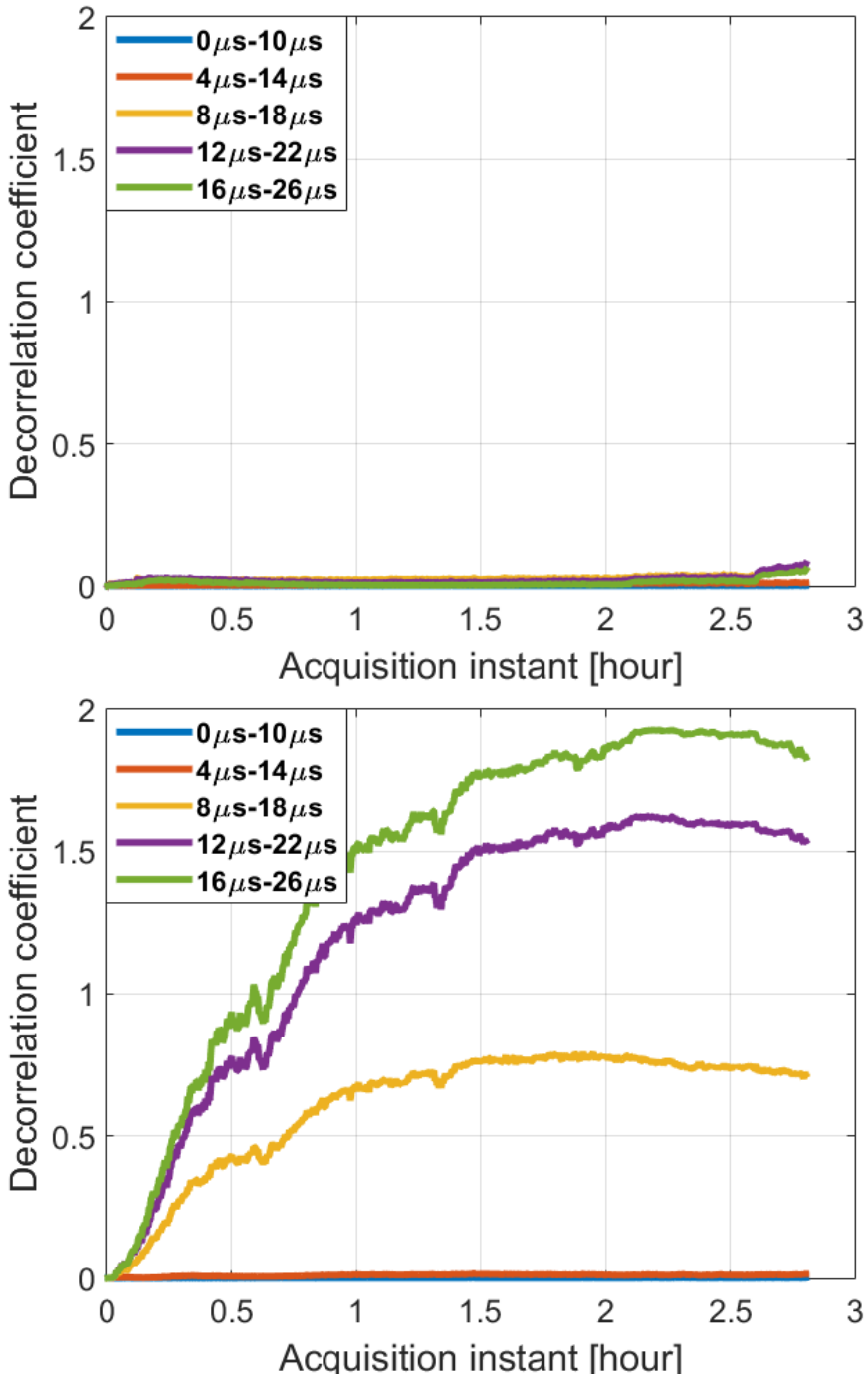

FIGURE 3.7 – Decorrelation coefficients : control sample (top) and wax cleaning process (bottom) ; The different colors represent the decorrelation coefficients of the signals within different windows. Blue : 0 $\mu s - 10$ μs ; Red : 4 $\mu s - 14$ μs ; Yellow : 8 $\mu s - 18$ μs ; Purple : 12 $\mu s - 22$ μs ; Green : 16 $\mu s - 26$ μs ; The sensitivity of the decorrelation coefficient depends on the window. The later the signal used, the higher the sensitivity of the result.

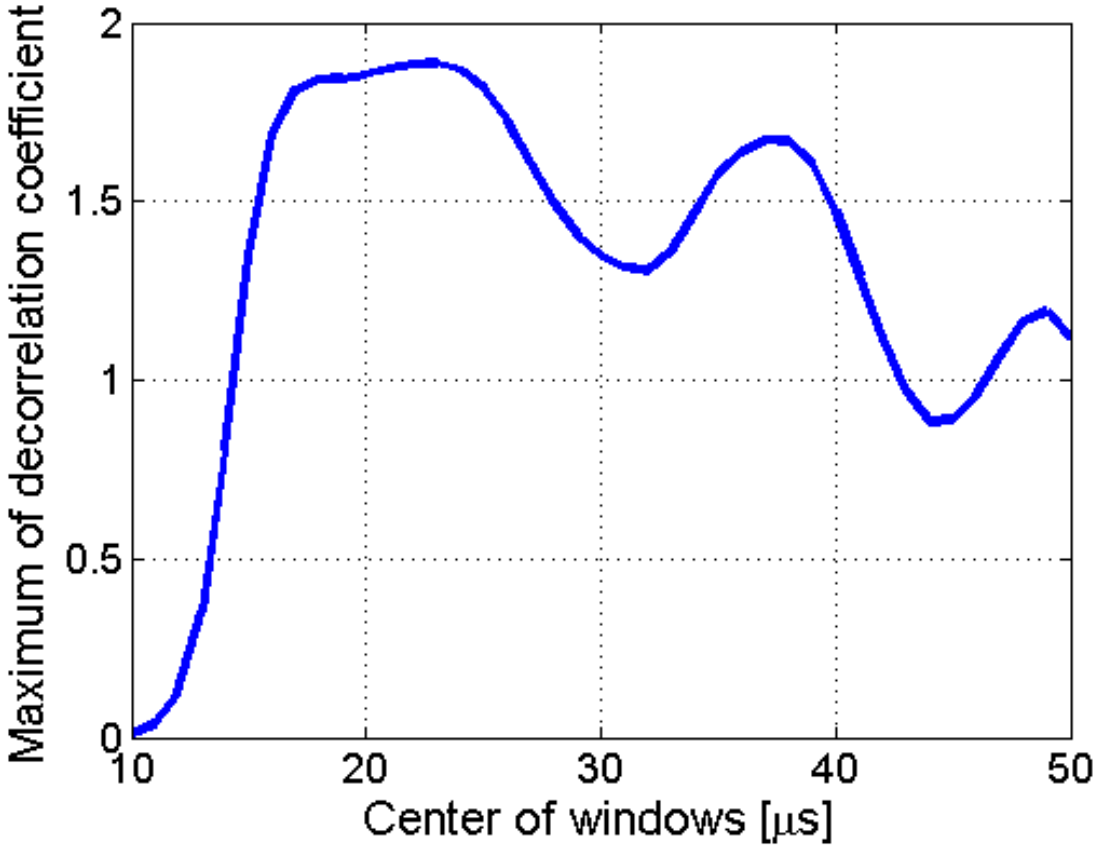

FIGURE 3.8 – The stable value (maximum value) of the decorrelation coefficient as a function of the center of the windows. The windows are always 10 μs wide.

similar ducts were rigorously identical, as the adhesion properties of wax on glass and on stainless steel plates could be different. In addition, slight variations in flow could have led to differences in the elimination process of the wax. However, the digital images obtained with the transparent duct are still pertinent and give an idea of the evolution of fouling over time.

Figure 3.9 clearly illustrates the capacity of the proposed monitoring tool to capture the evolution of the fouling state.

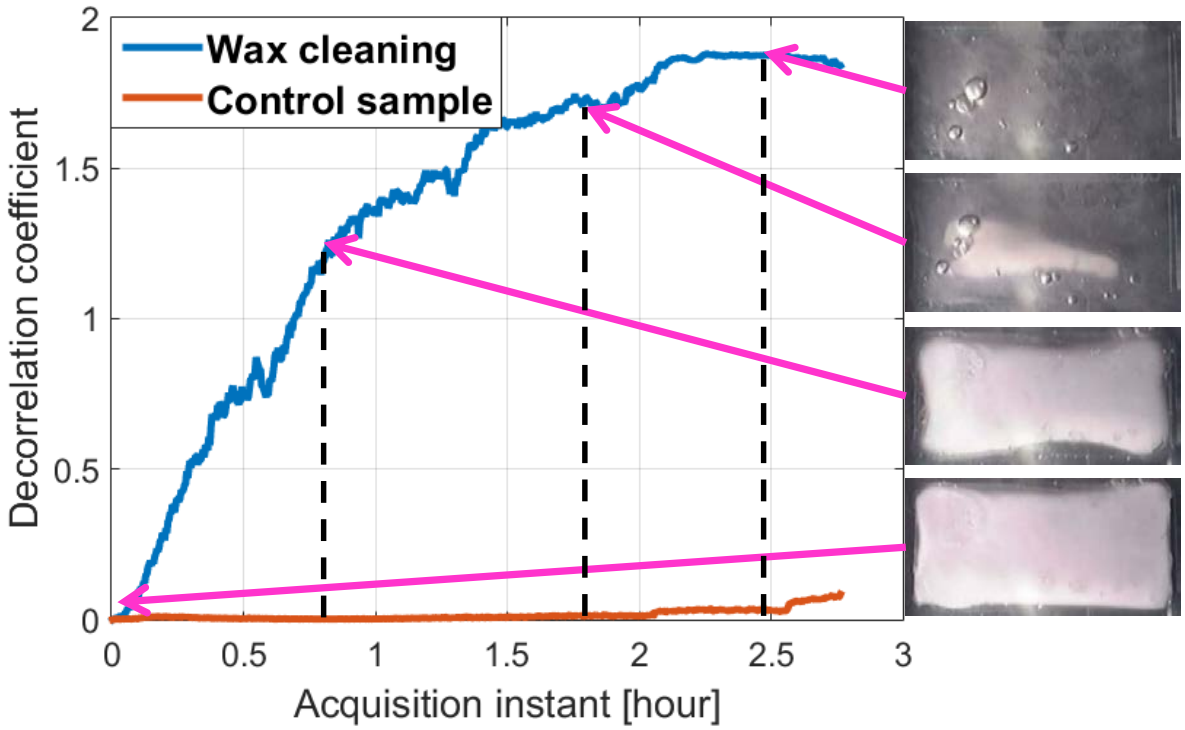

FIGURE 3.9 – Decorrelation coefficient curves : control sample (red) and wax cleaning process (blue) for the window 16 $\mu s - 26$ μs. Photo of wax at different moments (right, from bottom to top) : reference state, state at 0.8 h, state at 1.8 h, state at 2.5 h.

3.1.3 Discussion

In this section, an ultrasonic method based on Coda Wave Interferometry for monitoring the cleaning of fouling deposits on stainless steel ducts is presented. This method shows that the evolution of fouling can be captured non-invasively in an opaque channel.

Two sensors were installed to ascertain the feasibility of this innovative method, presented here for the first time. Sensor 2 was used to monitor the wax cleaning process, while sensor 1 was used as a control, with no wax deposit in the detection area.

The decorrelation coefficient was used as an indicator of a change in the acoustic signal during the cleaning process. The variation in the decorrelation coefficients obtained with the control and during cleaning is clear. A valuable advantage of this method is the capacity to adjust the sensitivity. Indeed, both the band-pass filter and the time-domain window chosen for the analysis have a direct influence on sensitivity. By adjusting

these parameters, the correct sensitivity to achieve accurate detection according to the conditions can be obtained. Moreover, there are no critical requirements concerning the quality of the sensors. Hence, the cost would be low.

In the following parts, the suitability of the method to follow the elimination of whey protein deposits in the dairy industry and the formation of biofilms will be addressed.

3.2 Cleaning of protein deposit

Proteineous deposit are very common in the milk industry and their composition (mineral and organic) are significantly different from wax which contains only organic compounds.

The preliminary result concerning wax cleaning monitoring by coda wave interferometry revealed satisfactory but additional and further trials are required to convince definitively dairy industry that basic principle reported by coda wave interferometry could be transposed to detect end of cleaning of surface fouled when heat processing dairy derivatives. So additional cleaning tests with proteineous deposits were decided and monitoring carried out by coda wave interferometry. The fouling deposit is made of whey protein built up off line on a substrate.

For these additional cleaning tests, the cleaning conditions are fully different than previous one for wax cleaning. Indeed cleaning agents inducing chemical reactions were used (basic detergent is used instead of water). Moreover the cleaning mechanisms are far away from the previous one since detachment of the wax deposit is driven by melting consideration whereas destruction of the proteinaceous deposit is known to be governed by chemical reactions, leading to its dissolution.

Two main questions were addressed in our work : is the principle of coda wave interferometry for monitoring cleaning is still valid ? What is the difficulty of the monitoring method for such application ?

The material and method for the fouling/cleaning tests will be presented in this section. Then, the monitoring results regarding the detachment of deposit will be discussed.

3.2.1 Materials and method

a) Cleaning protocol

The monitoring of cleaning by acoustic waves interferometry for proteinaceous deposit is observed in a tube (Figure 3.10) instead of a channel with a rectangular cross section. A stainless steel plate on which a layer of proteinaceous fouling adheres is located on the outer lateral wall of the tube. The deposit is in contact with the flowing detergent (process side) whereas the acoustic sensor is installed on the outside surface of the stainless steel.

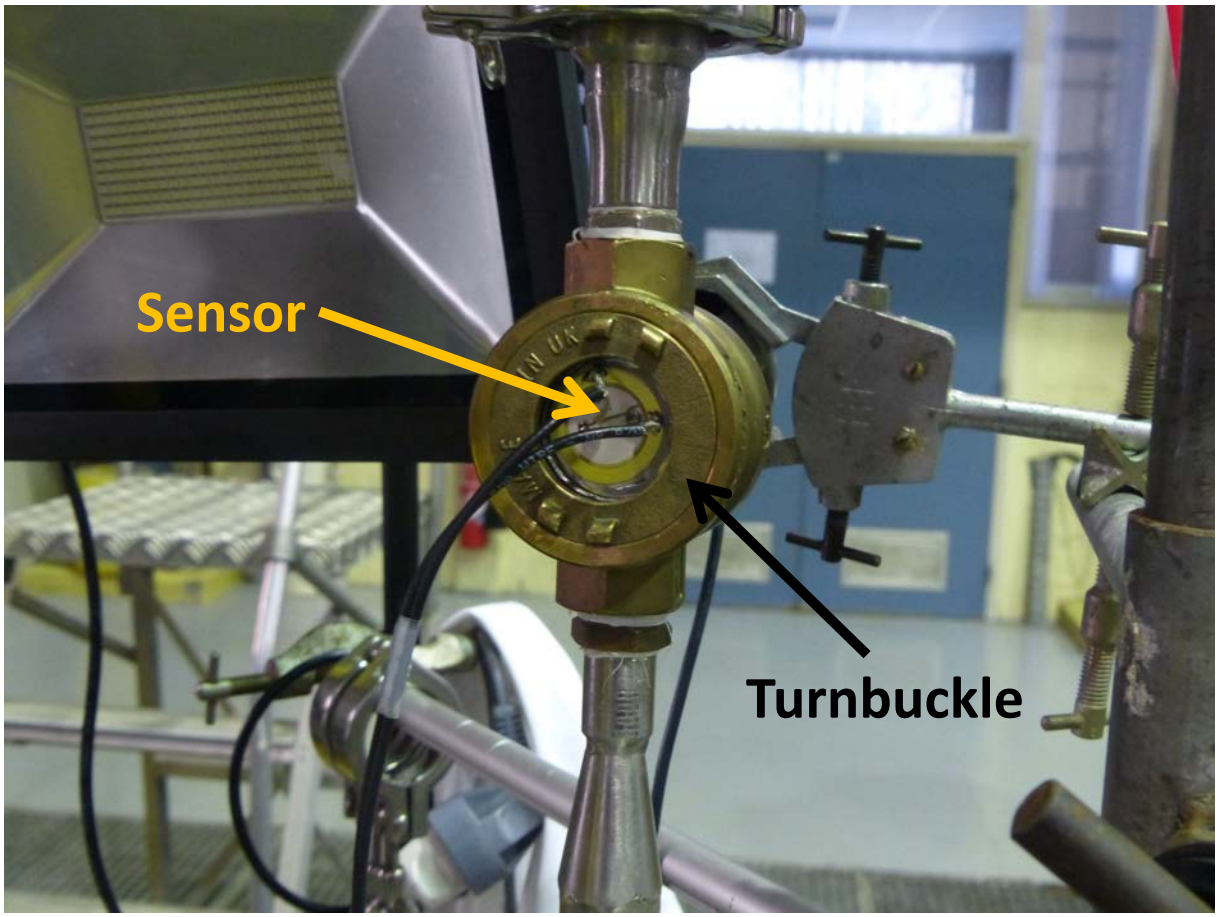

FIGURE 3.10 – Views and sketch of the sensor embedded in the tube containing the fouled substrate

On the opposite lateral surface of the tube (in front of the sensor device), a transparent surface in glass exists. This transparent substrate is used for a optical observing of the deposit detachment when cleaning.

The tube (with fouled substrate and sensor) is connected to a Cleaning In Place (CIP) loop. This CIP device can achieve a detergent circulation (either water for rinsing or sodium hydroxide solution -NaOH, strong alkaline- as cleaning agents), circulating through the tube, containing the fouled plate at given temperature and flow rate.

A schema of CIP loop is presented in Figure 3.11. The circulation of detergent liquids in the cleaning loop is delivered by a pump, maintaining a constant flow rate. The inlet circulation temperature of detergent is ensured by a heating loop. When there is a need of changing the cleaning liquid (from water to sodium hydroxide solution or inverse) in

order to progress in the cleaning sequence, the inlet connection was switch to the adequate cleaning agent storage tank.

A by-pass valve allows the detergent to pass either in the fouled tube or to cut off the circulation in the fouled tube for a while. This device is required to make sure that the cleaning of the fouled tube occurs under permanent regime.

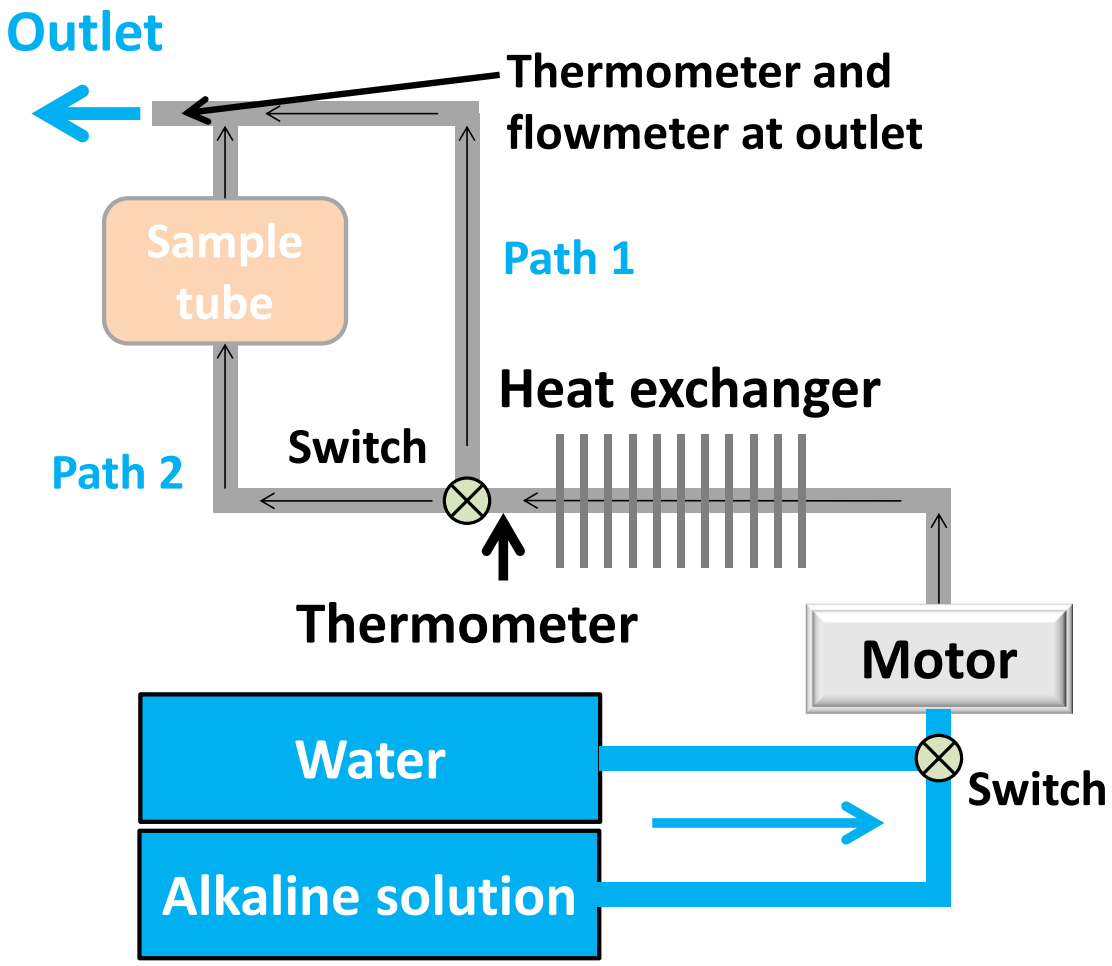

FIGURE 3.11 – Schema of cleaning in place loop : a given cleaning liquid (water or soda) is stored in a tank and the circulation is launched, vehiculated by a pump. Then the cleaning liquid passes through a heat exchanger and continue to either Path 1 (outlet directly) or Path 2 (fouled tube - outlet). A flowmeter and two thermometers (inlet/outlet) are installed in the cleaning in place loop to monitor cleaning process parameters (flow rate and temperature)

b) Preparation of protein fouling

For preparing the fouled substrates, a tube placed in a thermostatic enclosure Figure 3.10 is used. This tube is in fact a substrates-holder filled with foulant protein solution. In our case, a round wafer made by stainless steel is used as coupon. The diameter of this substrate is 41 mm and the thickness is 0.9 mm.

The foulant protein solution (5% whey protein solution) used in these experiments is prepared by the following steps :

1. Concoction of 5% whey solution
   Put 100g whey powder (PROMILK 852 FB1) into 2L reverse osmosis water.
2. Adjustment of the calcium rate at 500ppm
   Add 1.88g $CaCl_2$ (pureness : 96%) in the solution.

The temperature inside the thermostatic enclosure is set at about 80 °C. The sample tube is mounted on a rotating device (Figure 3.12). This rotating device keep the tube rotated at a constant angular velocity (the period is about 2s), so that the whey solution in the tube can generate a layer of protein fouling uniformly.

During the fouling formation in the thermostat cabinet, whey protein deposit build up and a depletion in protein occurs in the foulant solution. So, for this batch process, the whey solution need to be manually renewed in order that the fouling formation could be continued. Practically, about every 1 hour, the sample tube is taken out from the thermostat cabinet and the operation of renewing whey protein solution is performed. Then, the tube is resealed and reinstalled in the thermostat cabinet to continue the fouling formation. For the whole fouling formation operation, the whey solution in the sample tube is renewed 4 times. The entire preparation of protein fouling deposit takes about five hours.

Finally, a layer of protein fouling is successfully generated on the substrate of sample tube (Figure 3.13). This protein layer adhering on the substrate will be used for the next steps : cleaning monitoring. Even through the structure and the form of fouling layers is not rigorously repeatable and are likely to induce a slight change in cleaning course, but the the monitoring of fouling cleaning could be achieved anyway which was our purpose.

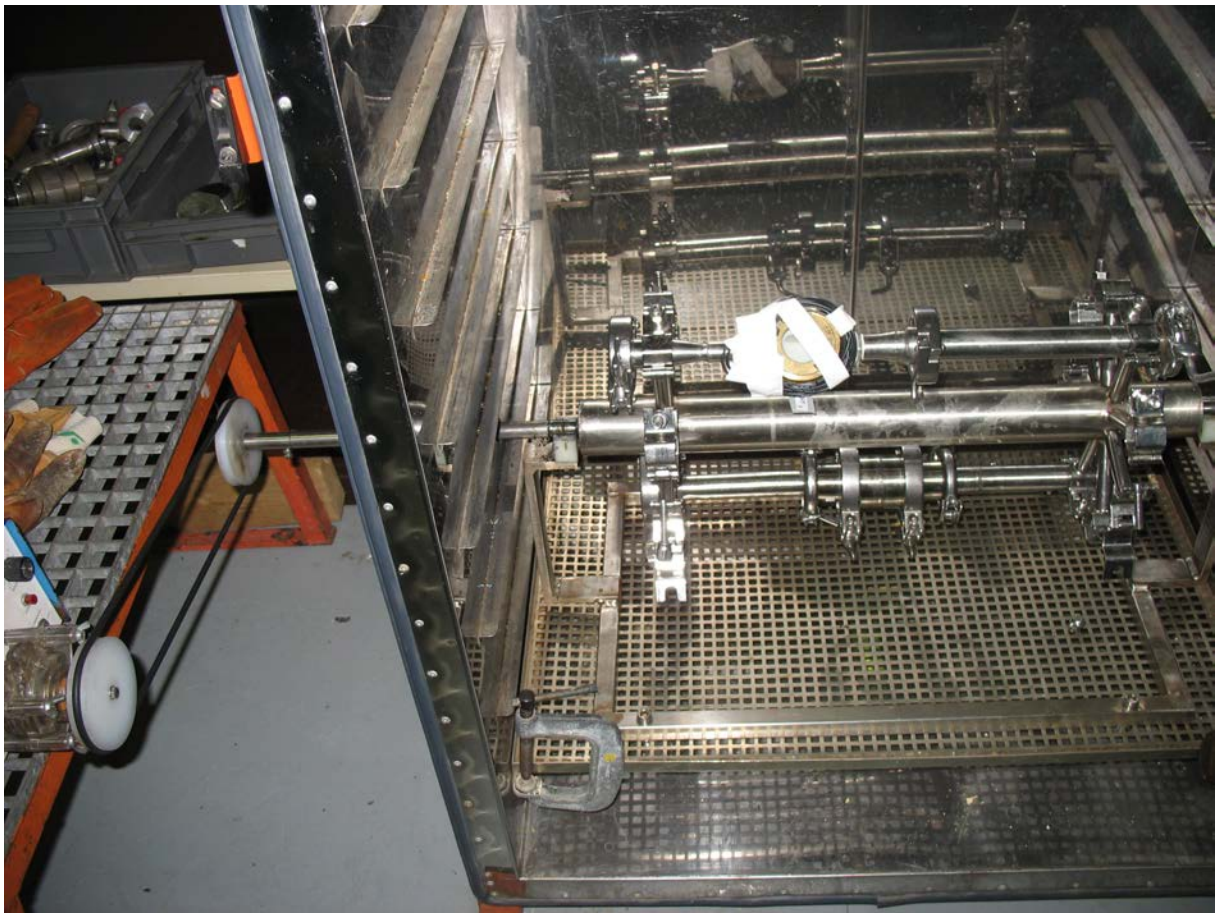

FIGURE 3.12 – Thermostat cabinet for the fouling formation

c) Operation of cleaning and acquisition of signals

After installing the fouled sample tube in the pilot, the circulation could be started in the pilot. The paths of entire pilot are complex with many turnings. Consequently, these turnings lead to a problem that lots of air bubbles may stay in the canalization after the start circulation. These air bubbles usually adhere loosely on the inner surface of pilot and they could leave the wall at any time.

As is known to all, the existence of undesired air in acoustic propagation field will cause an impact on the result which cannot be ignored for acoustical measurements. Thus, we need to be sure that there is no air in the pilot before launching the acoustic acquisition. So, at the beginning of each experiment, a circulation of water with strong flow rate is applied on the pilot to eliminate the air in the pilot.

FIGURE 3.13 – Protein fouling layer formed on the substrate

After the elimination of air, a circulation of water at a given temperature (50 °C) and a given flow rate (100 L/h) is launched in the pilot continuously. A sufficient quantity of sodium hydroxide solution at a concentration of 1% is prepared to replace the water as a cleaning liquid for the fouling cleaning. This condition is chosen for that the time of cleaning is less than 30 minutes.

The substrate fouled with whey protein (Figure 3.13) is installed on one of the plane surface of the sample tube. The sensor is on the outside surface of fouled substrate with a strong adhesive and connected to the acoustic acquisition system. On the other plane surface of sample tube, the installed substrate is a clean transparent substrate (which is made of glass). This transparent substrate is used for an optical observing.

The acoustic sensor on the fouled substrate is connected to an acoustical acquisition system (Figure 3.14). This acquisition system consist of 3 parts : Acoustic Generator,

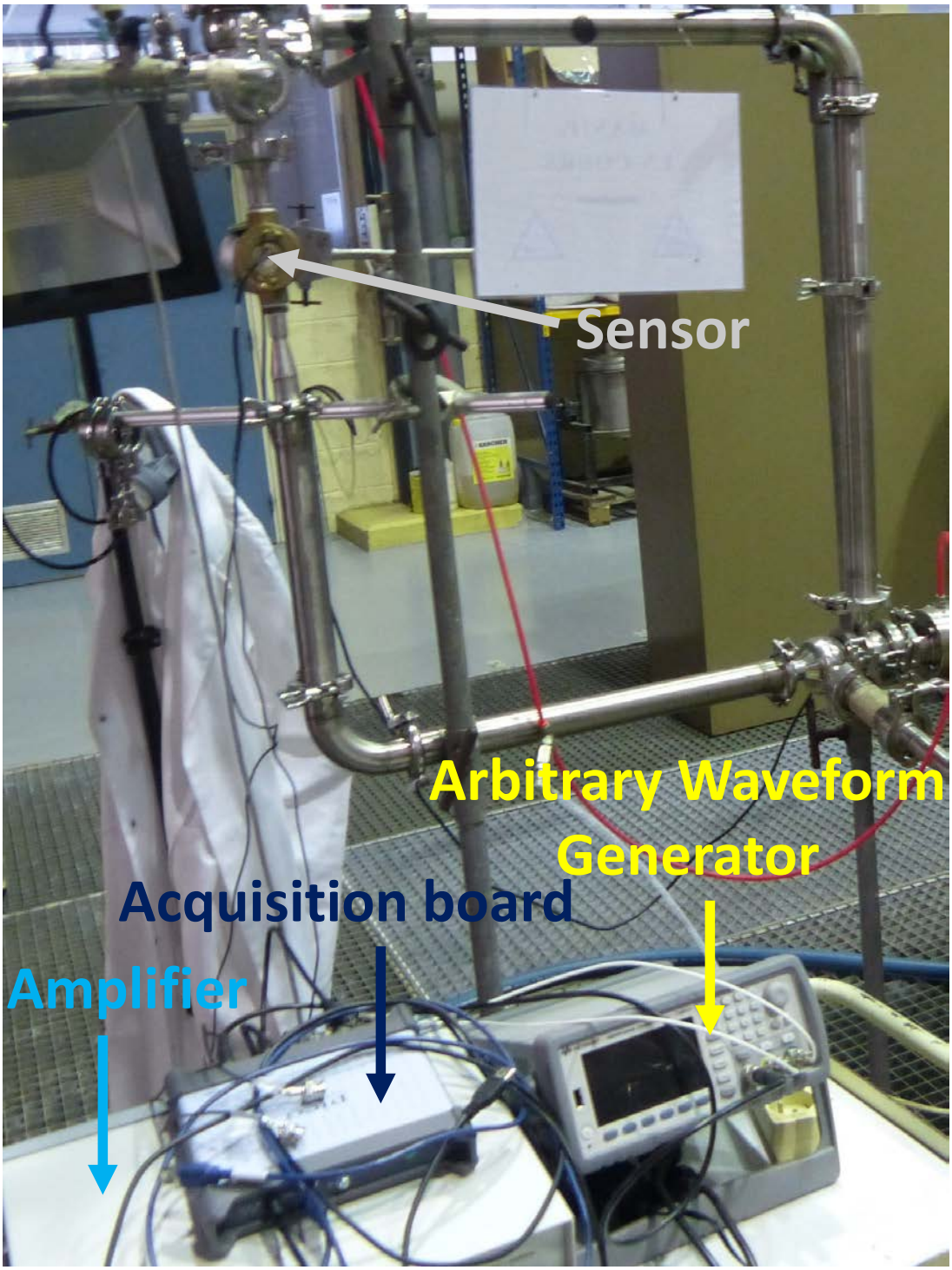

FIGURE 3.14 – Photo of acoustic acquisition devices with pilot ; (Piezoelectric sensor, Amplifier, Acoustic Arbitrary Waveform Generator, Acquisition Board)

Acquisition Board, Amplifier. The acoustic sensor used in this experiment is the same as in the previous work (experiment with wax).

Experimentally, the emission transducer will transform the electrical signals (which are received from generator) to acoustic waves (longitudinal waves), and send them into the test area. After propagations along numerous paths in the substrate and the tube, reflected acoustic waves are received by the reception transducer. The reception transducer will turn the acoustic waves into electrical signals and send them to the acquisition board (Figure 3.15).

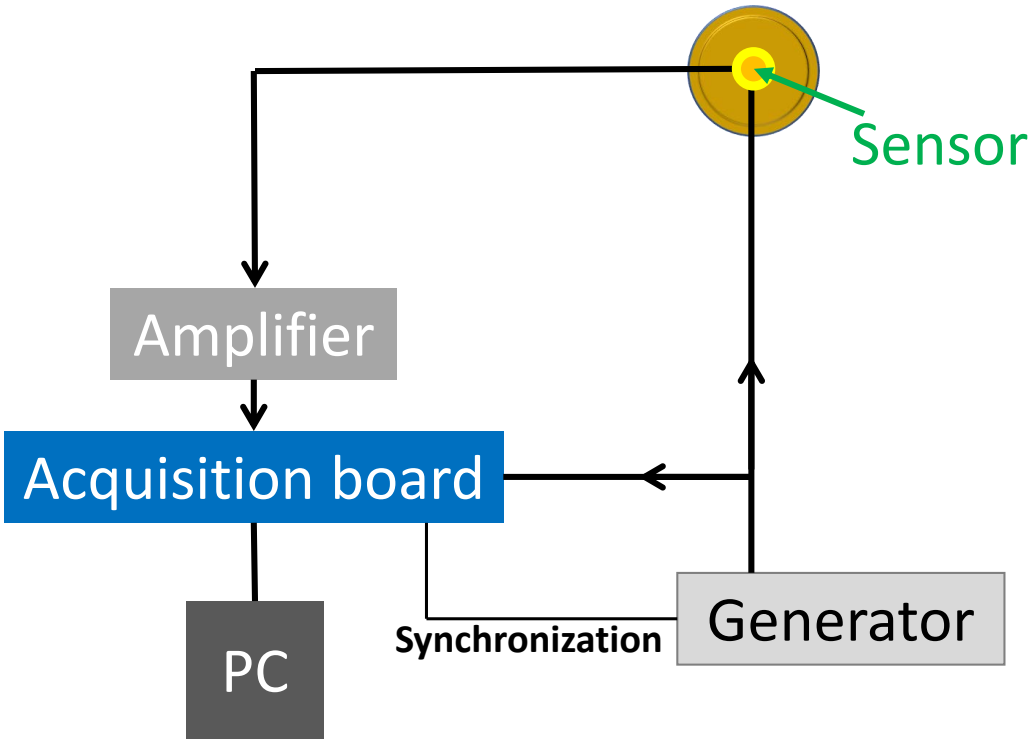

FIGURE 3.15 – Schema of acoustic acquisition system

In this experiment, the acoustic generator used in the acquisition system is 'Function / Arbitrary Waveform Generators, Keysight 33600A Series', which is able to generate arbitrary signals in high frequency band. One period of sinus signal at 10 MHz is used as the emission signal for all the measurements.

The acquisition board is 'PicoScope 5000 Series', which is used for recording the signals received by sensor (reception part). This acquisition board can be connected to a PC

with a USB interface. By communicating with PC, the acquisition parameters (sampling frequency, synchronization set up, time interval between different acquisitions,etc.) could be defined and the acquired signals could be stored on hard disk permanently. In this experiment, the sampling frequency is set to 125MHz. The acquisition is always synchronized with the emission of acoustic waves by using a connection between the acquisition board and acoustic generator. The time interval between different acquisitions depends on the particular needs.

In order to decrease the influence of ambient noise, each record of signal is an average of a certain number of measurements at a short duration. In this experiment, the average number is set as 100. For each acquisition, the acquisition board will execute 100 measurements continuously within a short duration and store the average of these 100 signals as the final record of this acquisition.

2 channels on the acquisition board are used for the acquisition in measurements. One channel is for the measurement of emission signals, which is connected directly to the acoustic generator/emission part of transducer, giving the real acoustic emission waveform. The recording of signals measured by the reception part of sensor is executed through the other channel.

The reception transducer and the acquisition board is not connected directly. A amplifier is installed between them to amplify the received signals. The amplifier used in this acquisition system is able to support the amplification of signals in high frequency (the upper limit is higher than 20MHz which is enough for this experiment). As there is so much attenuation and many reflections/transmissions in the acoustic propagation field, the received acoustic signals may be too weak for the recording and analyzing. With this amplifier, the amplitude of recorded signals could be within a suitable interval. Another function of the amplifier is the filter. Signals which are not interested in the experiment (such as the vibration of support, low frequency noise, etc.) will be filtered out by the amplifier.

In the sample tube, the acoustic waves sent by the transducer will propagate through the substrate and enter the detection zone perpendicularly. The detection zone is the field after the substrate, which is the flowing liquid with (or without) an additional layer of whey fouling deposit (Figure 3.16). The acoustic waves will propagate arbitrarily in the detection zone (or propagation field) and return to the reception transducer by passing

through the substrate.

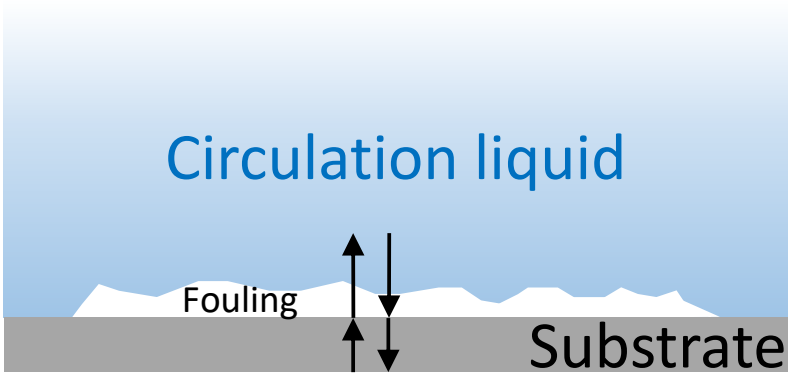

FIGURE 3.16 – The detection zone of this implementation in the experiment

While the installation of pilot and acoustic monitoring system is complete, the circulation could be applied on the sample tube and the cleaning process could start. The acoustic acquisition will also start to monitor the cleaning process.

The initial state of sample tube is as in Figure 3.17. One surface is a clean transparent substrate. The other surface is the stainless steel substrate with prepared whey protein fouling.

Water and sodium hydroxide solution is used as two kinds of circulation liquid in the experiment. When the sodium hydroxide solution passes through the samples tube, the whey protein fouling could be eliminated effectively because of the intense chemical reaction between sodium hydroxide and whey protein. On the other hand, there is no reaction between water and whey protein at all. So, the whey protein fouling will not change when water is used as the circulating liquid.

In order to make the experiment evident and to study how the different fouling behavior affect the acoustic indicator, the whole cleaning process could be classified into 3 principal steps :

— Pre-cleaning rinsing

— Cleaning

— Post-cleaning rinsing

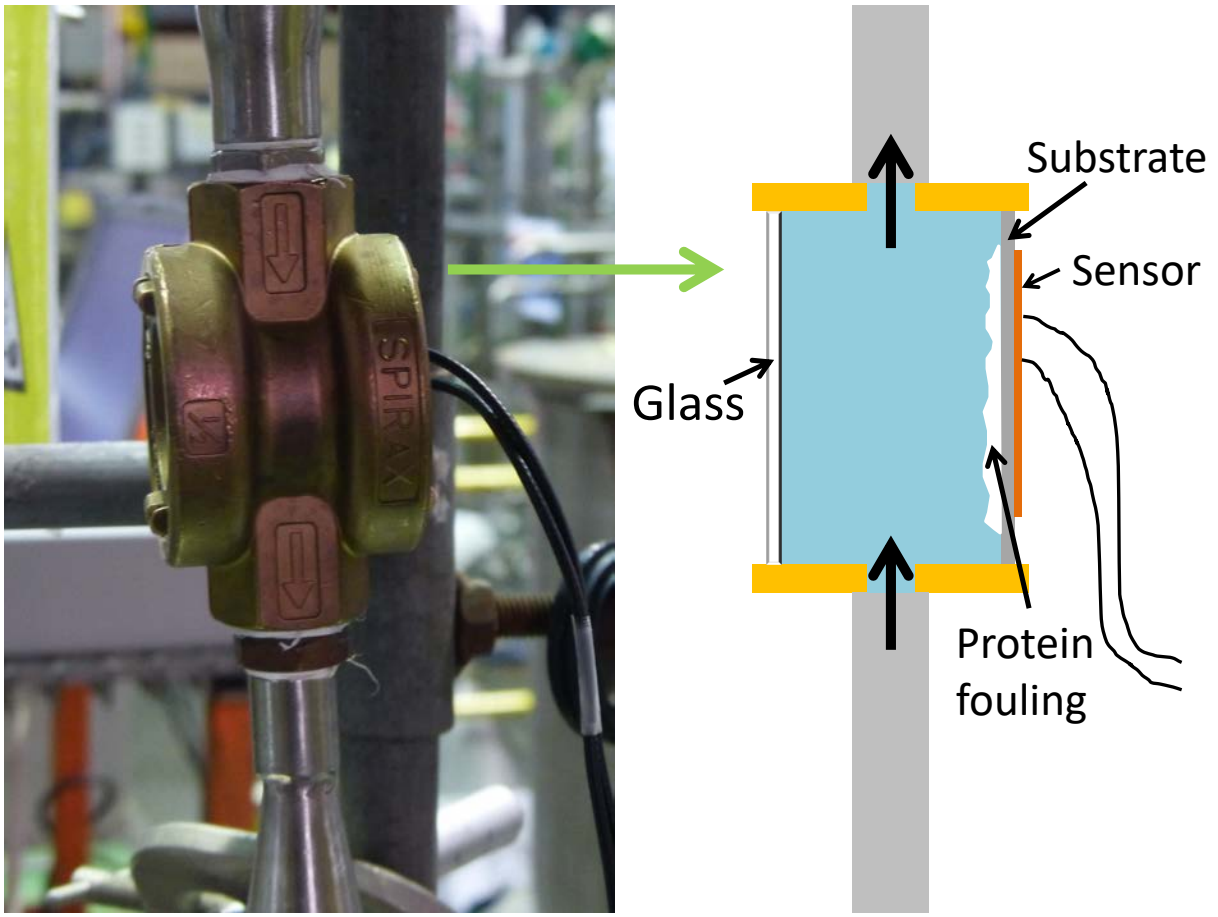

FIGURE 3.17 – The circulation in the sample tube

The first step 'Pre-cleaning rinsing' is a rinsing before eliminating the fouling. At this step, water is used as the circulation liquid. The circulation in the pilot will be switched to the sample tube (Path 2). At the same time, the acoustic acquisition is carried on to monitor the fouling behavior. And the monitoring of temperature and flow rate has also been executed to ensure that there is no influence in the sample tube caused by the variation of these two parameters. This rinsing step lasts for 10 minutes. Then the switch of circulation in the pilot is turned to the other path (Path 1) and the flow in the sample tube stop. The acoustic acquisition, temperature monitoring and flow rate monitoring are also finished. It has been verified visually through the transparent substrate that there is no change in the fouling during the circulation of water. 100 acquisitions are executed during this step. The time interval between each acquisition is about 6 seconds.

The second step 'Cleaning' is to eliminate the whey protein fouling by sodium hy-

droxide solution. As the circulation liquid of this step (sodium hydroxide solution) is different from the first step (water), the first operation on the pilot is to change the circulation liquid correctly. Practically, the storage of circulation liquid which connected to the pump (as presented in Figure 3.11) is change to the storage of sodium hydroxide solution, so that the input liquid of pilot could be change to the sodium hydroxide solution. Then the water in the pilot will be slowly discharged and finally replaced by the sodium hydroxide solution. Mention that the switch is always stay at Path 1 during the operation of changing circulation liquid, so that the fouling in the sample tube will not be influenced by this operation. After the pilot is filled with sodium hydroxide solution, the circulation returns to a stable state and the operation of changing the circulation liquid is finished. At this moment, the cleaning of whey protein fouling is ready to start. The switch is turned to the sample tube (Path 2) and the thermometers and flowmeter start to record the temperature and flow rate variation in the Path 2. The acoustic acquisition is also applied on the test sample to monitor the cleaning process.

The sodium hydroxide solution has a good effect in eliminating whey protein fouling. In fact, during the circulation of sodium hydroxide solution in the sample tube, the elimination of fouling is evident and it could be confirmed visually through the transparent substrate.

The whole cleaning step lasts for about 35 minutes while all the fouling on the substrate is totally cleaned. The number of acquisitions is also 100. The time interval between acquisitions is then about 20 seconds.

The last step 'Post-cleaning rinsing' is a rinsing after eliminating the protein fouling. In this step, water will be reused as the circulation liquid and the circulation is the same as first step. The circulation liquid is changed back to the water and the rinsing step could start. The switch is turned to Path 2 and all the monitoring systems begin to record data (temperature, flow rate and acoustic signals). This step also takes 10 minutes for the measuring respecting the first step. Since there is no more fouling on the substrate, no modification of structure exists in the sample tube. Hence, there is no variation in the acoustic propagation field.

While all the steps is finished, the data of all the parameters (temperature, flow rate and acoustic acquisition signals) will be recorded on hard disk for further signal processing. The signal processing method has already been used in the previous works [152].

d) Optical observing by camera

The known fouling states in the experiment are only the initial state and the final state (clean state). As the acoustic signals present the indicators of fouling at each moment, it is not enough to have only two known states for the corresponding between the actual fouling state and the acoustical monitoring results.

In this case, we need to know the detail of fouling at each moment of cleaning or rinsing steps. So, an optical method is used to monitor the state of fouling in real time. As a kind of visual and direct method, this monitoring is also easy to implement. In practice, a camera is fixed in front of the sample tube (Figure 3.18). The fouling could be observed by the camera through the transparent substrate (Figure 3.19). Light is provided by a high power lamp in order to meet the needs of photography. The recorded zone of video is focus on the protein fouling. By using this camera, a video of fouling is recorded for each step.

The beginning and the ending of video are synchronized with the acoustic monitoring. During the recording of video, the camera will take 7 photos per second. This frequency of acquisition by camera is enough for the experiment as the interval between each 2 acquisitions of acoustic measurement is more than 6 seconds.

During all the measurements, videos of fouling at each cleaning step are recorded by optical observing. These videos are then converted to images for extracting more information.

The acoustic monitoring result is quantified by using decorrelation coefficient as indicator. Therefore, it is useful to have the optical observing result quantified. In this experiment, the average of color is used as the indicator of fouling pictures.

Since the light cannot cover every corner in the sample tube, shadow will always exist on the stainless steel substrate. Consequently, in the analyzing of pictures, only a zone without shadow is taken into account. With a graphic software (ImageJ), the color of each pixel in the same zone of pictures for a video could be quantified. The average value of all the pixel in the zone is used as the indicator of a picture. Gathering the results of all the pictures, a video could be quantified.

The acoustic monitoring and the optical observing are executed at the same time period. Then, once the results of both methods are all quantified, they could be compared

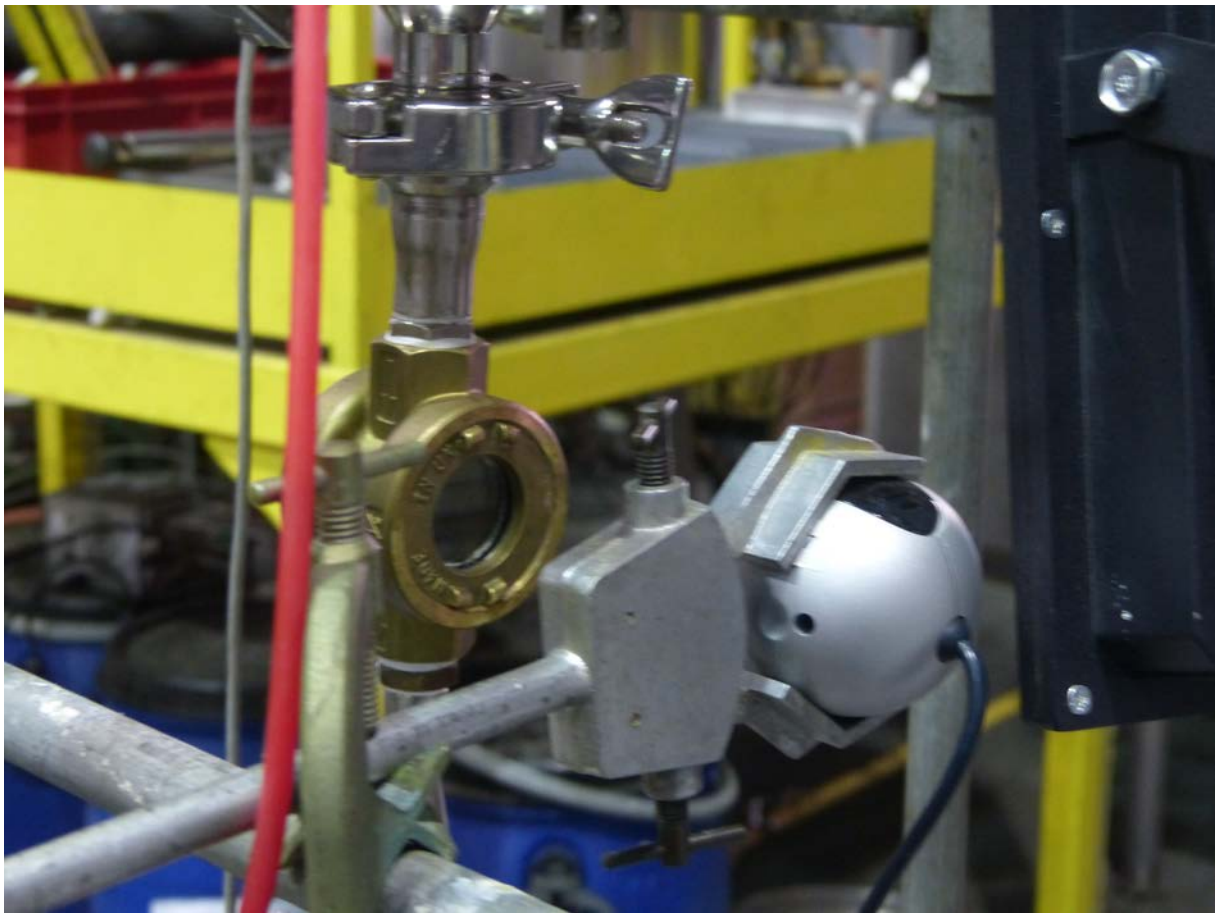

FIGURE 3.18 – Camera for the optical observing

with each other. Hence, it is able to confirm the acoustic monitoring with the optical observing result.

3.2.2 Experimental results

The signals measured by the acoustic acquisition system are presented in Figure 3.20. In the Figure 3.20, direct waves is received at about 5 μs with limited amplitude. The coda waves after the first arrived waves are around 10 $\mu s - 30$ μs. It is evident that several echoes appear in the signal after 30 μs (at 40 $\mu s, 80$ $\mu s, ...$). These echoes are the waves arrived at the other surface of sample tube (transparent substrate) and reflected to the receiver. Considering that in the circulation of liquid there is always the risk of appearance of undesired elements (small bubbles, particles,...), there may be many influences other

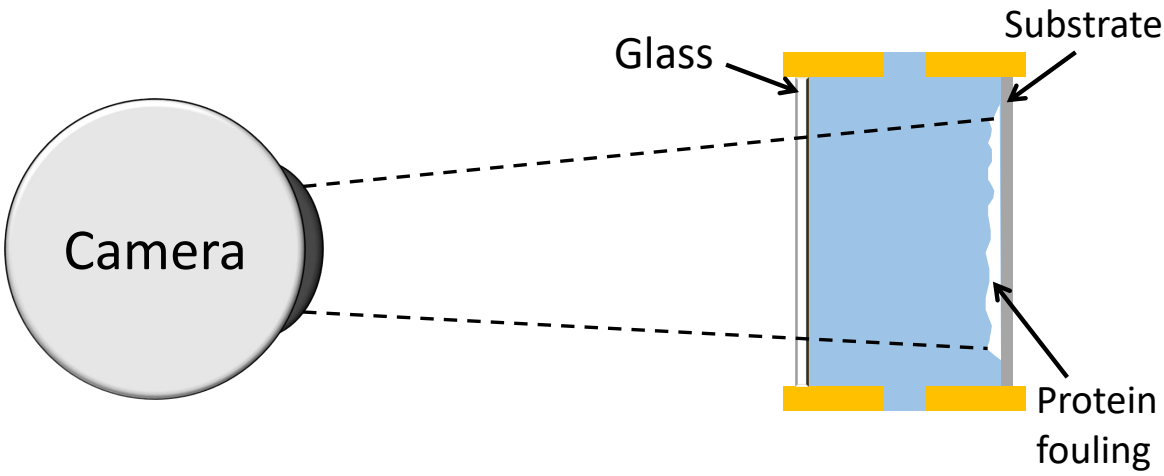

FIGURE 3.19 – Camera for the optical observing

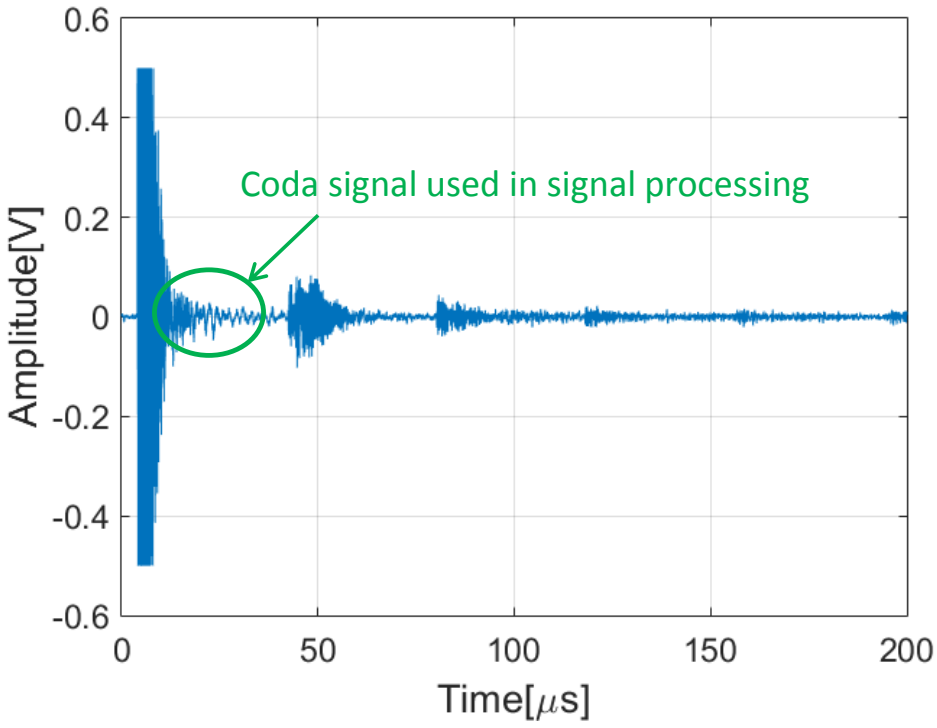

FIGURE 3.20 – Acoustic signal measured by the acquisition system

than the fouling modification at very late part of signals, especially after the second echo.

While choosing the time window for the signal processing, in order to make sure that the waves have propagated many times in the test part (fouling layer) and keep the penetration of waves not too far from the test layer, the time window should be the coda after the first arrived waves and before the echoes, which means it should be within [10 μs30 μs]. In particular, the window [20 μs25 μs] is used here for calculating the decorrelation coefficient.

The emission signals is at the frequency of 10 MHz, which is also close to the resonance frequency of sensor. The components of signal at other frequency with weak amplitude (which mixed with other kinds of waves like guide wave, noise,...) may not be useful for the analyze. Some components at the frequency far from emission frequency may decrease the sensitivity of results. Therefore, the frequency band is chosen to be $[9MHz - 11MHz]$ in this experiment.

After the time window and frequency filter band are all settled. Decorrelation coefficient could be obtained from the series of signals. With the optical observing, we can be sure that the stainless steel substrate surface is clean after the three steps. This final state is defined as the reference state and all the series of signals is compared with the reference signal. And the decorrelation coefficient in function of real time could be obtained.

Figure 3.21 (Blue curve) shows the evolution of decorrelation coefficient during the cleaning cycle . In 3.21, the decorrelation coefficient stay stable at 0.15 for the first 10 minutes, which is the pre-cleaning rinsing step. For the fouling cleaning step (10-35 minutes), the decorrelation coefficient decrease to 0 within 4 minutes. Then it stay at 0 till the end of step 3.

According to the optical observation, the fouling state does not change at the first step while there is only a circulation of water. During the cleaning step, the video shows that the fouling layer is eliminated rapidly and the substrate become clean after about 3.5 minutes. As the fouling layer has already been totally eliminated at that moment, there is no change in the detection zone after, including the step 3.

Several images capture from the video are presented in Figure 3.22, verifying that there is no change on the surface of substrate in step 1 and 3 (Figure 3.22 top) and fouling layer is cleaned during step 2 (Figure 3.22 bottom).

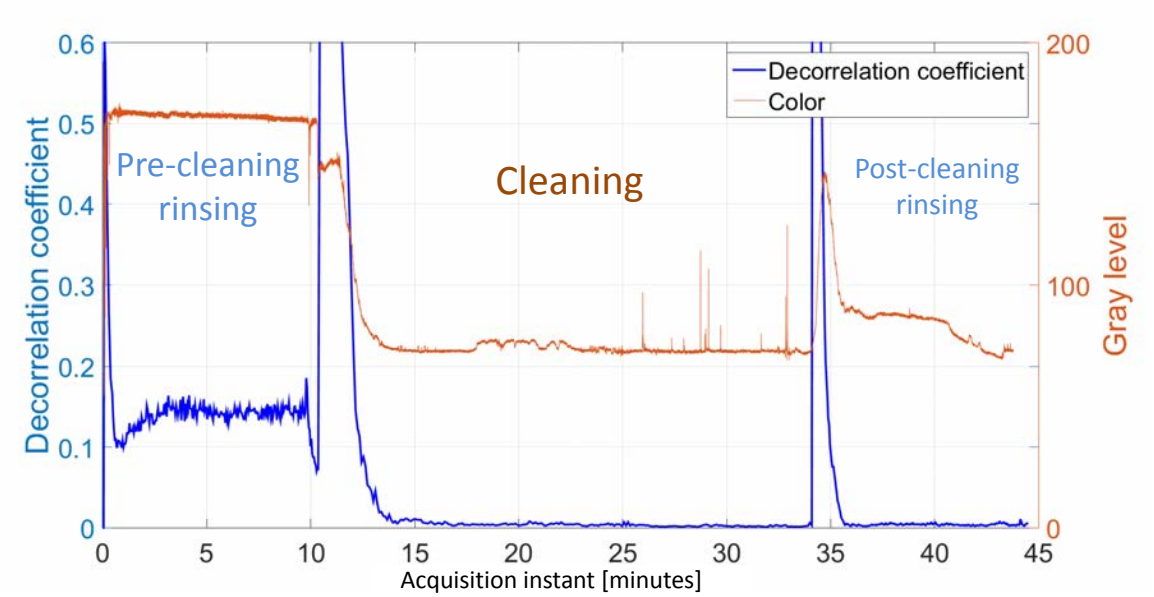

FIGURE 3.21 – The decorrelation coefficient (Blue) and Gray level evolutions during cleaning of proteianeous (Red)

The record of temperature and flow rate in the pilot during all 3 cleaning steps is presented in Figure 3.23. The inlet temperature is always constant at 50 °C, but the outlet temperature changes a lot at the beginning of each step. When the flow of Path 2 is stopped, the temperature of components and liquid in Path 2 will decrease immediately. Therefore, each time the switch is turned on the Path 2 to start a new step of measurement, the temperature takes some time to return to the constant value. This is the reason why there are abnormal rises in the decorrelation coefficient in Figure 3.21. Fortunately, outlet temperature is stable during the other parts of cleaning process. It can be noted that the flow rate is relatively stable during all the cleaning cycle. Only a small increase of flow rate of about $5\% - 10\%$ is observed at step 3.

Consequently, the result of decorrelation coefficient corresponds to the optical observation in each step in Figure 3.21. The peak between each two steps (at 10 minutes and 35 minutes) is caused by the switch of circulation. Each time the circulation in the sample tube is started or stopped, the change of temperature in the detection zone will influence the wave propagation and lead to the peaks.

As introduced before, videos of each step of measurement are recorded by a camera. The color of these videos are quantified and presented together with the decorrelation

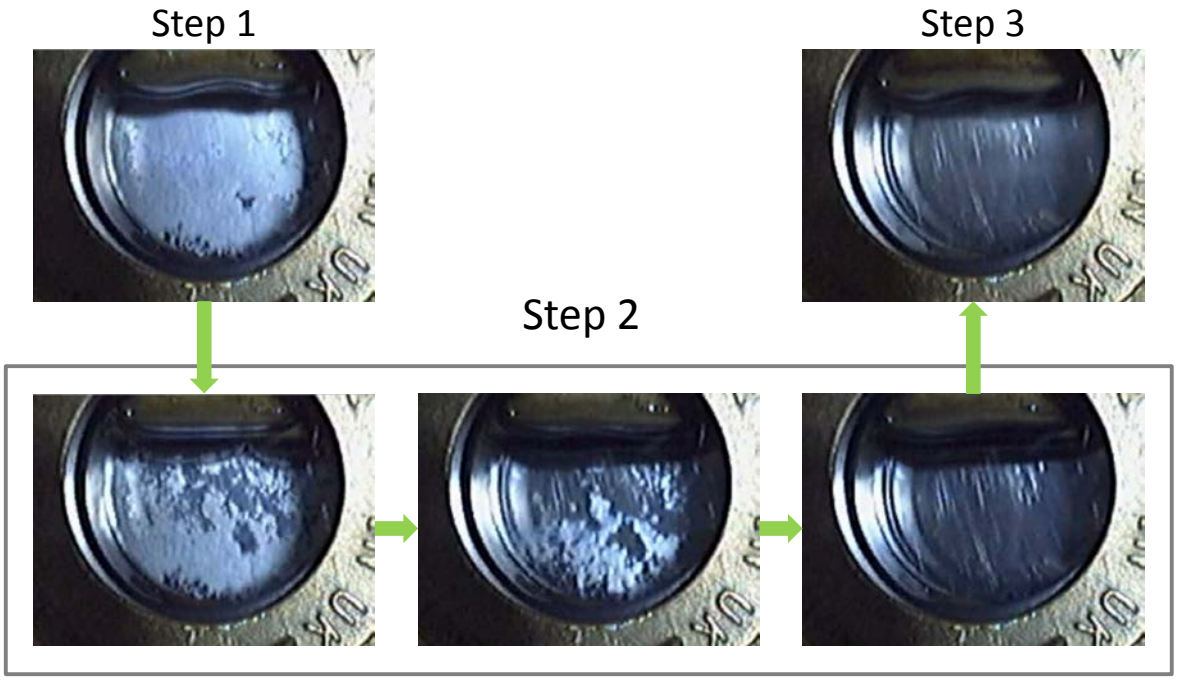

FIGURE 3.22 – The state of fouling layer during the whole experiment observed by camera (captured from video) : Step 1 (Pre-cleaning rinsing), Step 2 (Cleaning) and Step 3 (Post-cleaning rinsing)

coefficient in Figure 3.21 (Red curve). This parameter gives a tendency similar to the decorrelation coefficient. The color of substrate surface is constant value (167) at first (step 1 while the fouling state is stable), then change to another value (step 2) and stabled at the new value (80).

However, this optical record is not perfect. There are still some abnormal values in the curve of color. At later part of step 2, there is several peaks which are not supposed to exist. This phenomenon may be caused by the unpredictable appearance of air bubble (Figure 3.24-(a)). The acquisition frequency of acoustic measurement (about 20s for one acquisition) is much lower than the optical observing (7 image per second). Thus, the short duration appearance of air bubbles is difficult to be recorded by the acoustic monitoring.

Another abnormal part is the curve of step 3. The color value is a little higher than the normal value at the beginning. In fact, this phenomenon is caused by the difference of ambient brightness. As in Figure 3.24-(b) and (c), due to unexpected reasons, the brightness is changed for a certain period. But visually, the surface of substrate in the video

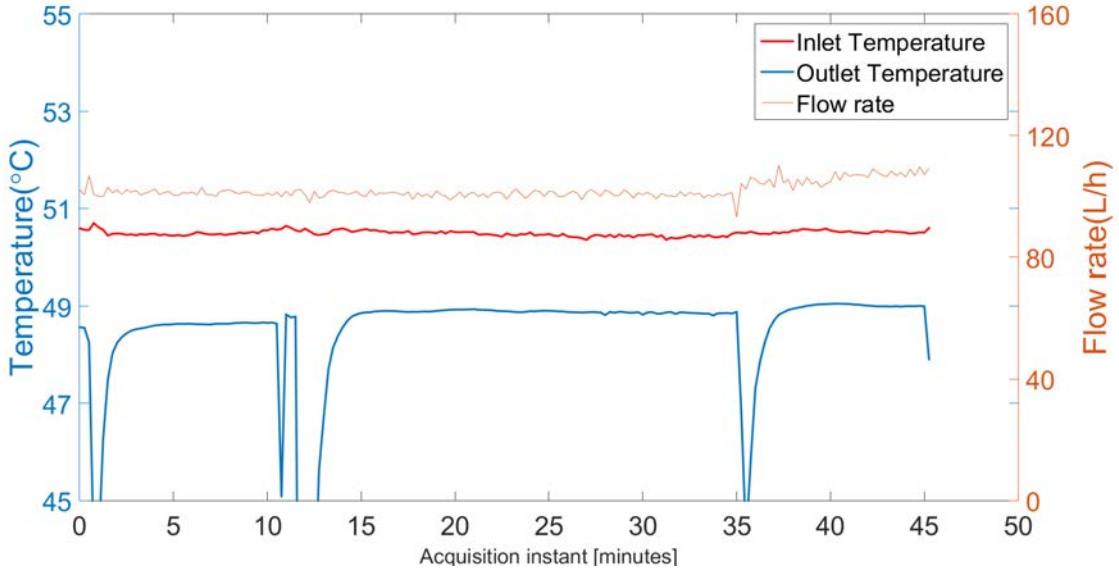

FIGURE 3.23 – The temperatures and flow rate evolutions during the cleaning cycle. Red thick curve : Inlet temperature ; Blue thick curve : Outlet temperature ; Red thin curve : Flow rate

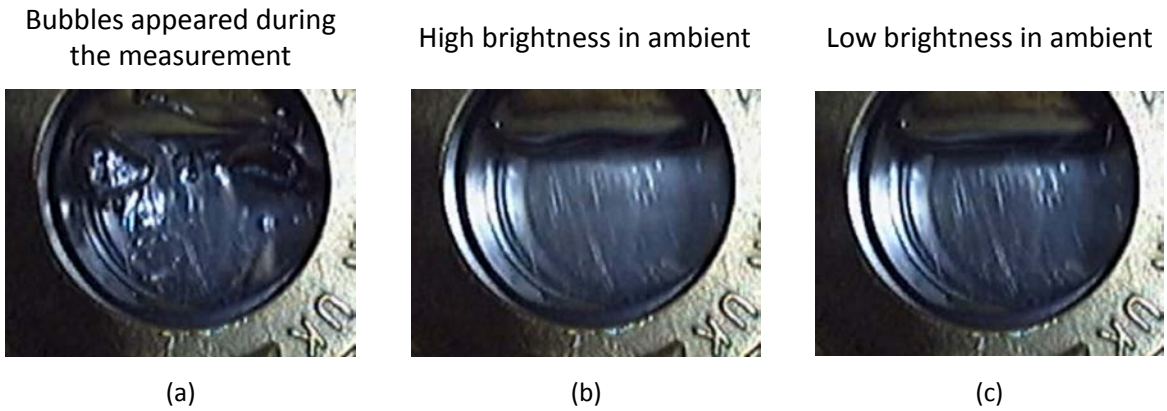

FIGURE 3.24 – The undesired influences in the sample tube : (a) Appearance of air bubbles ; (b) high brightness ; (c) Low brightness ;

is always clean. The difficulty encountered for monitoring cleaning by images acquisition is another fact which show the necessity of developing new sensors for following fouling factor of process equipment.

Overall, even though there is some errors in the acoustic monitoring record and the op-

tical observing record at several particular moments, the entire tendency will not change. Neglecting those particular error moments, the Figure 3.21 is still convincible for the correspondence between decorrelation coefficient and color of images. Hence, it is possible to use the coda wave to quantify the state of substrate surface.

3.2.3 Conclusion

In this section, cleaning of protein deposit is carried out. Whey protein deposit is used in order to demonstrate the feasibility of monitoring cleaning by CWI for agroalimentary applications, especially for the dairy industry.

The results of this experiment are relatively good. Indeed, when circulation of water is applied on step 1 and 3, the decorrelation coefficient is stable which is quite logical since no cleaning takes place. In step 2, the cleaning process is performed by a circulation of sodium hydroxide. For this step, the decorrelation coefficient changes and seems able to describe fouling factor decrease.

An optical observing is carried on during the whole measurements by a camera. With the optical record, the correctness of the acoustic monitoring result could be correlated.

This work clearly show that decorrelation coefficient change with the fouling state, which ascertain the feasibility of applying the acoustic method for monitoring fouling factor state. Considering that the cost of this technique is quite low, its potential in industrial applications is promising.

Chapitre 4

Detection of biofilm formation

After the measurement of cleaning process of deposit, an experiment of fouling formation monitoring will be addressed in this chapter. The problems caused by the presence of biofilm and the applications of biofilm detection have been already detailed in context. An effective non-invasive detection method for biofilm is widely needed in many sectors.

The thickness of biofilm is usually very small. The sensitivity of detection method has to be high enough to discover the presence of biofilm. The classic acoustic detection techniques, which use direct waves, might be difficult to achieve such sensitivity because the sensitivity is related to the wavelength. In order to overcome the limit of sensitivity without modifying the wavelength of signals, coda wave is still the technique that is used in this chapter to monitor the fouling formation.

In this chapter, the materials (including transducers, acoustic monitoring system and biological equipment) and the experimental protocol will be detailed. The experiment contain a monitoring of biofilm formation. *Staphylococcus aureus* is used as the contamination source of biofilm. Then, the results of biofilm monitoring will be discussed. (This chapter is principally taken from the submitted article 'Detection of biofilm formation by ultrasonic Coda Wave Interferometry')

4.1 Materials and method

4.1.1 The biofilm formation assay

The biofilm formation was performed on the upper face of the circular slides of stainless steel (1) Figure 4.1 (diameter : 4.1 cm). The CWI sensor is attached to the lower face of the stainless steel slides in order to detect the biofilm formation (Figure 4.1-(A),(B)). In order to obtain the formation of the biofilm, the circular slide of stainless steel is placed in a static reactor (Figure 4.1-(C)). The reactor consists of several assembled pieces of stainless steel and a rubber O-ring (Figure 4.1-(C)), as previously described by Abdallah et al. [154]. The circular base of this reactor (1) is made of stainless steel and can receive an O-ring (2) which is used to fit perfectly one circular test slide (3). Then a stainless steel cylinder (4) can be placed in order to form the well of the biofilm formation. A collar clamp (5) was used to provide tightness and a metal cover (6) was used to ensure the sterility of the closed system (7) (Figure 4.1-(D)). Two similar reactors are used to evaluate the ability of the sensor for detecting the deposit formation (Figure 4.1-(D)). The first one is for monitoring the biofilm formation (marked as reactor 1), and the second one is used as a negative control or witness (marked as reactor 2).

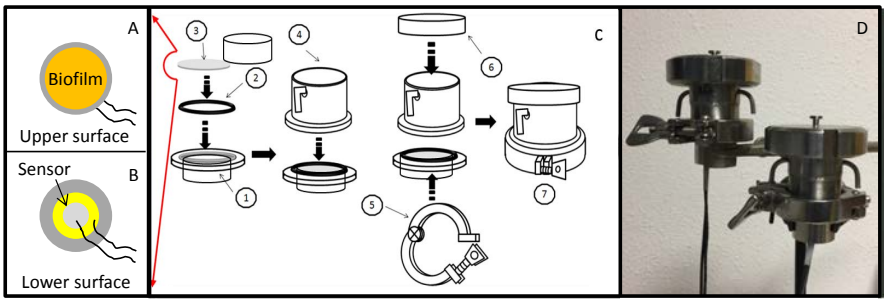

FIGURE 4.1 – The configuration of reactors for the biofilm formation. (a) Upper surface of substrate ; (b) Lower surface of substrate ; (c) Installation of reactor ; (d) Photo of the reactors

Prior to their use, the reactors were cleaned and disinfected using ethanol 95° to ensure the sterility of them.

The formation of biofilm was performed according to Abdallah et al [154]. The biofilm formation was initiated by the bacterial adhesion to surfaces, which constitutes the first

FIGURE 4.2 – Photo of biofilm formed on the substrate of reactor 1

step of the biofilm formation. Then the formation of biofilm layers was pursued by adding the culture medium in the wells and placing reactors in an incubator with a controlled temperature. In details, the step 1 was performed by the deposition of 5 mL of bacterial suspension (10^7 CFU/mL) in the well of reactor 1 and, then, incubated at 20 °C for 1 h to allow the bacterial adhesion into substrate. For the negative control (or witness), 5 ml of sterile physiological saline water were used. The counts of bacterial cells after step 1 showed that the number of attached cells in reactor 1 was around 1×10^5 CFU/cm^2. As expected, on the contrary, no adhered bacterial cells were found in reactor 2 (named witness or control condition). After the bacterial adhesion, the step 2 was started. For that, the 5 mL of bacterial suspension were removed and the slides were washed twice using physiological saline water (8.5% of Nacl) in order to remove loosely attached cells. Then 25 mL of Tryptone Soy Broth (TSB ; Biokar Diagnostics, Pantin, France)) were deposited in each well. Thereafter, reactors are sealed by lids and incubated at controlled temperature of 30 °C to allow the biofilm formation (Figure 4.2). The average thickness of biofilm layer, after 30 h, has been checked visually and is around 50 μm as measured by Abdallah et al. [154]. All experiments were done under sterile environment to avoid undesired contamination and to control as much as possible the biofilm growth.

For the quantification of bacterial biofilm biomass, stainless steel slides were placed in sterile containers and bacterial cells were detached in 20 ml of phosphate buffer (100 mM) by vortexing for 30 s followed by a sonication for 5 min. Then tenfold serial dilutions of each bacterial suspension were made in tryptone salt broth (TS ; Biokar Diagnostics, Pantin, France). 100 μl of each dilution were spread onto tryptic soy agar plates (TSA ; Biokar Diagnostics, Pantin, France). Agar plates were incubated at 37 °C and the number of

viable and culturable cells was counted after 24 h of incubation. The results are expressed in log CFU/cm^2 and represent the means of three independent experiments.

Time (h)	Biofilm biomass (Log CFU/cm^2)
0	5,1 ± 0,2
6	5,7 ± 0,1
12	6,2 ± 0,2
18	7,0 ± 0,1
24	7,9 ± 0,4
30	8,1 ± 0,3

TABLE 4.1 – Biofilm biomasses as a function of incubation time

4.1.2 Ultrasound acquisition and description of coda processing

During the different steps of biofilm formation, a continuous ultrasound monitoring is applied to the two reactors (referenced 1 and 2, respectively). The signal acquisition system consists of 5 components : a laptop PC with acquisition software (Matlab, instruments drivers), a waveform generator (Keysight 33600A Series), an acquisition board (PicoScope 5000 Series), an amplifier with internal high-pass filters and two transducers. The transducers used in this experiment are low-cost piezoelectric patches (Figure 4.3), consisting of two separate electroded parts for emission and reception. Their thickness resonance frequency is around 10 MHz. As mentioned above, they are glued on the lower face of the circular stainless steel substrate as described in Figure 4.1. This device allowed the monitoring of the biofilm formation occurring on the upper face of the circular slides.

The excitation signal is one period of sinus at 10 MHz. The transducers convert the electrical signals to ultrasound waves through piezoelectric effect. After propagation and multiple reflections and scattering in the sample (see more detailed explanation below), parts of these waves are returned towards the transducer and converted back into electrical signals at the reception electrode. After high-pass filtering (aimed at filtering out low frequency vibrations coming from the environment) and amplification, the received signals are fed into the acquisition board with sampling frequency 125 MHz and recorded in the PC after averaging over 100 signal acquisitions. This acquisition process is then repeated every five minutes, from the beginning of biofilm formation and for a total mo-

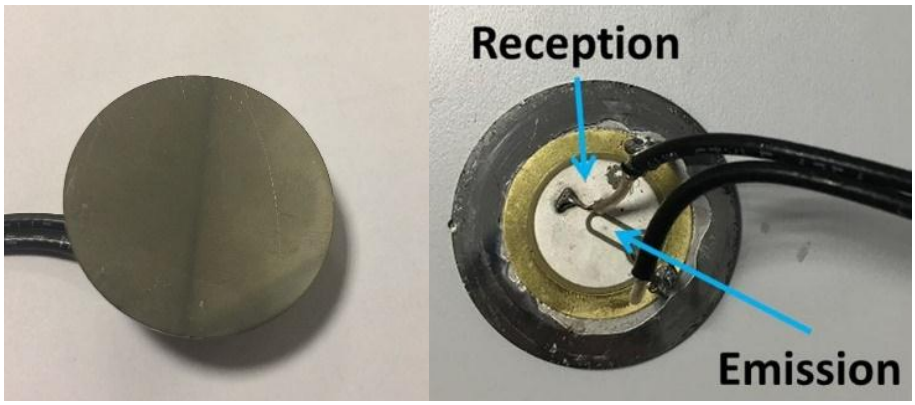

FIGURE 4.3 – Piezoelectric transducer used for the acquisition

nitoring duration of thirty hours. The biofilm formation on the surface will modify the substrate/biofilm interface properties and therefore lead to subsequent changes of reflected and back-scattered ultrasound signals.

4.1.3 Environmental temperature

Acoustic waves are very sensitive and influenced by temperature changes, in particular when using codas. Therefore, a monitoring of temperature in the incubator is carried on by a thermometer at the same time as the ultrasound acquisition. Since the signal recording time is very short and the biofilm formation is very slow, the temperature change of sample and the growth of biofilm during one single acquisition can be neglected. Temperature evolution measured during the biofilm formation in the reactor is shown in Figure 4.4.

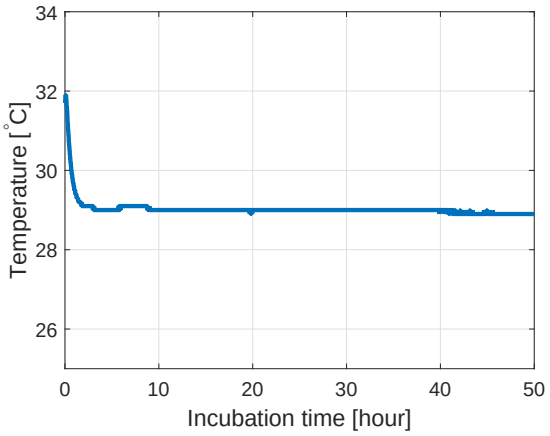

FIGURE 4.4 – Temperature in the incubator during the measurement

The curve shows that temperature inside the reactor stabilizes approximately two hours after setting in the incubator. Therefore, the initial (or reference) state for the decorrelation coefficient estimation is defined at two hours of incubation time, in order to avoid the influence of temperature variation.

4.2 Experimental results and interpretation

Two series of signals are obtained from reactors 1 and 2 and are recorded from 2 hours of incubation time (taken as reference) and every 5 minutes. First, all these signals are numerically band-pass filtered between 9 and 11 MHz (relative bandwidth 20%) and then decorrelation coefficients between the reference signal and every subsequent signals are computed using Eq. (2.29) for sliding time-windows of duration $\Delta T = 5$ μs. This satisfies the mentioned above conditions on frequency bandwidth and time-window duration.

Figure 4.5-(a) and (b) show the evolution of the decorrelation coefficient as a function of incubation time for the control and the biofilm samples, respectively. In both cases, decorrelation values computed in four time-windows are shown : $0\ \mu s - 5\ \mu s, 3\ \mu s - 8\ \mu s, 5\ \mu s - 10\ \mu s, 16\ \mu s - 21\ \mu s$.

In the negative control reactor (Figure 4.5-(a)), the decorrelation coefficients are always close to 0 for any incubation time and whatever the selected time window. This indicates the absence of any significant change from the initial surface property state. This is coherent with the absence of biofilm formation, observed with naked eyes, on the negative control substrate. In addition, these results confirm that no apparent variable factor other than the biofilm formation on substrate influence the propagation of acoustic waves.

On the contrary, the results in Figure 4.5-(b) show that the decorrelation coefficients of biofilm monitoring sample rises significantly as incubation time increases. It also shows that the sensitivity of the state change detection depends on the time windows. The first window ($0\ \mu s - 5\ \mu s$) is not sensitive at all since the decorrelation coefficients are close to 0. On the contrary for the other time windows, corresponding to later parts of the coda, significant increases of the decorrelation coefficient can be observed. Finally, the decorrelation coefficients become stable after about 22 hours, which is probably due to the reaching of quasi-steady state of the biofilm formation.

In order to verify the correlation between the evolution curves in Fig. 4.5-(b) and the

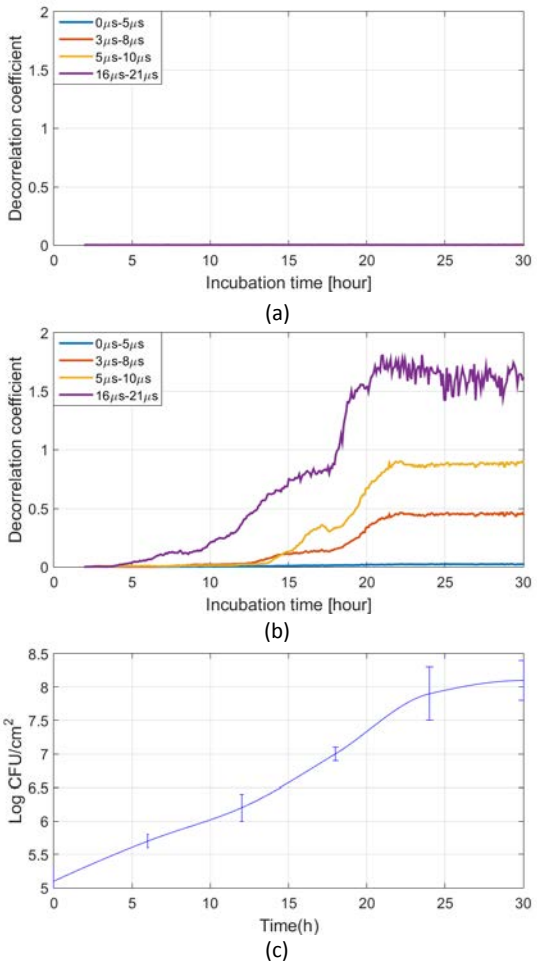

FIGURE 4.5 – Decorrelation coefficient evolution as a function of incubation time for : (a) control sample, (b) biofilm formation sample, with different time windows : 0 μs – 5 μs, 3 μs – 8 μs, 5 μs – 10 μs, 16 μs – 21 μs (frequency band 9 MHz-11 MHz) ; (c) Kinetic of *S. aureus* biofilm formation on stainless steel substrate.

biofilm formation on substrate, the kinetic of *S. aureus* biofilm formation on the stainless steel were investigated by enumeration of biofilm cells on agar plates, as explained in Sec. 4.1.1. The results showed that the counts of the initial adhered bacteria were in the range of 5 log CFU/cm^2 (Table 4.1). The results also showed that the biofilm biomasses increased with the increase of the incubation time and reached the steady state around 24 h of incubation time. In fact, the biofilm biomasses were stable and in the range of 8 log CFU/cm^2 (Figure 4.5-(c)). The biomass evolution could be compared with the decorrelation coefficient (Figure 4.5-(b)). Indeed, the data of the bacterial cell enumeration are well described by the decorrelation coefficient evolution. These data proved that this

method has the potential to detect and monitor the biofilm formation on a substrate in a non-invasive way.

4.3 Conclusion

The detection of biofilm formation on surfaces is of critical importance to sectors that directly affect human health. In fact, biofilm represents a reservoir of pathogens which lead to serious human infections. Thus, an efficient biofilm monitoring on surfaces, commonly used in food and medical sectors, is needed in order to reduce the microbiological risks and associated human and economic losses. In this context, our work described a monitoring method based on Coda Wave Interferometry to detect the biofilm formation on stainless steel.

The principle of this monitoring technique is to compare the acoustic signals received at different instants, which is based on CWI. Decorrelation coefficient of multiply-reflected or scattered (coda) waves is used as an indicator of state changes in the samples. The method described herein presents several advantages over conventional methods based on optical, heat transfer, pressure drop, fluid dynamic gauging, direct weighing and thickness measurements. Indeed, conventional methods are usually invasive. On the contrary, the method described in this paper is non-invasive, cheap and easy to apply in food and medical environments. In addition, this method is highly sensitive that a layer less that $50\mu m$ could be detected (in the particular condition considered in this work, an area of 12 cm^2 has been monitored using a single sensor).

Our results show that this technique has the potential for performing continuous real-time biofilm detection and monitoring in sealed opaque equipment. In addition, this method interestingly succeeded to detect the early stage of biofilm formation. In fact, the decorrelation coefficient started increasing from a bacterial concentration of 10^5 CFU/cm^2.

Conclusion and perspectives

The work of this thesis principally concerns detection/monitoring of fouling factor of a solid substrate by ultrasonic coda waves. This study focus mainly on type of fouling which could be encoutered in food industry. There is no direct contact between sensor and test sample, and the acoustic waves for the detection ought to propagate through the substrate. Then, with the multiple reflections in the substrate layer, the coda waves last for a long duration, which helps the numerical analyze.

The principle of this detection technique is to relate the state change of test sample (fouling) to the coda signals. Once there is a perturbation in the test sample, the propagation paths of acoustic waves will be modified, and the received coda signals will be different. Then, knowing a reference fouling state (usually the initial state or clean state), the fouling states at other moments could be obtained and compared. The quantification of fouling states is achieved by decorrelation coefficient which gives the difference of two coda signals.

The feasibility of the coda wave detection method has been validated successfully by several experiments, including wax and whey protein deposit cleaning and monitoring of biofilm formation. The different fouling states is well indicated by different values of decorrelation coefficient. The result shows that this technique is able to monitor thin layer (thickness less than 50 μm). The success of monitoring cleaning (wax which mimick chocolate cleaning by melting and whey protein deposit by detergents) reveals that there is no difficulty to apply this technique on real industrial equipment.

The method of coda wave detection itself does not require a specific type of acoustic transducer. Thus, the cost of sensor is relatively cheap. Like other acoustic detection techniques, coda wave monitoring is noninvasive. But the sensitivity of coda wave is much better than the classic acoustic techniques which use the information of direct waves.

The sensitivity of coda wave detection could be defined by the time window. Therefore, the sensitivity could be easily modified to meet the requirements of detection. The signal processing of this technique is not complicated. Real time monitoring with a frequency of 1 acquisition per second could be achieved.

The drawbacks of coda wave technique is that some environmental variations may also cause the change of coda signals and make the detection result incorrect. Like other acoustic detection techniques, the environmental temperature is always a parameter which could lead to a variation on signals. Keeping the temperature constant is indispensable for the signal processing of coda wave detection. The existence of air near substrate is another risk. Air will affect the propagation of ultrasonic waves. During the measurement, it should be confirmed that there is no air in substrate and test sample. An unstable substrate could also influence the monitoring result in an unpredictable way, but it is rare to meet this situation in applications.

According to the experimental results, this ultrasonic coda wave detection technique has promising potential on industrial monitoring. The following work that needs to be done is to construct a complete monitoring system that could be applied on real industrial equipment. For some applications that the temperature could not be controlled strictly, there will be some difficulties to monitor the fouling states. In this case, the instability of temperature may be overcome by knowing the coda signals of the reference state (clean state) at every possible temperature.

This coda wave method is a technique for local measurement. However, control of a large surface could be achieved with numerous transducer. For that, the influence of fouling position to the detection result for a single transducer have to be investigated.

For the interest of many applications, it is also valuable to know the type of fouling. The detection technique proposed in this thesis cannot identify the fouling type for now. However, ANN (Artificial Neural Network) may able to make it possible to detect fouling type. With a large database of the coda signals measured with known types of fouling, an unknown fouling may be recognized by comparing the coda signal with the database.

Bibliographie

[1] T. Kuppan. *Heat Exchanger Design Book*. Marcel Dekker Inc, New York, 2000.

[2] Bipan Bansal and Xiao Dong Chen. A Critical Review of Milk Fouling in Heat Exchangers. *Comprehensive Reviews in Food Science and Food Safety*, 5(2) :27–33, April 2006.

[3] Anwar K. Sheikh, Syed M. Zubair, Muhammad Younas, and M. O. Budair. A risk based heat exchanger analysis subject to fouling : Part II : Economics of heat exchangers cleaning. *Energy*, 25(5) :445–461, 2000.

[4] Matthias Bohnet. Fouling of heat transfer surfaces. *Chemical engineering & technology*, 10(1) :113–125, 1987.

[5] Nicholas John Ashbolt. Microbial contamination of drinking water and disease outcomes in developing regions. *Toxicology*, 198(1-3) :229–238, 2004.

[6] Joël Hardy, Michel Parmentier, and Jacques Fanni. Functionality of nutrients and thermal treatments of food. *Proceedings of the Nutrition Society*, 58(03) :579–585, August 1999.

[7] Nicolas Collier. *Développement d'un Outil Ultrasonore de Caractérisation Des Propriétés d'adhésion de Milieux Modèles Avec Application Aux Dépôts Laitiers*. PhD thesis, Lille 1, 2014.

[8] J. Taborek, T. Aoki, R. B. Ritter, J. W. Palen, and J. G. Knudsen. Fouling : The major unresolved problem in heat transfer. 1972.

[9] T. R. Bott. Crystallisation Fouling — Basic Science and Models. In *Fouling Science and Technology*, NATO ASI Series, pages 251–260. Springer, Dordrecht, 1988.

[10] Y. Toure, N. Mabon, and M. Sindic. Synthèse bibliographique des souillures modèles utilisées en laboratoire pour l'évaluation de l'adhérence des souillures, l'en-

crassement et la nettoyabilité des surfaces. *Biotechnologie, Agronomie, Société et Environnement*, 17(3) :527–539–539, September 2013.

[11] R. Sheikholeslami. Composite fouling - inorganic and biological : A review. *Environmental Progress*, 18(2) :113–122, June 1999.

[12] Cristiane Boxler. *Fouling by Milk Constituents and Cleaning of Modified Surfaces*. Cuvillier Verlag, 2015.

[13] J. Visser and Th. J. M. Jeurnink. Fouling of heat exchangers in the dairy industry. *Experimental Thermal and Fluid Science*, 14(4) :407–424, May 1997.

[14] Michael C. Georgiadis and Sandro Macchietto. Dynamic modelling and simulation of plate heat exchangers under milk fouling. *Chemical Engineering Science*, 55(9) :1605–1619, May 2000.

[15] S. D. Changani, M. T. Belmar-Beiny, and P. J. Fryer. Engineering and chemical factors associated with fouling and cleaning in milk processing. *Experimental Thermal and Fluid Science*, 14(4) :392–406, May 1997.

[16] Th. J. M Jeurnink. *Milk fouling in heat exchangers*. PhD thesis, [publisher not identified], Wageningen, 1996. OCLC : 35793300.

[17] Hans Müller-Steinhagen. *Heat Exchanger Fouling : Mitigation and Cleaning Techniques*. IChemE, 2000.

[18] T. Casanueva-Robles and T. R. Bott. THE ENVIRONMENTAL EFFECT OF HEAT EXCHANGER FOULING. 2005.

[19] R. Oliveira, L. Melo, M. Pinheiro, and M.J. Vieira. Surface Interactions and Deposit Growth in Fouling of Heat Exchangers. *Corrosion Reviews*, 11(1-2) :55–96, 2011.

[20] P J Fryer, G K Christian, and W Liu. How hygiene happens : Physics and chemistry of cleaning. *International Journal of Dairy Technology*, 59(2) :76–84, May 2006.

[21] Mostafa M. Awad. Fouling of heat transfer surfaces. In *Heat Transfer-Theoretical Analysis, Experimental Investigations and Industrial Systems*. InTech, 2011.

[22] W. J. Rebello, S. L. Richlen, and F. Childs. The cost of heat exchanger fouling in the US industries. 1988.

[23] Sushilla Changani. *An Investigation into the Fouling and Cleaning Behaviour of Dairy Deposits*. PhD thesis, University of Birmingham, 1999.

[24] G. Daufin, J. P. Labbé, A. Quemerais, G. Brulé, Françoise Michel, M. Roignant, and M. Priol. Fouling of a heat exchange surface by whey, milk and model fluids. An analytical study. *Le Lait*, 67(3) :339–364, 1987.

[25] M. Jimenez, G. Delaplace, N. Nuns, S. Bellayer, D. Deresmes, G. Ronse, G. Alogaili, M. Collinet-Fressancourt, and M. Traisnel. Toward the understanding of the interfacial dairy fouling deposition and growth mechanisms at a stainless steel surface : A multiscale approach. *Journal of colloid and interface science*, 404 :192–200, 2013.

[26] P. Blanpain-Avet, C. Faille, G. Delaplace, and T. Bénézech. Cell adhesion and related fouling mechanism on a tubular ceramic microfiltration membrane using Bacillus cereus spores. *Journal of Membrane Science*, 385-386 :200–216, December 2011.

[27] J. Sadeghinezhad, C. Sorteni, G. Di Guardo, C. D'Agostino, U. Agrimi, R. Nonno, and R. Chiocchetti. Neurochemistry of myenteric plexus neurons of bank vole (Myodes glareolus) ileum. *Research in Veterinary Science*, 95(3) :846–853, December 2013.

[28] N. Andritsos, S. G. Yiantsios, and A. J. Karabelas. Calcium Phosphate Scale Formation from Simulated Milk Ultrafiltrate Solutions. *Food and Bioproducts Processing*, 80(4) :223–230, December 2002.

[29] Tuan Ho Truong. *Fouling of Stainless Steel Surfaces by Heated Whole Milk : A Thesis Presented in Partial Fulfilment of the Requirements for the Degree of Doctor of Philosophy in Food Technology.* PhD thesis, Massey University, 2001.

[30] Theodore Reginald Bott. *Fouling of Heat Exchangers.* Elsevier, 1995.

[31] J. Yoon and D. B. Lund. Effect of operating conditions, surface coatings and pretreatment on milk fouling in a plate heat exchanger. In *Fouling and Cleaning in Food Processing*, volume 59, page 80. Taylor & Francis Perin, 1989.

[32] Michel Britten, Margaret L. Green, Marcel Boulet, and Paul Paquin. Deposit formation on heated surfaces : Effect of interface energetics. *Journal of Dairy Research*, 55(4) :551–562, 1988.

[33] D. B. Lund and D. Bixby. Fouling of heat exchange surfaces by milk. *Process Biochemistry*, 1975.

[34] H. Burton. A laboratory method for the investigation of milk deposits on heat exchange surfaces. *Journal of Dairy Research*, 28(3) :255–263, 1961.

[35] H. Burton. Reviews of the progress of dairy science. *J. Dairy Res.*, 35 :317–330, 1968.

[36] Sami M. Al-Roubaie and Harold Burton. Effect of free fatty acids on the amount of deposit formed from milk on heated surfaces. *Journal of Dairy Research*, 46(3) :463–471, 1979.

[37] Th JM Jeurnink. *Effect of Proteolysis in Milk on Fouling in Heat Exchangers*. NIZO, 1991.

[38] Hayden Albert Edward Bennett. ASPECTS OF FOULING IN DAIRY PROCESSING. page 249.

[39] Pieter Walstra and Robert Jenness. *Dairy Chemistry & Physics.* John Wiley & Sons, 1984.

[40] Th JM Jeurnink. Fouling of heat exchangers by fresh and reconstituted milk and the influence of air bubbles. *Milchwissenschaft*, 50(4) :189–192, 1995.

[41] R. Thom. Formation of milk deposits in plate heaters. *Milchwissenschaft*, 30(2) :84–89, 1975.

[42] R. W. Bell and C. F. Sanders. Prevention of Milestone Formation in a High-Temperature-Short-Time Heater by Preheating Milk, Skim Milk and Whey. *Journal of Dairy Science*, 27(6) :499–504, 1944.

[43] P. De Jong, S. Bouman, and HJLJ Van der Linden. Original Papers and Proceedings : Fouling of heat treatment equipment in relation to the denaturation of $\beta -$lactoglobulin. *International Journal of Dairy Technology*, 45(1) :3–8, 1992.

[44] Carl Suetens. ECDC Point Prevalence Survey of healthcare- associated infections and antimicrobial use in European acute care hospitals, 2011-2012. page 64.

[45] Nathan K. Archer, Mark J. Mazaitis, J. William Costerton, Jeff G. Leid, Mary Elizabeth Powers, and Mark E. Shirtliff. Staphylococcus aureus biofilms. *Virulence*, 2(5) :445–459, September 2011.

[46] Cynthia B. Whitchurch, Tim Tolker-Nielsen, Paula C. Ragas, and John S. Mattick. Extracellular DNA Required for Bacterial Biofilm Formation. *Science*, 295(5559) :1487–1487, February 2002.

[47] Thien-Fah C. Mah and George A. O'Toole. Mechanisms of biofilm resistance to antimicrobial agents. *Trends in Microbiology*, 9(1) :34–39, January 2001.

[48] Luanne Hall-Stoodley and Paul Stoodley. Evolving concepts in biofilm infections. *Cellular Microbiology*, 11(7) :1034–1043, July 2009.

[49] Sachdeva Sharma, Pooja Sachdeva, and Jugsharan Singh Virdi. Emerging waterborne pathogens. *Applied Microbiology and Biotechnology*, 61(5-6) :424–428, 2003.

[50] Panagiota Gousia, Vagelis Economou, Hercules Sakkas, Stamatina Leveidiotou, and Chrissanthy Papadopoulou. Antimicrobial resistance of major foodborne pathogens from major meat products. *Foodborne pathogens and disease*, 8(1) :27–38, 2011.

[51] S. Sasidharan, B. Prema, and Latha L. Yoga. Antimicrobial drug resistance of Staphylococcus aureus in dairy products. *Asian Pacific journal of tropical biomedicine*, 1(2) :130, 2011.

[52] Mehdi Zarei, Siavash Maktabi, and Masoud Ghorbanpour. Prevalence of Listeria monocytogenes, Vibrio parahaemolyticus, Staphylococcus aureus, and Salmonella spp. in seafood products using multiplex polymerase chain reaction. *Foodborne pathogens and disease*, 9(2) :108–112, 2012.

[53] Xin Wang, Xiaoya Tao, Xiaodong Xia, Baowei Yang, Meili Xi, Jianghong Meng, Jing Zhang, and Benjin Xu. Staphylococcus aureus and methicillin-resistant Staphylococcus aureus in retail raw chicken in China. *Food Control*, 29(1) :103–106, 2013.

[54] M. Sharma and S. K. Anand. Characterization of constitutive microflora of biofilms in dairy processing lines. *Food Microbiology*, 19(6) :627–636, 2002.

[55] Diana Gutiérrez, Susana Delgado, Daniel Vázquez-Sánchez, Beatriz Martínez, Marta López Cabo, Ana Rodríguez, Juan J. Herrera, and Pilar García. Incidence of Staphylococcus aureus and analysis of bacterial-associated communities on food industry surfaces. *Applied and environmental microbiology*, pages AEM. 02045–12, 2012.

[56] Antonia S. Gounadaki, Panagiotis N. Skandamis, Eleftherios H. Drosinos, and George-John E. Nychas. Microbial ecology of food contact surfaces and products of small-scale facilities producing traditional sausages. *Food Microbiology*, 25(2) :313–323, 2008.

[57] Kamel Chaieb, Bochra Kouidhi, Hanene Jrah, Kacem Mahdouani, and Amina Bakhrouf. Antibacterial activity of Thymoquinone, an active principle of Nigella sativa

and its potency to prevent bacterial biofilm formation. *BMC Complementary and Alternative Medicine*, 11 :29, April 2011.

[58] Kateryna Bazaka, Mohan V. Jacob, Russell J. Crawford, and Elena P. Ivanova. Efficient surface modification of biomaterial to prevent biofilm formation and the attachment of microorganisms. *Applied Microbiology and Biotechnology*, 95(2) :299–311, July 2012.

[59] Karen E. Beenken, Jon S. Blevins, and Mark S. Smeltzer. Mutation of sarA in Staphylococcus aureus Limits Biofilm Formation. *Infection and Immunity*, 71(7) :4206–4211, January 2003.

[60] Gibson H., Taylor J. H., Hall K. E., and Holah J. T. Effectiveness of cleaning techniques used in the food industry in terms of the removal of bacterial biofilms. *Journal of Applied Microbiology*, 87(1) :41–48, December 2001.

[61] T. Schmid, U. Panne, J. Adams, and R. Niessner. Investigation of biocide efficacy by photoacoustic biofilm monitoring. *Water Research*, 38(5) :1189–1196, March 2004.

[62] J. W. Costerton, Philip S. Stewart, and E. P. Greenberg. Bacterial Biofilms : A Common Cause of Persistent Infections. *Science*, 284(5418) :1318–1322, May 1999.

[63] Paula Watnick and Roberto Kolter. Biofilm, City of Microbes. *Journal of Bacteriology*, 182(10) :2675–2679, May 2000.

[64] R. Van Houdt and C.w. Michiels. Biofilm formation and the food industry, a focus on the bacterial outer surface. *Journal of Applied Microbiology*, 109(4) :1117–1131, October 2010.

[65] Marwan Abdallah, Corinne Benoliel, Djamel Drider, Pascal Dhulster, and Nour-Eddine Chihib. Biofilm formation and persistence on abiotic surfaces in the context of food and medical environments. *Archives of Microbiology*, 196(7) :453–472, July 2014.

[66] Jyotsna Chandra, Duncan M. Kuhn, Pranab K. Mukherjee, Lois L. Hoyer, Thomas McCormick, and Mahmoud A. Ghannoum. Biofilm Formation by the Fungal PathogenCandida albicans : Development, Architecture, and Drug Resistance. *Journal of Bacteriology*, 183(18) :5385–5394, September 2001.

[67] Philippe Vogeleer, Yannick D. N. Tremblay, Akier A. Mafu, Mario Jacques, and Josée Harel. Life on the outside : Role of biofilms in environmental persistence of Shiga-toxin producing Escherichia coli. *Frontiers in Microbiology*, 5, 2014.

[68] Lars D. Renner and Douglas B. Weibel. Physicochemical regulation of biofilm formation. *MRS bulletin*, 36(5) :347–355, 2011.

[69] Rolf Bos, Henny C. Van der Mei, and Henk J. Busscher. Physico-chemistry of initial microbial adhesive interactions–its mechanisms and methods for study. *FEMS microbiology reviews*, 23(2) :179–230, 1999.

[70] Ece Karatan and Paula Watnick. Signals, regulatory networks, and materials that build and break bacterial biofilms. *Microbiology and molecular biology reviews*, 73(2) :310–347, 2009.

[71] Christopher Weidenmaier and Andreas Peschel. Teichoic acids and related cell-wall glycopolymers in Gram-positive physiology and host interactions. *Nature Reviews Microbiology*, 6(4) :276, 2008.

[72] Hans-Curt Flemming and Jost Wingender. The biofilm matrix. *Nature reviews microbiology*, 8(9) :623, 2010.

[73] Aamir Ghafoor, Iain D. Hay, and Bernd HA Rehm. The role of exopolysaccharides in Pseudomonas aeruginosa biofilm formation and architecture. *Applied and environmental microbiology*, pages AEM. 00637–11, 2011.

[74] W. Michael Dunne. Bacterial adhesion : Seen any good biofilms lately ? *Clinical microbiology reviews*, 15(2) :155–166, 2002.

[75] T. R. De Kievit. Quorum sensing in Pseudomonas aeruginosa biofilms. *Environmental microbiology*, 11(2) :279–288, 2009.

[76] P.J. Fryer and K. Asteriadou. A prototype cleaning map : A classification of industrial cleaning processes. *Trends in Food Science & Technology*, 20(6-7) :255–262, July 2009.

[77] F. Smaïli, V. S. Vassiliadis, and D. I. Wilson. Optimization of cleaning schedulesin heat exchanger networkssubject to fouling. *Chemical Engineering Communications*, 189(11) :1517–1549, November 2002.

[78] N. Alvarez, G. Daufin, and G. Gésan-Guiziou. Recommendations for rationalizing cleaning-in-place in the dairy industry : Case study of an ultra-high temperature heat exchanger. *Journal of Dairy Science*, 93(2) :808–821, February 2010.

[79] Adnan Y. Tamime. *Cleaning-in-Place : Dairy, Food and Beverage Operations*, volume 13. John Wiley & Sons, 2009.

[80] Albrecht GRASSHOFF. Efficiency assessment of a multiple stage CIP-procedure for cleaning a dairy plate heat exchanger. *EUR*, pages 117–124, 1996.

[81] W. G. Jennings, A. A. McKillop, and J. K. Luick. Circulation Cleaning1. *Journal of dairy science*, 40(11) :1471–1479, 1957.

[82] D. A. Timperley and C. N. M. Smeulders. Cleaning of dairy HTST plate heat exchangers : Comparison of single and two stage procedures. *International Journal of Dairy Technology*, 40(1) :4–7, 1987.

[83] A. Graßhoff. Cleaning of heat treatment equipment. In *Fouling and Cleaning of Heat Treatment Equipment*, pages 32–44. IDF Monograph# 328, publ. IDF, Brussels, 1997.

[84] Ruben Mercadé-Prieto, William R. Paterson, Xiao Dong Chen, and D. Ian Wilson. Diffusion of NaOH into a protein gel. *Chemical Engineering Science*, 63(10) :2763–2772, 2008.

[85] Camilla A.-C. Karlsson, Marie C. Wahlgren, and A. Christian Trägårdh. Some surface-related aspects of the cleaning of new and reused stainless-steel surfaces fouled by protein. *International dairy journal*, 8(10-11) :925–933, 1998.

[86] T. R. Tuladhar, W. R. Paterson, and D. I. Wilson. Investigation of alkaline cleaning-in-place of whey protein deposits using dynamic gauging. *Food and Bioproducts Processing*, 80(3) :199–214, 2002.

[87] Michael Roger Bird. *Cleaning of Food Process Plant.* PhD thesis, University of Cambridge, 1993.

[88] Pascale MARTY. Maîtrise de la consommation d'eau dans les industries agro-alimentaires : Dossier eau. *Industries alimentaires et agricoles*, 118(5) :35–39, 2001.

[89] M. Sage. Valorisation des eaux de procédés de l'industrie laitière en méthanisation et dénitrification. *Unpublished PhD thesis, École Nationale Supérieure d'Agronomie de Rennes, Rennes, France*, 2005.

[90] A. J. Van Asselt, M. M. M. Vissers, F. Smit, and P. De Jong. In-line control of fouling. In *Proceedings of Heat Exchanger Fouling and Cleaning-Challenges and Opportunities, Engineering Conferences International, Kloster Irsee, Germany*, 2005.

[91] LM Freitas Dos Santos and A. G. Livingston. Novel membrane bioreactor for detoxification of VOC wastewaters : Biodegradation of 1, 2-dichloroethane. *Water Research*, 29(1) :179–194, 1995.

[92] Th JM Jeurnink, D. W. Brinkman, and A. D. Stemerdink. Distribution and composition of deposit in heat exchangers. In *Proceeding of the Third International Conference on Fouling and Cleaning in Food Processing (25–35). Munich, Germany : University of Munich*, 1989.

[93] T. Truong, S. Anema, K. Kirkpatrick, and K. T. Tuoc. In-line measurements of fouling and CIP in milk powder plants. In *Fouling and Cleaning in Food Processing*, pages 6–8. Jesus College, University of Cambridge Cambridge, 1998.

[94] Franck Delplace. *Identification Des Échangeurs de Chaleur à Plaques : Application à l'étude de l'encrassement Par Les Produits Laitiers*. PhD thesis, Nancy 1, 1995.

[95] H. Burton. Seasonal variation in deposit formation from whole milk on a heated surface. *Journal of Dairy Research*, 34(2) :137–143, June 1967.

[96] Paul J. Skudder, Elmer L. Thomas, John A. Pavey, and Allen G. Perkin. Effects of adding potassium iodate to milk before UHT treatment : I. Reduction in the amount of deposit on the heated surfaces. *Journal of Dairy Research*, 48(1) :99–113, February 1981.

[97] Marc Lalande, Jean-Pierre Tissier, and Georges Corrieu. Fouling of a plate heat exchanger used in ultra-high-temperature sterilization of milk. *Journal of Dairy Research*, 51(4) :557–568, November 1984.

[98] J. Hiddink, M. Lalande, A. J. R. Maas, and A. Streuper. Heat treatment of whipping cream. I. Fouling of the pasteurization equipment. *Milchwissenschaft (Germany, FR)*, 1986.

[99] Jean-Claude Leuliet. *Comportements Hydraulique et Thermique Des Échangeurs à Plaques Traitant Des Produits Non-Newtoniens*. PhD thesis, 1988.

[100] Yoon Jungro and Lund Daryl B. Magnetic Treatment of Milk and Surface Treatment of Plate Heat Exchangers : Effects on Milk Fouling. *Journal of Food Science*, 59(5) :964–969, August 2006.

[101] F. Delplace, J. C. Leuliet, and J. P. Tissier. Fouling experiments of a plate heat exchanger by whey proteins solutions. *Food and bioproducts processing : transactions of the Institution of Chemical Engineers, Part C*, 1994.

[102] P. J. Fryer, P. T. Robbins, C. Green, P. J. R. Schreier, A. M. Pritchard, A. P. M. Hasting, D. G. Royston, and J. F. Richardson. A statistical model for fouling of

a plate heat exchanger by whey protein solution at UHT conditions. *Food and Bioproducts Processing*, 74(4) :189–199, 1996.

[103] Romuald Guérin, Gilles Ronse, Laurent Bouvier, Pascal Debreyne, and Guillaume Delaplace. Structure and rate of growth of whey protein deposit from in situ electrical conductivity during fouling in a plate heat exchanger. *Chemical Engineering Science*, 62(7) :1948–1957, April 2007.

[104] J. P. Tissier and M. Lalande. Experimental device and methods for studying milk deposit formation on heat exchange surfaces. *Biotechnology Progress*, 2(4) :218–229, 1986.

[105] K. R. Goode, J. Bowen, N. Akhtar, P. T. Robbins, and P. J. Fryer. The effect of temperature on adhesion forces between surfaces and model foods containing whey protein and sugar. *Journal of Food Engineering*, 118(4) :371–379, 2013.

[106] M. R. Bird and M. Bartlett. CIP optimisation for the food industry : Relationships between detergent concentration, temperature and cleaning time. *Food and bioproducts processing : transactions of the Institution of Chemical Engineers, Part C*, 1995.

[107] C Riverol and V Napolitano. Estimation of fouling in a plate heat exchanger through the application of neural networks. *Journal of Chemical Technology & Biotechnology*, 80(5) :594–600, May 2005.

[108] Holger Martin. The generalized Lévêque equation and its practical use for the prediction of heat and mass transfer rates from pressure drop. *Chemical Engineering Science*, 57(16) :3217–3223, August 2002.

[109] Helga Ingimundardóttir and Sylvain Lalot. Detection of Fouling in a Cross-Flow Heat Exchanger Using Wavelets. *Heat Transfer Engineering*, 32(3-4) :349–357, March 2011.

[110] S. Lecoeuche, S. Lalot, and B. Desmet. Modelling a non-stationary single tube heat exchanger using multiple coupled local neural networks. *International Communications in Heat and Mass Transfer*, 32(7) :913–922, July 2005.

[111] P. K. Nema and A. K. Datta. A computer based solution to check the drop in milk outlet temperature due to fouling in a tubular heat exchanger. *Journal of food engineering*, 71(2) :133–142, 2005.

[112] P. K. Nema and A. K. Datta. Improved milk fouling simulation in a helical triple tube heat exchanger. *International Journal of Heat and Mass Transfer*, 49(19-20) :3360–3370, 2006.

[113] L. Perez, B. Ladevie, P. Tochon, and J. C. Batsale. A new transient thermal fouling probe for cross flow tubular heat exchangers. *International Journal of Heat and Mass Transfer*, 52(1) :407–414, January 2009.

[114] C. M. Astorga-Zaragoza, A. Zavala-Río, V. M. Alvarado, R. M. Méndez, and J. Reyes-Reyes. Performance monitoring of heat exchangers via adaptive observers. *Measurement*, 40(4) :392–405, May 2007.

[115] Xiao Dong Chen, Dolly X.Y. Li, Sean X.Q. Lin, and Necati Ozkan. On-line fouling/cleaning detection by measuring electric resistance equipment development and application to milk fouling detection and chemical cleaning monitoring. *Journal of Food Engineering*, 61(2) :181–189, February 2004.

[116] M. A. Ayadi, J. C. Leuliet, F. Chopard, M. Berthou, and M. Lebouché. Continuous ohmic heating unit under whey protein fouling. *Innovative Food Science & Emerging Technologies*, 5(4) :465–473, December 2004.

[117] M. A. Ayadi, T. Benezech, F. Chopard, and M. Berthou. Thermal performance of a flat ohmic cell under non-fouling and whey protein fouling conditions. *LWT - Food Science and Technology*, 41(6) :1073–1081, July 2008.

[118] J. Y. M. Chew, W. R. Paterson, and D. I. Wilson. Fluid dynamic gauging for measuring the strength of soft deposits. *Journal of Food Engineering*, 65(2) :175–187, November 2004.

[119] Y.M.J. Chew, W.R. Paterson, and D.I. Wilson. Fluid dynamic gauging : A new technique for studying membrane fouling. *Water Science & Technology : Water Supply*, 7(5-6) :175, December 2007.

[120] Rowan J. Hooper, Wei Liu, Peter J. Fryer, W. R. Paterson, D. Ian Wilson, and Zhibing Zhang. Comparative studies of fluid dynamic gauging and a micromanipulation probe for strength measurements. *Food and Bioproducts Processing*, 84(4) :353–358, 2006.

[121] Peter M. Withers. Ultrasonic, acoustic and optical techniques for the non-invasive detection of fouling in food processing equipment. *Trends in Food Science & Technology*, 7(9) :293–298, September 1996.

[122] N. Collier, P. Debreyne, G. Delaplace, B. Chen, D. Callens, P. Campistron, and B. Nongaillard. Contribution of the shear wave ultrasonic reflectometry to the stickiness measurements. *Ultrasonics*, 89 :187–194, September 2018.

[123] Charlotte Modin, Anne-Louise Stranne, Morten Foss, Mogens Duch, Jeannette Justesen, Jacques Chevallier, Lars K. Andersen, Anne G. Hemmersam, Finn S. Pedersen, and Flemming Besenbacher. QCM-D studies of attachment and differential spreading of pre-osteoblastic cells on Ta and Cr surfaces. *Biomaterials*, 27(8) :1346–1354, March 2006.

[124] J. J. da Silva, M. G. Wanzeller, P. de Almeida Farias, and J. S. da Rocha Neto. Development of Circuits for Excitation and Reception in Ultrasonic Transducers for Generation of Guided Waves in Hollow Cylinders for Fouling Detection. *IEEE Transactions on Instrumentation and Measurement*, 57(6) :1149–1153, June 2008.

[125] Thomas R. Hay and Joseph L. Rose. Fouling detection in the food industry using ultrasonic guided waves. *Food Control*, 14(7) :481–488, October 2003.

[126] Kenneth R. Lohr and Joseph L. Rose. Ultrasonic guided wave and acoustic impact methods for pipe fouling detection. *Journal of Food Engineering*, 56(4) :315–324, March 2003.

[127] B. Merheb, G. Nassar, B. Nongaillard, G. Delaplace, and J. C. Leuliet. Design and performance of a low-frequency non-intrusive acoustic technique for monitoring fouling in plate heat exchangers. *Journal of Food Engineering*, 82(4) :518–527, October 2007.

[128] A. Pereira, R. Rosmaninho, J. Mendes, and L. F. Melo. Monitoring Deposit Build-up using a Novel Mechatronic Surface Sensor (MSS). *Food and Bioproducts Processing*, 84(4) :366–370, December 2006.

[129] Renato Teixeira, Ana Pereira, Joaquim Mendes, and Luís F. Melo. Identifying the Nature of Fouling Layers by Online Monitoring of the Propagation of Vibrations Along the Deposition Surface. *Heat Transfer Engineering*, 35(3) :251–257, February 2014.

[130] E. Wallhäußer, M.A. Hussein, and T. Becker. Detection methods of fouling in heat exchangers in the food industry. *Food Control*, 27(1) :1–10, September 2012.

[131] Keiiti Aki and Bernard Chouet. Origin of coda waves : Source, attenuation, and scattering effects. *Journal of Geophysical Research*, 80(23) :3322–3342, August 1975.

[132] Alexandre A. Grêt. *Time-Lapse Monitoring with Coda Wave Interferometry*. PhD thesis, Colorado School of Mines, 2004.

[133] Alexandre Grêt, Roel Snieder, and John Scales. Time-lapse monitoring of rock properties with coda wave interferometry. *Journal of Geophysical Research : Solid Earth*, 111(B3) :B03305, March 2006.

[134] Alexander Grêt, Roel Snieder, Richard C. Aster, and Philip R. Kyle. Monitoring rapid temporal change in a volcano with coda wave interferometry. *Geophysical Research Letters*, 32(6) :L06304, March 2005.

[135] Roel Snieder. Coda wave interferometry and the equilibration of energy in elastic media. *Physical Review E*, 66(4) :046615, October 2002.

[136] Roel Snieder. The Theory of Coda Wave Interferometry. *Pure and Applied Geophysics*, 163(2-3) :455–473, March 2006.

[137] Yuxiang Zhang. *Contrôle de Santé Des Matériaux et Structures Par Analyse de La Coda Ultrasonore*. PhD thesis, Université du Maine, 2013.

[138] D. A. Weitz, J. X. Zhu, D. J. Durian, Hu Gang, and D. J. Pine. Diffusing-wave spectroscopy : The technique and some applications. *Physica Scripta*, 1993(T49B) :610, 1993.

[139] M. L. Cowan, I. P. Jones, J. H. Page, and D. A. Weitz. Diffusing acoustic wave spectroscopy. *Physical Review E*, 65(6), June 2002.

[140] Keiiti Aki. Analysis of the seismic coda of local earthquakes as scattered waves. *Journal of Geophysical Research*, 74(2) :615–631, January 1969.

[141] Roel Snieder and Mike Hagerty. Monitoring change in volcanic interiors using coda wave interferometry : Application to Arenal Volcano, Costa Rica. *Geophysical research letters*, 31(9), 2004.

[142] C. Friedrich and U. Wegler. Localization of seismic coda at Merapi volcano (Indonesia). *Geophysical research letters*, 32(14), 2005.

[143] Alexandre Grêt, Roel Snieder, and Ugur Özbay. Monitoring in situ stress changes in a mining environment with coda wave interferometry. *Geophysical Journal International*, 167(2) :504–508, 2006.

[144] Matthew M. Haney, Kasper van Wijk, Leiph A. Preston, and David F. Aldridge. Observation and modeling of source effects in coda wave interferometry at Pavlof volcano. *The Leading Edge*, 28(5) :554–560, 2009.

[145] Jean Battaglia, Jean-Philippe Métaxian, and Esline Garaebiti. Earthquake volcano interaction imaged by coda wave interferometry. *Geophysical Research Letters*, 39(11), 2012.

[146] Francesca Martini, Christopher J. Bean, Gilberto Saccorotti, Fatima Viveiros, and Nicolau Wallenstein. Seasonal cycles of seismic velocity variations detected using coda wave interferometry at Fogo volcano, São Miguel, Azores, during 2003–2004. *Journal of Volcanology and Geothermal Research*, 181(3-4) :231–246, 2009.

[147] Yuxiang Zhang, Odile Abraham, Vincent Tournat, Alain Le Duff, Bertrand Lascoup, Ahmed Loukili, Frédéric Grondin, and Olivier Durand. Validation of a thermal bias control technique for Coda Wave Interferometry (CWI). *Ultrasonics*, 53(3) :658–664, 2013.

[148] Yuxiang Zhang, Odile Abraham, Frédéric Grondin, Ahmed Loukili, Vincent Tournat, Alain Le Duff, Bertrand Lascoup, and Olivier Durand. Study of stress-induced velocity variation in concrete under direct tensile force and monitoring of the damage level by using thermally-compensated coda wave interferometry. *Ultrasonics*, 52(8) :1038–1045, 2012.

[149] Benoit Hilloulin, Yuxiang Zhang, Odile Abraham, Ahmed Loukili, Frédéric Grondin, Olivier Durand, and Vincent Tournat. Small crack detection in cementitious materials using nonlinear coda wave modulation. *NDT & E International*, 68 :98–104, December 2014.

[150] G. Poupinet, W. L. Ellsworth, and J. Frechet. Monitoring velocity variations in the crust using earthquake doublets : An application to the Calaveras Fault, California. *Journal of Geophysical Research : Solid Earth*, 89(B7) :5719–5731, July 1984.

[151] Christoph Sens-Schönfelder and Eric Larose. Temporal changes in the lunar soil from correlation of diffuse vibrations. *Physical Review E*, 78(4) :045601, October 2008.

[152] B. Chen, D. Callens, P. Campistron, E. Moulin, P. Debreyne, and G. Delaplace. Monitoring cleaning cycles of fouled ducts using ultrasonic coda wave interferometry (CWI). *Ultrasonics*, 96 :253–260, July 2019.

[153] Hiroaki Kamioka. Ultrasonic Behaviour of Paraffin Wax during Melting and Solidification Processes. *Japanese Journal of Applied Physics*, 33(5S) :2908, May 1994.

[154] Marwan Abdallah, Oussama Khelissa, Ali Ibrahim, Corinne Benoliel, Laurent Heliot, Pascal Dhulster, and Nour-Eddine Chihib. Impact of growth temperature and surface type on the resistance of Pseudomonas aeruginosa and Staphylococcus aureus biofilms to disinfectants. *International Journal of Food Microbiology*, 214 :38–47, December 2015.